RICE UNIVERSITY

Optical Imaging Techniques for the Detection of Esophageal Neoplasia in Barrett's Esophagus

by

Nadhi Thekkek

A THESIS SUBMITTED IN PARTIAL FULFILLMENT OF THE REQUIREMENTS FOR THE DEGREE

Doctor of Philosophy

APPROVED, THESIS COMMITTEE:

_____
Rebecca Richards-Kortum, Stanley C. Moore Professor and Chair
Bioengineering, Rice University

_____
Sharmila Anandasabapathy, Associate Professor of Medicine
Gastroenterology, Mount Sinai Medical Center

_____
John McDevitt, Brown-Wiess Professor
Bioengineering and Chemistry, Rice University

_____
Richard Baraniuk, Victor E. Cameron Professor
Electrical and Computer Engineering, Rice University

HOUSTON, TEXAS
JANUARY 2013

ABSTRACT

Optical Imaging Techniques for the Detection of Esophageal Neoplasia in Barrett's Esophagus

by

Nadhi Thekkek

The main objective of this research was to develop a two-stage optical imaging platform to improve detection of cancer in Barrett's esophagus (BE). BE caused by chronic reflux and patients with BE are at a higher risk for developing esophageal adenocarcinoma (EAC). However, neoplasia in BE is often unidentifiable under standard endoscopy, and studies have shown nearly half of early cancers can go unidentified by this method.

Widefield imaging (resolves ~100 microns) allows efficient surveillance of large BE segments. Two widefield imaging techniques were identified to improve contrast between benign and abnormal lesions during an ex vivo 15 patient feasibility study. Cross-polarized imaging (CPI) reduced specular reflection and improved vascular contrast. Vital-dye fluorescence imaging (VFI) using topically-applied proflavine improved visualization of glandular pattern. Moreover, relevant pathologic features visible during VFI were seen in corresponding histology slides as well as high resolution images of the same sites.

Based on these results, a cap-based Multispectral Digital Endoscope (MDE) was designed and built. The MDE can image in three different imaging modes: white light

imaging, CPI, and VFI. Modifications to a Pentax EPK-i video processor and a Pentax endoscope were made to incorporate these imaging modes into one system. A 21 patient in vivo pilot study with 65 pathologically correlated sites demonstrated the feasibility of using this system in vivo; image criteria were developed to classify neoplasia with a sensitivity and specificity of 100% and 76% respectively.

High resolution imaging (resolves ~2-5 micron) may verify the disease presence in suspicious areas identified using widefield techniques. 2-NBDG, a fluorescent metabolic marker, was used as to identify neoplastic biopsies. In a study with 21 patients yielding 38 pathologically correlated biopsies and 158 image sites, 2-NBDG imaging allowed classification of cancerous biopsies with a sensitivity of 96% and specificity of 90%.

The unique contributions of these results is the development of a multimodal cap-based endoscopic system to identify suspicious areas in BE, and using a metabolic marker to verify the presence of disease. This application extends beyond esophageal cancer detection and may be explored for cancer detection in other organ sites characterized by columnar epithelium.

ACKNOWLEDGEMENTS

First, I would like to thank Dr. Kortum for being an amazing mentor and advisor. You are a dedicated scientist, teacher, and mother and an inspiration to anyone you meet. I truly believe you are saving lives with the work you do and feel privileged to have been a part of that process.

I would like to especially thank Dr. Anandasabapathy for being an irreplaceable part of my graduate work and my education. Her dedication to her patients is inspiring and makes bioengineers want to do their jobs better every day. I also would like to thank the rest of my committee members, Dr. Baraniuk and Dr. McDevitt for being accessible and enthusiastic about this work.

I would like to thank everyone who made this work possible including: Tim Muldoon, Rachna Khare Muldoon, Josephine Mitcham, Michelle Lee, and Yubo Tang. Each of them had an instrumental role in data collection and the patient studies would not have gone as smoothly without them.

I have learned a lot from mentors and friends, including Mark Pierce, Darren Roblyer, Richard Schwarz, Kelsey Rosbach, Noah Bedard, Donnie Shin, Anne Hellebust, Ben Grant, Veronica Leautaud, and Vivian Mack. Their knowledge and patience have been imperative in my learning process. I would not have learned so much without them, and have so much fun in the process.

My parents have been supportive in everything that I attempt, and are there for me whether I succeed or not. The opportunities that I have had in my life have been made available to me primarily because of their hard work and selflessness. I cannot even begin to thank them for everything they have done for me.

My husband, Roy is my biggest supporter and knows how to tell it to me straight. He knows what I am capable of sometimes even better than I do – in fact, he always sees me going further than I see myself. Having his support and love means the world to me.

This time in graduate school has been invaluable. I learned a lot about myself, my abilities, my limitations, and my passions. I could not have gone on this journey without dedicated advisors, teachers, mentors, family-members and friends.

TABLE OF CONTENTS

LIST OF TABLES AND FIGURES

CHAPTER 1: INTRODUCTION

1.1 Overview

Cancer accounts for more than 20% of deaths in many developed countries, and about 10% of deaths in developing countries [1]. Esophageal adenocarcinoma (EAC) is a small but rapidly increasing part of this global burden. The disease has one of the fastest rising rates of incidence in the United States with an estimated 463% increase among males and a 335% increase among females since 1975 [2]. This is of particular concern, since the five-year survival for patients diagnosed with EAC is can be as low as 12% [3], a dismal outcome resulting primarily from late-stage disease detection. Though treating esophageal neoplasia at an early stage has been reported to increase five-year survival rates to as high as 81% , only a fraction of these cancers are detected early [2].

EAC develops primarily in patients with Barrett's esophagus (BE), a prevalent condition of the esophagus caused by chronic acid reflux have an increased risk of developing EAC. Therefore patients with BE undergo regular endoscopic surveillance in an attempt to identify and treat early lesions. Surveillance for dysplasia and cancer in BE involves bi-annual endoscopic examination with random four-quadrant biopsies taken every 1-2 cm along the entire BE segment [4]. However, dysplasia in BE is often unidentifiable under standard white light endoscopy and studies have shown that as many as 43-57% of early cancers can go unidentified by the random biopsy protocol [5]. These limitations in the standard of care motivate the development of improved early detection strategies.

Optical imaging can measure signal alterations associated with light scattering, light absorption and tissue autofluorescence, properties which are not apparent under

standard white light endoscopy [6]. Various widefield optical imaging modalities that are capable of imaging these sources of endogenous contrast in real-time have been shown to improve the detection of neoplasia in BE [7, 8]; unfortunately, the high rate of false-positives associated with inflammation, the details of which will be reviewed further in Chapter 2, continues to be a major drawback [7].

The relatively poor specificity of widefield imaging motivates the need for high-resolution interrogation at the cellular level. Recent advances in instrumentation have allowed real-time evaluation of sub-cellular morphology *in vivo*. Coupled with the appropriate contrast agent, high resolution imaging modalities have been shown to improve specificity [9]. A limitation of high resolution imaging modalities is its small field of view (~1 mm x 1 mm); this constraint makes it difficult to survey the entire mucosal surface at risk during routine surveillance.

Due to limitations such as these, there is an important need to explore additional imaging techniques to improve detection. A potential solution may be a multimodal approach, combining the benefits of widefield and high resolution instrumentation. At the same time, advances in exogenous contrast agents such as a vital-dye (proflavine hemisulfate) or a metabolic marker (2-NBDG) may further enhance signal differences associated with neoplasia to better facilitate detection. The work described in this thesis is motivated by the need for a contrast-enhanced multimodal imaging platform that can survey large areas to identify suspicious regions with high sensitivity and can then interrogate those regions with increased resolution to potentially improve specificity.

1.2 Specific Aims

The overall goal of this dissertation was to develop contrast-enhanced multimodal optical imaging techniques to improve the detection of Barrett's-associated neoplasia during widefield and high resolution imaging. The specific aims achieved to accomplish this goal were to:

1) **Evaluate the use of a single contrast agent (proflavine) during widefield and high resolution imaging to characterize gastrointestinal conditions.** Using a multispectral digital microscope and a high resolution microendoscope, endoscopic and surgical resection specimens from 15 consenting patients were imaged to characterize the signal associated with proflavine enhancement. Image criteria were developed based on histopathology gold standard to assess architectural and morphologic changes associated with neoplastic progression for future *in vivo* studies.

2) **Design, construct, and test a modular video endoscope capable of imaging proflavine *in vivo* at multiple spatial resolutions.** Optical performance of the system was characterized by determining its resolution, field of view, and other performance indicators. A pilot study was conducted to assess system feasibility during *in vivo* Barrett's surveillance.

3) **Determine quantitative image criteria that aids the identification of neoplasia in widefield vital-dye fluorescence images obtained in vivo.** Vital-dye fluorescence images from 65 pathologically correlated in vivo image sites. Texture, frequency content, and granulometry metrics were calculated and sequential feature selection was used to determine the optimal features for linear discriminant analysis. Histopathology was used as a gold standard for comparison.

4) **Evaluate the use of 2-NBDG for identifying neoplasia and reducing false positives associated with inflammation.** Biopsy specimens from 26 consenting patients were incubated with 2-NBDG and imaged using a benchtop confocal microscope. Image analysis was conducted to determine whether 2-NBDG associated contrast allowed for identification of neoplastic specimens. Histopathology was used as a gold standard for comparison.

1.3 Chapter Summaries

This dissertation describes the development of contrast-enhanced widefield and high resolution optical imaging techniques to improve the detection of Barrett's-associated neoplasia. Many previous works have used widefield imaging to detect lesions missed by the random biopsy method. In those studies, the primary sources of contrast were endogenous signal alterations associated with neoplastic areas which in some cases are indistinguishable from benign inflammatory lesions by standard endoscopy [7, 8]. Additional studies have explored the use of high resolution imaging with both

intravenously and topically administered contrast agents [9, 10], but have been limited by their small field of view. This dissertation introduces the potential benefit of a vital-dye enhanced multimodal imaging platform to evaluate morphologic changes in the Barrett's-associated disease sequence. This work also details the instrumentation developed to measure those changes *in vivo*. Moreover, this dissertation extends the use of contrast agents not only to evaluate morphology at multiple spatial scales but also to take advantage of metabolic signatures that neoplastic cells present in an effort to understand the confounding effect of inflammation. A summary of each chapter follows.

Chapter 2 summarizes the motivation for this work, including relevant cancer-associated alterations in tissue, and current imaging approaches that have been explored to measure these changes. Current widefield and high resolution imaging approaches, some coupled with an appropriate contrast agent, can measure differences in glandular morphology, nuclear morphology, or vascular alterations associated with neoplasia. Advances in targeted contrast agents are further discussed. Studies that have explored these technologies are highlighted, as are the advantages and limitations of each.

Chapter 3 describes a study evaluating the feasibility of a single agent, proflavine hemisulfate, as a contrast medium during both widefield and high resolution imaging to characterize morphologic changes associated with a variety of gastrointestinal conditions. Surgical specimens were obtained from 15 patients undergoing esophagectomy or colectomy procedures. Proflavine, a vital fluorescent dye which stains cell nuclei was applied topically. Specimens were imaged with a widefield multispectral microscope and a high resolution microendoscope and compared to histopathology. Relevant widefield and high resolution morphologic features characteristic to metaplasia, neoplasia, and

inflammation are described. This study provided the rationale for the development of an instrument that could acquire these measurements *in vivo*.

Chapter 4 describes the development and testing of a multimodal digital endoscope (MDE). Specifically, this chapter details the design and implementation of two imaging modes, cross-polarized reflectance imaging and fluorescence imaging with vital-dye enhancement. This system was used to collect *in vivo* image data from esophageal tissue in order to identify suspicious lesions that may not be apparent during standard white light endoscopy. An ex vivo esophagectomy specimen with histologically-verified neoplasia was used to identify pathologically relevant CPI and VFI image features. The criteria was verified in vivo during routine endoscopic surveillance of BE. Image data from various tissue types were evaluated to identify relevant pathologic features associated with neoplasia. This initial examination of widefield image criteria in vivo motivated to the 20 patient in vivo pilot study.

Chapter 5 describes the quantitative analysis of data obtained during in vivo endoscopic surveillance during a 20 patient pilot study, yielding 65 pathologically correlated images. Optimal image criteria were determined by sequential feature selection and linear discriminant analysis. Classification accuracy was assessed using histopathology as the gold standard.

Chapter 6 describes a study evaluating 2-NBDG, a fluorescent metabolic marker, to help differentiate neoplasia from benign lesions. Surveillance biopsies from patients with varying pathologic grades of Barrett's esophagus were incubated *ex vivo* at 37°C with 2-NBDG and imaged with a fluorescence confocal microscope. Forty-four biopsies

were obtained from twenty-six patients; 206 sites were imaged. Images were categorized as neoplastic (high grade dysplasia, esophageal adenocarcinoma) or metaplastic (intestinal metaplasia, low grade dysplasia) based on the degree of glandular 2-NBDG uptake. Classification accuracy was assessed using histopathology as the gold standard.

Chapter 7 discusses the major conclusions of this work and elaborates on the implications on the advancing field of endoscopic surveillance. This research presented in this dissertation focuses on the development of optical imaging techniques that can be used for *in vivo* detection of esophageal precancers associated with EAC. These studies will provide information necessary to build a multi-faceted platform technology that can be used not only to detect precancer in Barrett's, but also abnormalities in other organ sites lined with glandular epithelium.

Chapter 7 also describes the future directions associated with instrument and contrast agent advances made in this dissertation. To summarize, a larger clinical trial is required to identify which widefield imaging mode achieves high sensitivity. Next, a study to assess the benefits of widefield imaging and high resolution imaging is necessary to compare the sensitivity and specificity of this multimodal platform to standard surveillance techniques. Furthermore, there exists a need to translate the use of 2-NBDG *in vivo*; necessary steps include identifying a medium for delivery and conducting delivery experiments in an appropriate animal model. These steps towards clinical translation are essential in assessing to what degree the technologies developed in this dissertation could improve disease management and ultimately, patient care.

CHAPTER 2: BACKGROUND

2.1 Motivation and significance

The incidence of esophageal adenocarcinoma (EAC) is rapidly increasing; over the last 40 years, the incidence rate of EAC has risen by over 300% in the United States [11]. This is of particular concern because the overall 5-year survival rate for patients diagnosed with EAC is only 12% [3]. Although detecting and treating esophageal neoplasia at an early stage has been reported to increase 5-year survival to rates as high as 81% [12], current methods of early detection have significant limitations. As a result, more than 60% of patients with EAC are diagnosed at a late stage, after local, regional, or distance metastases have occurred [13].

EAC arises primarily in patients with Barrett's esophagus (BE) [14, 15], which is a highly prevalent condition in which the squamous epithelium of the esophagus is replaced by intestinal metaplasia (IM) near the gastroesophageal (GE) junction [16-18]. Because of this increased risk, patients with BE undergo regular surveillance endoscopy at designated intervals in an attempt to identify neoplastic lesions at an early stage [4, 19]. Surveillance involves endoscopic examination with random four-quadrant biopsies taken every 1-2 cm of the Barrett's segment [4].

Despite surveillance efforts, routine biopsy protocols have been shown to miss up to 57% of neoplastic lesions in patients with BE [5]. This is largely due to the fact that dysplasia or neoplasia may be focal, flat, and endoscopically indistinguishable from non-neoplastic epithelium on routine white-light endoscopy (WLE). This ability to better delineate superficial mucosal changes associated with early neoplasia at a macroscopic

level, and subsequently, identify the subcellular changes associated with neoplastic progression would greatly enhance the yield and efficacy of current surveillance practices.

2.4 Changes in Optical Properties

In a standard white light endoscopic examination, the endoscopist views white light reflected from the surface of the esophagus; while visual examination of reflected white light can identify some changes in tissue morphology associated with neoplasia, it does not exploit the full range of changes in tissue optical properties which are associated with dysplasia and cancer. Neoplasia alters the light absorption and scattering properties of esophageal tissue [20, 21]; in addition, neoplasia is associated with changes in the autofluorescence properties of esophageal tissue [20, 22-24]. A number of new endoscopic approaches have been developed to more effectively probe neoplasia-related changes in optical properties to improve visualization of early neoplastic lesions. For example, the color of illumination light can be optimized to better probe changes in tissue absorption and/or scattering. Autofluorescence endoscopy can be used to image changes in tissue fluorescence which are associated with neoplasia. Moreover, improving spatial resolution of endoscopic imaging can help reveal changes in cellular architecture and morphology associated with neoplasia. Finally, optically active contrast agents can be used to further improve image contrast and probe specific molecular and morphologic features of neoplastic tissue which may not be associated with changes in native optical properties.

In this chapter, we first review changes in the optical properties of esophageal tissue associated with neoplasia, and then outline new endoscopic imaging approaches to

better use these changes to improve early detection of esophageal neoplasia. Finally, we discuss the use of targeted contrast agents to expand the range of molecular changes that can be imaged in vivo.

2.4.1 Neoplasia-Associated Changes in Tissue Light Scattering and Absorption

Light attenuation in esophageal tissue is governed by a combination of absorption and scattering. In the visible region of the spectrum, the primary source of light absorption in esophageal tissue is hemoglobin. Esophageal neoplasia is associated with increased angiogenesis [25], and endoscopic imaging approaches to enhance vascular contrast may improve early detection[26, 27]. Oxy-hemoglobin has absorption peaks at 420 nm, 542 nm, and 577 nm[20]; examining the tissue at these illumination wavelengths can enhance vascular contrast, with vasculature appearing visibly darker than the surrounding tissue due to the increase in light absorption[28]. Neovascularization is an important quantifiable tool for distinguishing neoplasia from non-neoplastic Barrett's epithelium. Irregular angiogenesis occurs within the lamina propria at various levels of the mucosal layer in high grade dysplasia and cancer. These features have been verified by analysis of microvessels and overexpression of relevant markers such as VEG-F and CD34 resulting in a statistically significant difference between the microvessel density in BE versus high grade dysplasia and cancer[26, 27].

Light scattering in tissue is a result of spatial fluctuations in the refractive index. In general, the scattering of stroma is significantly greater than that of the epithelium and is the dominant source of reflected white light from intact tissue. Neoplasia is associated with a small decrease in stromal scattering attributed to degradation in collagen fibers

possibly due to proteases secreted by pre-neoplastic epithelial cells[25, 29, 30]. The attenuation of light in tissue is wavelength dependent, with longer red wavelengths able to penetrate more deeply than shorter blue wavelengths. Thus, tuning the illumination wavelength provides some ability to control penetration depth, and highlight vascular contrast.

2.4.2 Neoplasia-Associated Changes in Tissue Autofluorescence

Some endogenous constituents of esophageal tissue can remit absorbed light in the form of fluorescence. Endogenous fluorophores are found in both the epithelium and the stroma of esophageal tissue, and fluorescence imaging provides a way to monitor changes in the concentration and composition of these fluorophores. When esophageal tissue undergoes malignant transformation, endogenous fluorophores undergo alterations[31-33], which can be probed via autofluorescence imaging (AFI), to detect abnormalities that may not be visible during standard white light endoscopy. Tuning the excitation wavelength provides a way to selectively probe various fluorophores which can then be quantified by measuring light intensity at specific emission wavelengths[33].

The primary fluorophores within the epithelium include mitochondrial NADH and FAD found in epithelial cells. Epithelial cells show cytoplasmic autofluorescence attributed to NADH using UV excitation wavelengths (~330-370 nm) and FAD using green excitation wavelengths (~510-550 nm)[34, 35]. Levels of mitochondrial NADH[23] and mitochondrial FAD increase due to dysplastic changes in the epithelium[36, 37].

Stromal fluorescence of esophageal tissue is predominantly associated with covalent collagen crosslinks, which are characterized by relatively high autofluorescence intensity across a broad range of UV, blue, and green excitation wavelengths[24].

Esophageal neoplasia is associated with a loss of stromal autofluorescence, which has been attributed to a decrease in collagen crosslinking[25, 29, 30]. Finally, invasive esophageal cancers are often associated with porphyrin fluorescence, with maximal excitation near 400 nm and emission in the red spectral region[20, 38, 39].

2.4.3 High-Resolution Imaging

The spatial resolution of optical imaging is governed by diffraction, and with visible wavelengths of light, sub-cellular resolution imaging is possible. Typically, standard endoscopic imaging approaches do not achieve diffraction-limited resolution, however, recent advances in high resolution imaging techniques such as optical coherence tomography, endocytoscopy, and endomicroscopy afford the ability to image with sub-cellular resolution. Such approaches are often termed 'optical biopsy,' because they allow visualization of glandular and cellular alterations associated with neoplasia. Optical contrast in high resolution imaging is governed by the same alterations in tissue absorption, scattering and fluorescence described above. In addition, optically active contrast agents are often used to increase contrast for high resolution imaging.

2.5 In Vivo Assessment of Imaging Technologies

In the past decade, advances in imaging technologies have enabled gastroenterologists to optically image and interrogate Barrett's-associated neoplasia with better contrast in vivo. The development of widefield imaging technologies affords clinicians a macroscopic view of the tissue, serving as a 'red-flag technique' for relevant abnormalities. High resolution technologies assess microscopic features of the tissue and, if coupled with an ideal source of contrast, may measure biochemical, molecular, and

vascular changes. Table 2-1 summarizes a number of different optical technologies currently under investigation, describes the advantages and disadvantages of each, and describes which stage they have reached in terms of clinical translation. Table 2-2 summarizes the accuracy of the technologies that have been translated to clinical use and have been used in large scale clinical trials.

Table 2-1. Advantages and disadvantages of optical technologies for identification of neoplasia in Barrett's esophagus

Technology	Advantages	Disadvantages	Stage
Standard WLE	Capable of scanning wide area, widely available outside of tertiary care centers, no exogenous contrast	Limited sensitivity and specificity	Commercially available
High-definition WLE	Capable of scanning wide area, increased image contrast, no exogenous contrast	Performance evaluated in moderate-sized studies	Commercially available
Autofluorescence Imaging	Capable of scanning wide area, consistently high sensitivity, no exogenous contrast	High rate of false positives, Performance evaluated only in small pilot studies	Commercially available
Narrow Band Imaging	Capable of scanning wide area, consistently high sensitivity, no exogenous contrast	Performance evaluated in small pilot studies	Commercially available
Optical Coherence Tomography	Resolves subsurface structure, no exogenous contrast	Technology still under development	Clinical Studies
Endocytoscopy	Histology-like imaging, high specificity	Low sensitivity, limited FOV, requires exogenous contrast	Commercially available
Confocal Microendoscopy	Nuclear morphology can be viewed, high	Limited FOV, high cost, uses IV exogenous	Commercially available

	sensitivity and specificity	contrast	
High Resolution Microendoscopy	Some nuclear morphology can be viewed , lower cost, adaptable to any endoscope	Limited FOV, requires exogenous contrast, technology in development	Clinical Studies

Table 2-2. Summary of performance of emerging optical technologies.

Type of detection	Study Size	Sensitivity, Specificity
Autofluorescence Imaging	60 patients; 116 images	91%, 43%[7]
Narrowband Imaging	63 patients; 175 images	94%, 76%[40]
	51 patients; 204 images	100%, 98%[41]
	21 patients; 75 images	89%, 95%[42]
High Resolution Imaging **(1-15µm resolution)**		
Optical Coherence Tomography	33 patients; 314 images	68%, 82%[43]
	55 patients; 177 images	83%, 75%[44]
Endocytoscopy	16 patients; 166 images	56%, 68% (425x) 42%, 83% (1125x)[45]
Confocal Imaging	63 patients; 433 images	93%, 98%[9]
	38 patients; 296 images	75%, 90%[46]

2.5.1 Narrow Band Imaging

Narrow band imaging (NBI) is a widefield imaging technology that takes advantage of changes in light scattering and absorption in neoplastic tissue. Systems that implement NBI illuminate tissue with one or more narrowband wavelength ranges corresponding to hemoglobin absorption peaks. Reflected light in these bandwidths is recombined to create a digital image with enhanced vascular contrast. This approach can also enhance visualization of villous mucosal patterns due to lining of vessels in mucosal folds[28]. An example is shown in Figure 2-1.

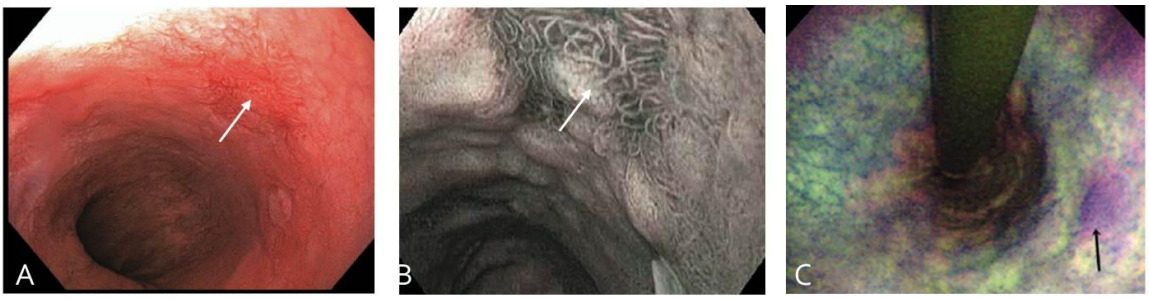

Figure 2-1. Endoscopic images from an area positive for esophageal adenocarcinoma. Abnormal areas (black arrows) can be seen in the high resolution white light image (A), and the narrow band image (B)[42]. In the narrow band image the irregular mucosal morphology is visible (black arrow). An abnormal area (black arrow) can be seen in the autofluorescence image (C) where areas with loss of fluorescence are indicated as purple regions in the pseudo-colored overlay[7].

For example, one NBI system combines information from three wavelength ranges; 400-430 nm (blue), 530-550 nm (green), and 600-620 nm (red). Higher relative intensity from the blue region is used to enhance surface level vasculature associated with neoplasia due to its shallow penetration depth. In a 63 patient study using this approach, researchers in Amsterdam used features such as mucosal morphology and vascular contrast to determine grade of disease. The presence and regularity of these patterns were

found to be essential for image evaluation. Out of the 175 areas, 52 were used as training material for endoscopists and the remaining 123 were used as a validation set. In the validation set, 94% of HGD images were noted to show irregular or disrupted villous/gyrous mucosal pattern, and 85% were noted to show irregular vascular patterns. Using these features and others, they developed a multi-step hierarchical classification system based on mucosal morphology including features such as type and regularity of mucosal patterns, regularity of vasculature patterns, and finally presence and type of abnormal blood vessels. Using this multistep evaluation, they determined the overall sensitivity and specificity to be 94% and 76%, respectively[40]. Similarly promising performance was also obtained using the same NBI system in a 51 patient study by Sharma and colleagues; sensitivity and specificity for detection of HGD were 100% and 99%[41].

Of continued debate, however, is the question of how NBI compares to high-definition white-light endoscopy (HD-WLE) using the current generation of endoscopes. This new generation of endoscopes offers markedly higher pixel densities and high-definition images resulting in increased contrast in villous mucosal patterns, and a marked improvement in resolution[7, 47] over standard WLE[8]. In a study with 65 patients, Wolfsen and colleagues, using a narrow band system where only two of the shorter wavelength-ranges associated with hemoglobin were used, observed that the combination of HD-WLE and NBI did find higher grades of dysplasia in 18% of the study patients using fewer biopsies than standard endoscopy. They also observed that out of 5 of the cases where HGD or EAC were detected, 3 were detected by HD-WLE as well. While results favored NBI, the study was not designed to determine the efficacy of one modality

over the other[42]. Another study by Curvers and colleagues observed that while expert endoscopists preferred the image contrast provided by NBI, this did not improve overall inter-observer agreement or accuracy when compared to HD-WLE[48, 49]. Larger-scale studies are needed to determine which is the more accurate technique.

2.5.2 Autofluorescence Imaging

Autofluorescence imaging can also increase contrast between non-neoplastic and neoplastic sites, as a result of the loss of autofluorescence associated with esophageal neoplasia. Typically, tissue autofluorescence is excited in the blue region (λ ~395-475 nm) and fluorescence emission is collected at longer wavelengths (>490 nm) to detect changes in fluorophores associated with malignant transformation. Because the intensity of autofluorescence can be low, this technique requires the use of highly sensitive CCDs to collect the autofluorescence signal. In recent systems, reflected light is also collected through a second CCD. Co-registered images can be used to compensate for changes in fluorescence intensity associated with variations in illumination and distance from the tip of the endoscope to the tissue, thereby further enhancing autofluorescence contrast. The resulting effect is pseudo-colored purple to highlight neoplastic lesions[7, 8]. An example is shown in Figure 2-1.

In a recent 60 patient study using a standard endoscope with an added AFI component, Kara was able to detect HGD in 22 patients, 14 of which were detected with AFI and WLE, and 6 of which were detected using AFI alone; thereby increasing the detection rate from 23% to 33% using AFI. Only one of the patients was diagnosed using four-quadrant biopsies alone [7]. Results suggest that AFI may aid in the detection of

addition HGD sites; however it may not exclude the need for the standard four quadrant biopsies. Sensitivity and specificity based on the 116 samples used for this study were 91% and 43%, respectively. While no patient was diagnosed without AFI and four quadrant biopsies, they cite a high rate of false positives using AFI alone due in part to the loss of autofluorescence associated with acute inflammation[7].

While individually these enhanced endoscopic technologies have shown success, the high rate of false positives is a major drawback. To address this limitation, a combination of modalities is being explored to utilize the benefits of each, potentially increasing the accuracy of detection at the point of surveillance. Kara and colleagues conducted a 20 patient pilot study where HD-WLE and AFI were used initially to locate suspicious lesions. Once the lesions were identified an NBI scope was introduced for detailed inspection of vascular and mucosal patterns. They found that 40% of the HGD lesions were discovered with AFI alone. However, the false positive rate of the modality was 40% and the positive predictive value was 60%. Following NBI inspection, the false positive rate was reduced to 10%; achieving a positive predictive value of 85%[50]. A more recent study with one scope containing both modalities achieved similar results. In this study, AFI was able to detect more lesions than high resolution WLE alone, however the false positive rate remained a high 81%; following detailed inspective with NBI the rate was reduced to 26%[42]. In both cases however, random four-quadrant biopsies detected additional lesions that the optical modalities did not identify – indicating the need for further development of these and other technologies.

2.5.3 High Resolution Imaging

Widefield imaging techniques, such as AFI and NBI, were developed to measure large surface areas of GI tissue. More recently, high resolution systems have been developed to achieve near diffraction-limited imaging from small fields of view. Four primary approaches have been pursued to increase spatial resolution. Optical coherence tomography (OCT) can image esophageal tissue with 10-15 micron resolution and a penetration depth of 1-2 mm. Endocytoscopy can image surface level esophageal tissue with up to 1-2 micron resolution using the highest magnification setting. Confocal microscopy can image esophageal tissue with 1-2 micron spatial resolution with a penetration depth of 300-400 microns. High resolution microendoscopy can image surface level esophageal tissue with 4-5 micron spatial resolution. Recent clinical studies with these modalities highlight the benefits and limitations of high resolution imaging.

Optical coherence tomography (OCT) uses variations in the time it takes light to be reflected from structures beneath the tissue surface to image sub-surface tissue structures as seen in Figure 2-2, in a manner analogous to ultrasound imaging. In a 55 patient study, researchers determined that OCT could differentiate HGD and EAC from BE with a sensitivity of 83% and a specificity of 75%[43]. An advantage of OCT is that it relies on endogenous differences in light scattering to generate image contrast. OCT may be a particularly useful tool in the detection and surveillance of sub-squamous BE because of its relatively great depth of penetration[51]. However, the technology is still under development [52] and further clinical studies are needed to assess performance in a wide variety of clinical settings.

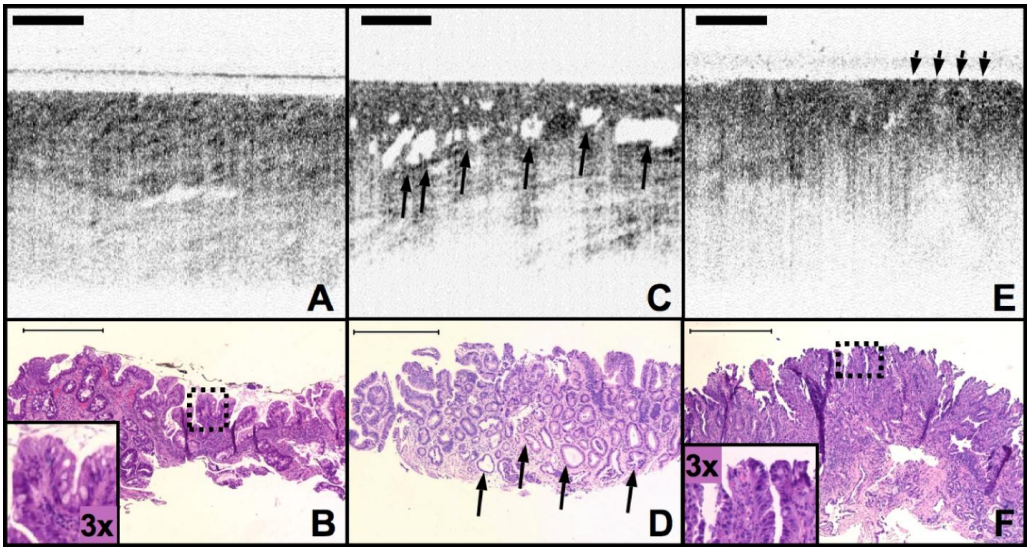

Figure 2-2. OCT images of intestinal metaplasia (A), and of neoplasia (C, E) are shown with corresponding histology images shown below[43]. Dilated glands (C) and increased surface reflectivity (E) can be seen in the OCT images of neoplastic tissue. Scale bars are 500 µm.

Endocytoscopy uses a probe which is passed through the instrumentation channel of an endoscope to image with sub-cellular resolution. Essentially, high resolution epi-reflectance microscopy is used with methylene blue contrast to highlight relevant nuclear features (Figure 2-3 first row). While models vary, there are generally two types each with different magnifications settings; one at 450x where the field of view can be as wide as 300x300 μm^2 and a higher magnification setting of 1125x where the field of view as small as 120x120 μm^2 is made visible[53]. A large study evaluating 166 sites in 16 patients with endocytoscopy by Pohl and colleagues reported a sensitivity and specificity of 42% and 83%, respectively[45]. While high specificity was encouraging, they did emphasize the need for an initial widefield surveillance technique to identify suspicious areas. This technology is certainly promising; however larger studies need to be performed.

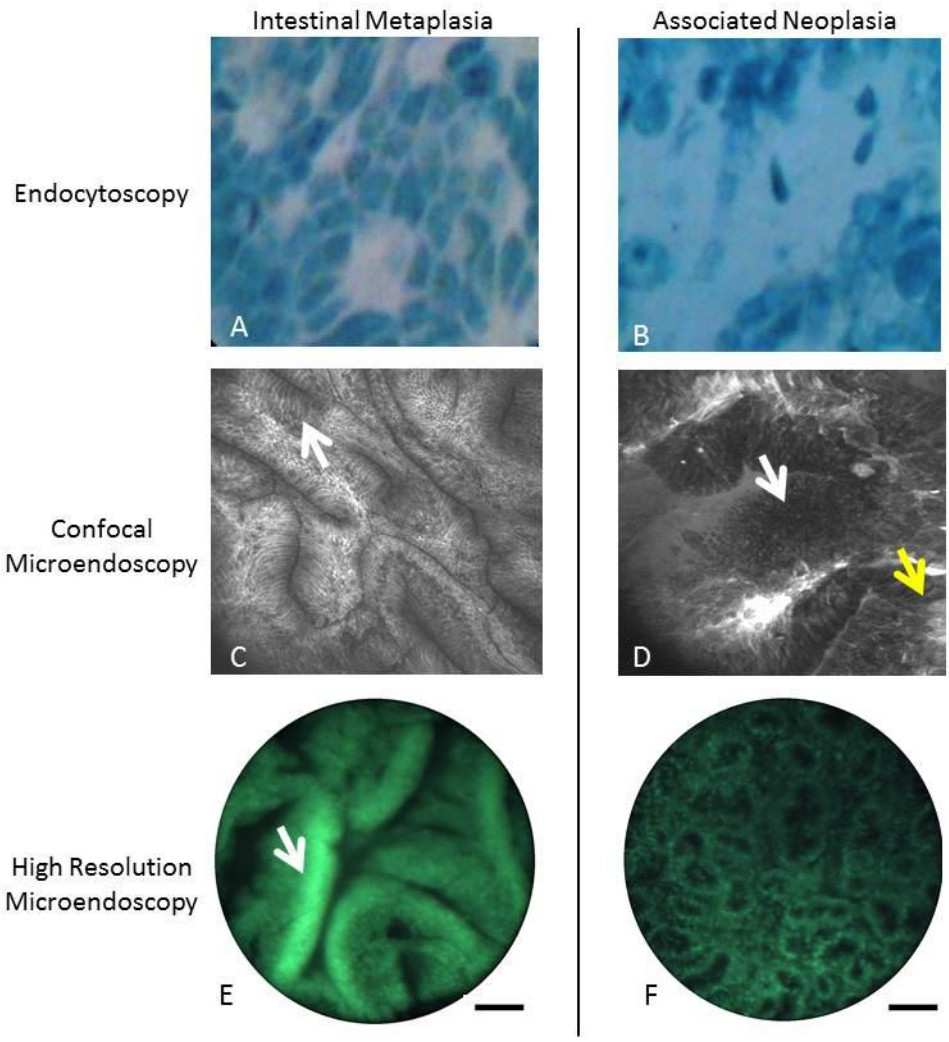

Figure 2-3: Images representing intestinal metaplasia and neoplasia collected using endocytoscopy (A,B)[45], confocal microendoscopy (C,D)[9], and high resolution microendoscopy (E,F)[54]. Topically applied methylene blue is used in endocytoscopy to highlight nuclear changes (A-B). In metaplasia (A), nuclei appear organized and regular; this is in stark contrast to neoplasia (B) where nuclei appear pleomorphic. Both images were taken using 1125x magnification. Confocal images were taken using intravenous fluorescein to enhance contrast of sub-epithelial capillaries (C-D). For intestinal metaplasia (C), confocal microendoscopy allows visualization of mucin-containing goblet cells (white arrow). For Barrett's-associated neoplasia (B), cells are irregularly oriented (white arrow) and malignant invasion of the lamina propria can be seen (yellow arrow). Confocal images are 500x500 µm. High resolution

microendoscopy uses proflavine for contrast enhancement, highlighting changes in glandular and nuclear patterns (E-F). High resolution images are 750 μm in diameter.

Confocal microendoscopy (CME) images subsurface tissue structure with high resolution by using a spatial filter to reduce the background signal produced by scattered out-of-focus light, producing images with 1-2 μm spatial resolution. While CME images can be generated either in reflectance mode or fluorescence mode, in the context of esophageal imaging, fluorescence CME has been primarily used. Since tissue autofluorescence is weak, typically fluorescent contrast agents are used to generate image contrast in CME. Kiesslich and researchers conducted a 63 patient study in Germany using an endoscope which incorporates both standard WLE and confocal microscopy; fluorescein (10%) was administered intravenously to generate vascular contrast. Sub-epithelial capillaries located in the upper and deeper layers of the lamina propria were identified due to fluorescein contrast. Leakage of fluorescein due to irregular capillary formation indicated neoplastic areas (Figure 2-3, second row). Indeed due to these irregularities, neoplasia could be detected with a sensitivity and specificity of 94% and 98% respectively[9]. In a prospective, randomized, double-blind, controlled, cross-over study with 39 patients using the same system, CME with targeted biopsy was shown to not only be accurate, but to nearly double the diagnostic yield of collected biopsies. In examining the biopsies identified by standard four-quadrant biopsies and the biopsies identified by CME, there was no statistically significant difference in detection of neoplasia between the two techniques[55]. However, although accuracy and diagnostic yield is impressive, the high cost may limit this technology to tertiary care centers.

A fiber-bundle, probe-based confocal system which can be passed through the instrument channel of any standard endoscope was used in a 38 patient study by Pohl and other researchers. A major benefit of this technology is its adaptability to existing endoscopes. This system also requires exogenous contrast; fluorescein was administered intravenously. The sensitivity and specificity of the two study endoscopists were 75% and 89% and 75% and 91%, respectively. They concluded that the confocal fiber probe showed a high negative predictive value for detecting unapparent neoplasia in BE, however sensitivity was not ideal[46].

An alternative approach to high resolution fluorescence imaging uses a coherent fiber bundle placed in direct contrast with the surface of tissue labeled with fluorescent dyes to yield high resolution images revealing sub-cellular structure (Figure 2-3, last row). This low-cost alternative to confocal imaging may be suited for large-scale surveillance outside of tertiary care centers. In a small pilot study of 9 patients, with topical proflavine for contrast enhancement of cell nuclei, researchers achieved a sensitivity and specificity of 87% and 85% using fluorescence microendoscopy[56].

2.5.4 Contrast Enhancement

As optical imaging technology continues to advance, the concurrent development of appropriate contrast agents that target bio-markers of neoplasia is crucial. Two general classes of optical contrast agents have been explored to improve image contrast: vital dyes and targeted contrast agents. Absorbing or fluorescent dyes which have an affinity for specific tissue constituents have often been used to improve the ability to visualize specific features associated with neoplasia. Often referred to as vital dyes, these stains

can help delineate features such as angiogenesis, leaky vasculature, and cell morphology. In contrast, targeted contrast agents use a high affinity probe molecule to target a specific molecular biomarker associated with neoplasia[57]. The probe molecule must be coupled to an optically active component, such as a fluorescent dye or scattering nanoparticle. Here we briefly review the utility of both types of contrast agents for improved detection of esophageal neoplasia.

Vital dyes can be utilized to better delineate morphologic changes associated with epithelial neoplasia. For example, the absorptive dye methylene blue localizes primarily in nuclei and can enhance visualization of nuclei when coupled with appropriate high resolution instrumentation. Using an endocytoscope, nuclear characteristics associated with neoplasia such as homogeneity, nuclear-to-cytoplasmic ratio, and organization can be resolved. However, since methylene blue dye has been known to induce oxidative damage of DNA when exposed to white light illumination[58], the risks of the contrast agent need to be weighed against benefits to determine potential use.

Fluorescent vital dyes may be advantageous due to the lack of interference with standard endoscopy. Fluorescein is a dye that is administered intravenously thus enhancing the view of vasculature in epithelial tissue. When coupled with confocal imaging, subsurface vasculature can be seen. The illumination and collection wavelengths of commercially available confocal systems correspond to fluorescein excitation (~490 nm) and emission (~520 nm) wavelengths[9, 46]. Acriflavine is another vital fluorescent dye that can be seen using similar excitation (~450 nm) and emission (~510 nm) wavelengths. Acriflavine stains cell nuclei, highlighting nuclear

characteristics such as size, shape, and spacing and has been used previously in vivo for GI imaging[59].

Targeted contrast agents serve as beacons that signal specific molecular events associated with precancer formation. The benefit of targeted agents is the potential to achieve a high signal to background ratio by virtue of selective binding to a molecular target. Lu and researchers used a phage display library with ~$2.8x10^9$ unique sequences to select a cancer-specific peptide. The library was biopanned against three cultured human esophageal cell types: adenocarcinoma, metaplasia, and normal to identify a peptide with specificity for the adenocarcinoma cell line. They used the selected peptide labeled with FITC to image Barrett's associated neoplasia in vivo. The agent was topically applied and imaged with a concurrently developed prototype fluorescence endoscope. Initial results showed a significant increase in binding to Barrett's-associated neoplasia over Barrett's alone when imaged with widefield fluorescence imaging (Figure 2-4)[10]. In a different study, Hsiung and colleagues fluorescently labeled a high affinity heptapeptide sequence selected with similar phage display techniques for the colon and were able to differentiate dysplastic from non-dysplastic colonic crypts using confocal imaging[60]. In both these of these cases, the topically applied contrast agent was incubated in vivo for a short period of time before the unbound agent was washed off to reduce non-specific signal. While the excitation and emission wavelengths of these agents correspond well with commercially available confocal endoscopes, another important advantage demonstrated by these studies is the ability to image these agents with both widefield fluorescence and CME.

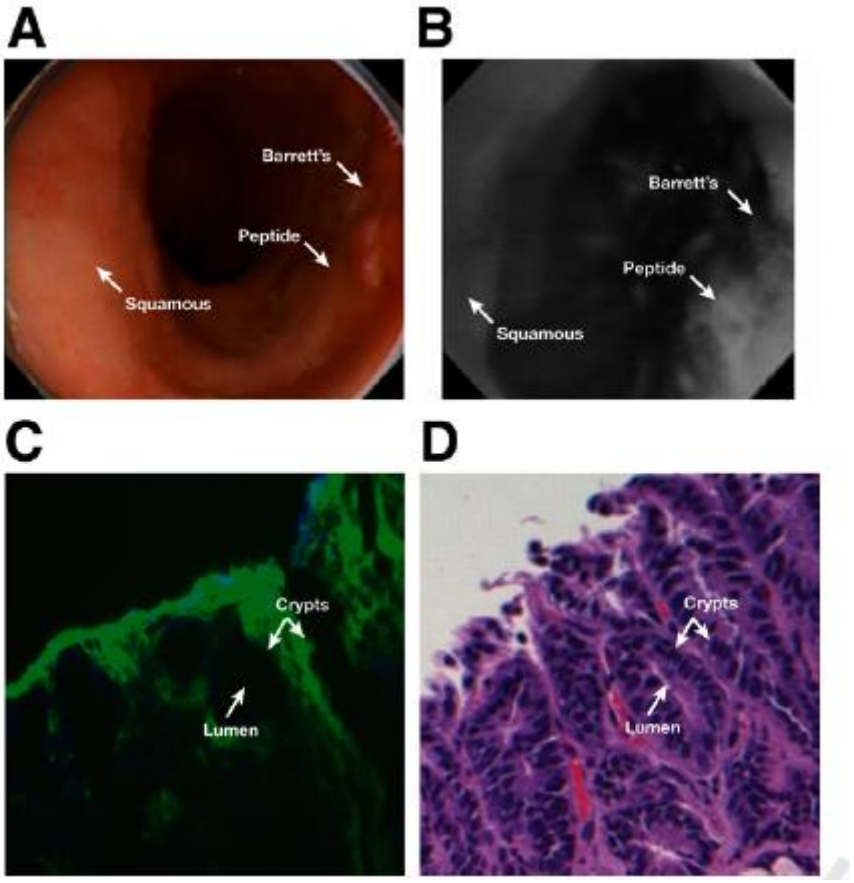

Figure 2-4: In vivo localization of contrast agent localized to a neoplasia region visualized using widefield fluorescence endoscopy. White light endoscopic image (A) shows no evidence of lesion. Topical administration of peptide-targeted fluorescent dye reveals neoplastic area (B)[10]. Targeted neoplastic crypts seen with fluorescence microscopy (C) and corresponding histology (D) [61].

2.6 Discussion

Recent advances in imaging technologies afford visualization of endogenous optical alterations associated with GI neoplasia. NBI shows contrast associated with light absorption due to hemoglobin. High sensitivity and specificity is cited in studies using this technology, however some indicate that there is no significant difference between contrast associated with NBI imaging and HD-WLE, which is becoming increasingly

available. Autofluorescence imaging measures the signal decrease associated with loss of stromal collagen fluorescence and increased fluorescence associated with porphyrin. Various studies evaluating AFI have cited high sensitivity, but a high rate of false positives. The combination of NBI and autofluorescence imaging may afford better sensitivity and specificity rates; NBI has shown to reduce the number of false positives identified by AFI from 81% to 26%[42].

High resolution imaging will also play a major role in improving detection, affording clinicians an 'optical biopsy' of epithelial tissue. Confocal imaging allows for optical sectioning of up to 250 μm deep and coupled with vital dyes such as fluorescein allows evaluation of vascular regularity. High sensitivity and specificity have been cited; however, high cost and the limited field of view remain concerns. Endocytoscopy allows for histology-like reflectance imaging where nuclei appear dark blue due to methylene blue contrast. The technology achieves high specificity however the dye has been shown to interfere with white light imaging and image quality has been an issue. When combined with widefield imaging techniques, high resolution technologies may reduce false positive rates if coupled with the appropriate contrast agent.

Unfortunately, despite all the advances in optical imaging methods, there are still lesions that are only detected by standard four quadrant biopsies. Improvements in contrast agents are also needed to facilitate better early detection. A number of contrast agents are commercially available, primarily vital dyes such as fluorescein and methylene blue. However, recent in vivo testing of optically labeled high affinity peptide and heptapeptide sequences has paved the way for molecule specific contrast agents for GI neoplasias[10, 60]. While advances have translated the use of vital dyes and contrast agents

in vivo, there are still many unanswered questions regarding their ultimate clinical role. What will be the ideal mechanism of delivery? How will the development of in vivo imaging technologies accommodate the use of new contrast agents? And finally, will the addition of contrast agents create a multifaceted platform that can improve overall accuracy of surveillance?

While these new imaging technologies may be appropriate for tertiary care centers, additional considerations are necessary as these technologies are disseminated more widely. A potential solution may be a lower cost technology such as the high resolution microscope or an adaptable technology such as the confocal miniprobe with topically applied contrast agents, both of which have been cited to achieve reasonably high sensitivity and specificity. Objective, quantitative algorithms will also be important since clinicians outside of tertiary care clinics may not be as familiar with optical characteristics of abnormal lesions detected with new technologies. Various groups have begun work in this area however larger trials will need to be conducted to determine effectiveness[44, 56].

At this point, larger scale studies are needed to test the combination of multi-scale, multi-modal technologies against the current surveillance standard, and to test whether the use of contrast agent is advantageous. This multifaceted optical approach has the potential to improve surveillance in BE; once validated it has the potential to utilized for surveillance of neoplasia along the GI tract and can be further developed for screening.

CHAPTER 3: VITAL-DYE ENHANCED FLUORESCENCE IMAGING OF GASTROINTESTINAL MUCOSA: METAPLASIA, NEOPLASIA, INFLAMMATION

3.1 Introduction

In the surveillance of both Barrett's esophagus (BE) and Inflammatory Bowel Disease (IBD), dysplasia is often focal, flat and indistinguishable from non-dysplastic mucosa[5, 62]. Current white-light endoscopic platforms lack the resolution required to accurately identify dysplasia. As a result, over half of such lesions can be missed [5, 63, 64].

Confocal endomicroscopy has revolutionized endoscopy by offering sub-cellular images of gastrointestinal epithelium [65-67]. However, the increase in spatial resolution comes at the expense of decreased field of view, leaving large areas unsurveyed. Therefore, there exists a need for multi-scale endoscopy platforms that use widefield imaging to better direct placement of high-resolution fluorescent imaging devices, including the recently described high-resolution microendoscope, an inexpensive (<$5000), probe-based technology for imaging histologic features in vivo [54, 68, 69].

Our goal in this *ex vivo* feasibility study was to evaluate the feasibility of a single topical contrast agent (0.01% proflavine hemisulfate) using a prototype multi-scale, fluorescence-based platform using both widefield and high-resolution imaging of the esophagus and colon. Resulting images were compared to standard H&E-stained histopathology to determine what morphologic features associated with metaplasia, neoplasia, and inflammation can be visualized using this novel approach. These criteria

may be used in future *in vivo* studies to determine its impact on diagnostic accuracy and margin determination.

3.2 Materials and Methods

3.2.1 Specimen Preparation and Imaging

Patients at UT MD Anderson Cancer Center and Mount Sinai Medical Center undergoing endoscopic mucosal resection (EMR) or surgery for adenocarcinoma or intractable IBD gave written informed consent to participate.

Immediately following resection, the mucosal surface of each specimen was rinsed with saline and imaged under white light illumination. Abnormal and normal areas were identified by the study pathologist based on appearance; borders of these regions were marked on the white light image. Proflavine hemisulfate (0.01% w/v), which has been shown to localize in cell nuclei[54, 70], was applied to the mucosal surface for 30 seconds. Excess proflavine was removed with dry gauze.

Widefield fluorescence images of areas identified as grossly normal and abnormal were obtained using a multispectral digital microscope (MDM) [71]. High-resolution fluorescence images were subsequently obtained from areas imaged with the MDM using a high resolution microendoscope (HRME)[54, 68]. In an effort to reduce sampling error, a dot of India ink was placed at each area imaged with the HRME, fixed with acetic acid, and photographed. Since the ink spread to ~2-4 mm in diameter and the field of view of the HRME is 750 μm, the photograph guided the approximation of image sites on large resected specimens; necessary to facilitate registration between widefield imaging, high resolution imaging, and subsequent histopathologic evaluation.

The specimen was then fixed in formalin and submitted for standard histopathologic analysis; vertical cross-sections were examined to grade and verify presence of disease. The study pathologist, blinded to the image results, assigned diagnoses to histologic sections of inked areas using standard histologic criteria.

3.2.2 Instrumentation

The MDM, a surgical microscope modified for fluorescence imaging, has been described previously [71]. In this study, widefield images were obtained at 450 nm excitation, and fluorescence was collected through a 515 nm long-pass filter. The field of view of the MDM is 2.5 cm, with a spatial resolution of 50-100 um. The average illumination intensity was 2.14 mW/cm^2 and images were acquired with a 1 s integration time.

The HRME system has also been described [68]. Illumination was provided via a 450 nm LED coupled to a coherent fiber-optic bundle. Fluorescence collected by the bundle while in contact with the tissue was delivered to a CCD camera through a 490 nm long pass filter. The field of view of the HRME is 750 μm in diameter and the spatial resolution is 4.5 microns.

3.2.3 Image Assessment

Fluorescence images were qualitatively compared to histology images. Features evaluated in widefield images included the presence or absence of glandular epithelium in the esophagus (Barrett's metaplasia), and the architectural characteristics of the colonic epithelium (shape, size, and spatial distribution of crypts, presence/absence of glandular

distortion). Features evaluated in high-resolution images included nuclear size, density, orientation and homogeneity as well as the composition of the lamina propria.

3.3 Results

Resected specimens from 15 patients were evaluated, including; 9 EMRs and 2 esophagectomies from patients with Barrett's-associated neoplasia, 3 colectomies from patients with colorectal adenocarcinoma, and 3 colectomies from patients with IBD (2 with ulcerative colitis and 1 with Crohn's disease). Images were obtained from 36 individual histologically-verified sites. Each figure shows a white light image, a widefield proflavine-fluorescence image, corresponding high resolution fluorescence image, and pathology. The inked area is approximated by a circle in each of the widefield proflavine-fluorescence images.

Figure 3-1 shows images of esophageal mucosa. The top region of the white light image (Figure 3-1A) depicts an area of normal esophageal squamous mucosa. The corresponding area in the widefield proflavine-fluorescence image (Figure 3-1B) shows homogeneous fluorescence, with uniform intensity except for some apparent proflavine pooling in tissue folds (arrow). A representative high-resolution image of the squamous region (Figure 3-1C) exhibits hexagonally-shaped cells with bright, small, round, evenly-spaced nuclei, which were consistently observed. These features are apparent in the corresponding histology section of the epithelial surface (Figure 3-1D).

During white light imaging, the glandular architecture of BE is difficult to visualize. In contrast, during widefield proflavine-fluorescence imaging, the glandular architecture is easily appreciated (Figure 3-1B). A high-resolution image (Figure 3-1E)

obtained from the circled area shows glands with central dark lumens, lined by evenly spaced cells with small, regular and polarized nuclei. Similar features are seen in histologic sections from the corresponding area (Figure 3-1F), which include metaplastic columnar epithelium with intestinal-type goblet cells.

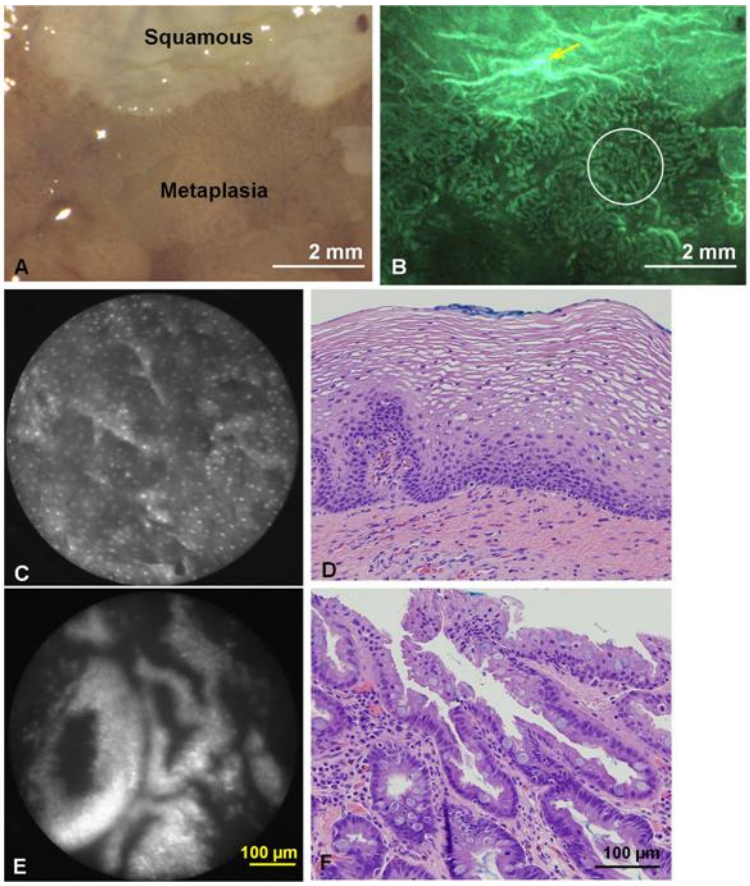

Figure 3-1. White-light image of squamo-columnar junction is shown (A). Widefield proflavine-fluorescence image (B) shows glandular detail in the Barrett's region. High-resolution fluorescence image of squamous mucosa is shown (C) with corresponding histopathology (D). High-resolution image of BE from area, indicated in (B), shows large glands typical of intestinal metaplasia (E). Corresponding histopathology is shown in (F).

Figure 3-2 shows images of Barrett's-associated neoplastic changes. Figure 3-2A shows a standard, white-light image of an area of BE with high grade dysplasia (HGD)

and adenocarcinoma. In the corresponding widefield proflavine-fluorescence image (Figure 3-2B), glands appear irregular compared to the glands associated with BE. Note the visible India ink (arrow). The high-resolution image (Figure 3-2C) obtained from the circled area shows glands that are smaller, more irregular in shape and irregularly spaced, compared to the glands in non-neoplastic BE. In addition, nuclei are more numerous, crowded, pleomorphic, and have lost polarity (arrow), mirroring the appearance of HGD and adenocarcinoma seen in the corresponding histologic section (Figure 3-2D).

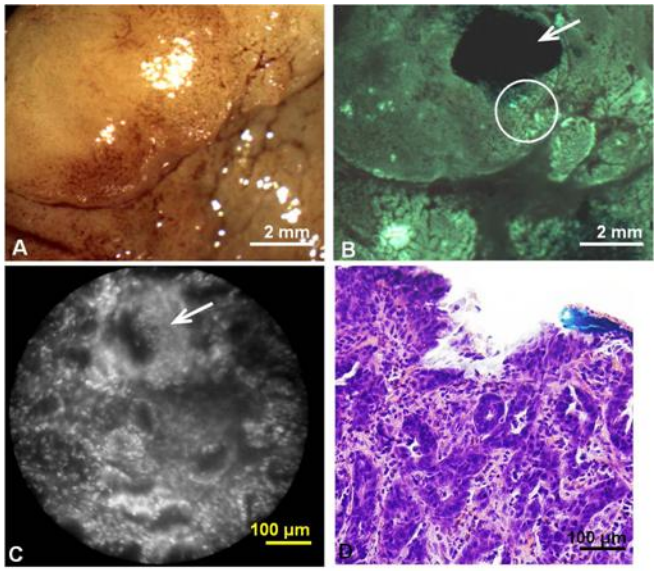

Figure 3-2. White-light image of Barrett's-associated neoplasia is shown (A). Widefield proflavine-fluorescence image depicts irregular glands (B). High-resolution fluorescence image from area indicated in (B) shows areas of nuclear crowding (arrow) (C). Corresponding histopathology is shown (D).

Figure 3-3 shows images of normal colonic mucosa. Figure 3-3A depicts normal colonic mucosa under white light illumination. The glandular pattern of colonic mucosa

is more apparent with widefield proflavine-fluorescence imaging (Figure 3-3B). The corresponding high-resolution image (Figure 3-3C) from the circled region is characterized by evenly distributed, round tubular structures of similar shape and diameter (yellow arrow) with basally oriented, small, fluorescent nuclei (white arrow), features that correlate well with the transverse histologic section from the same area (Figure 3-3D).

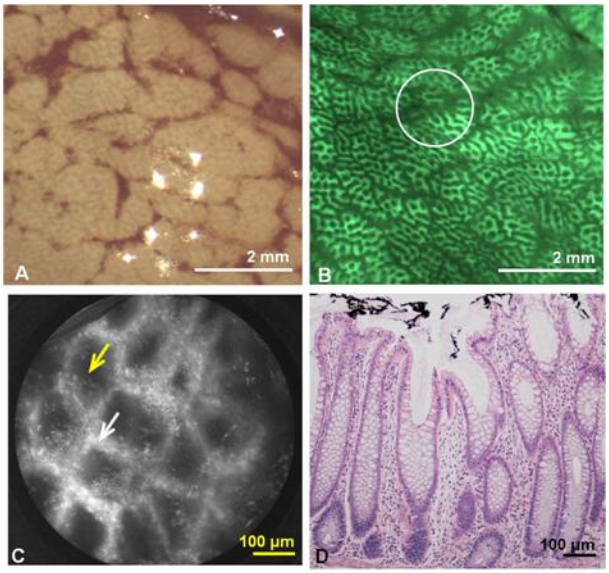

Figure 3-3. White-light image normal colonic mucosa is shown (A). Widefield proflavine-fluorescence image shows evenly-spaced colonic crypts (B). High-resolution fluorescence image from area in (B) shows evenly spaced tubular structures (yellow arrow) and polarized nuclei at the crypt edges (white arrow) (C). Corresponding histopathology is shown (D).

Figure 3-4 shows images from the edge of colonic dysplasia. Under white light (Figure 3-4A) colonic ridges are visualized as well as the transition to an area of irregular growth. With proflavine-enhanced widefield imaging (Figure 3-4B), dysplastic glandular structures appear larger than normal colonic crypts and are not as evenly spaced. In the

corresponding high-resolution fluorescence imaging (Figure 3-4C) of the circled area, glands appear elongated and irregular (yellow arrow) with apparent nuclear crowding (white arrow). These features correspond to the dysplastic colonic mucosa in the histologic section (Figure 3-4D).

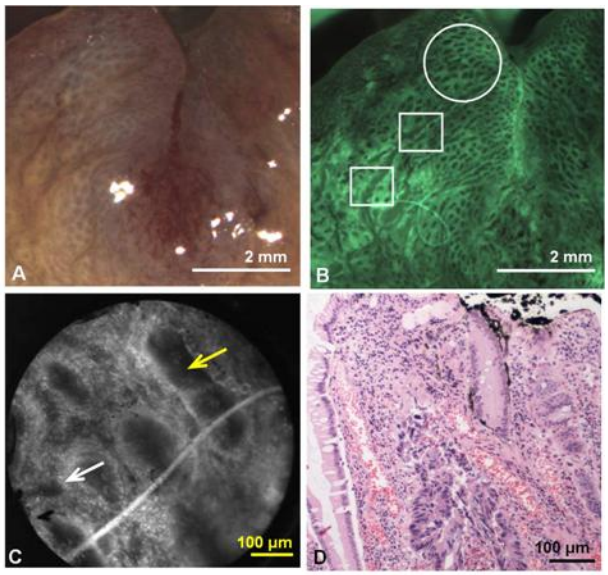

Figure 3-4. White-light image dysplastic colonic mucosa is shown (A). Widefield proflavine-fluorescence image shows unevenly-spaced colonic crypts (B). The brightness of the lamina propria is variable (white boxes). High-resolution proflavine-fluorescence image from inked area indicated in (B) shows unevenly spaced tubular structures (yellow arrow) and areas of crowded nuclei (white arrow) (C). Corresponding histopathology is shown (D).

Figure 3-5 shows images of severe dysplasia. Under white light (Figure 3-5A), the surface of a lesion can be appreciated, but without much glandular detail. In the corresponding widefield proflavine-fluorescence image (Figure 3-5B), barely-visible glands appear distorted. High-resolution imaging (Figure 3-5C) of the region indicated by the circle reveals irregular and unevenly spaced glandular structures (yellow arrow)

composed of crowded cells with enlarged, fluorescent nuclei that are heterogeneously oriented (white arrow), features that correspond to the diagnosis of HGD seen in the corresponding histologic section (Figure 3-5D).

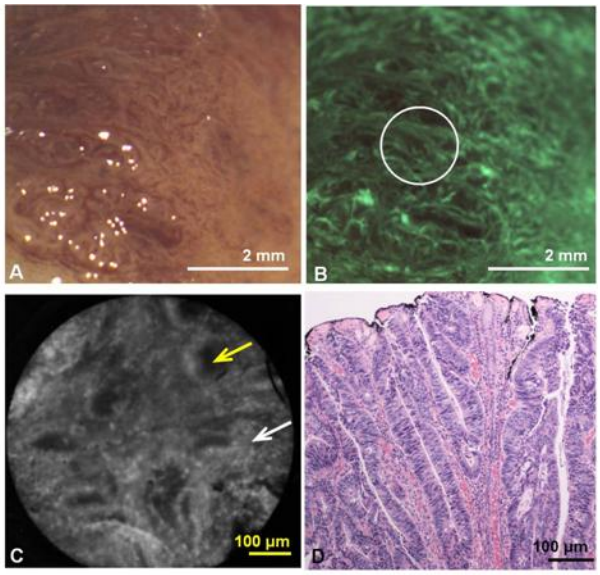

Figure 3-5: White-light image of severely dysplastic colonic mucosa with sub-surface adenocarcinoma is shown (A). Widefield proflavine-fluorescence image depicts irregularly shaped colonic crypts (B). High-resolution fluorescence image from area indicated in (B) shows irregularly shaped, unevenly spaced tubular structures (yellow arrow) and areas of crowded nuclei (white arrow) (C). Corresponding histopathology is shown (D).

Figure 3-6 shows images from an area of invasive adenocarcinoma. A mass is visible under white light (Figure 3-6A) and poorly-formed glandular structures can be seen during widefield proflavine-fluorescence imaging (Figure 3-6B). The high-resolution image (Figure 3-6C) of the circled area reveals highly irregular and uneven tubular structures lined by enlarged, fluorescent nuclei lacking orientation and polarity. The intervening stroma appears crowded, contributing to the visible increase in

fluorescence. These features mirror the appearance of dysplastic glands amidst desmoplastic stromal reaction in the corresponding histologic section (Figure 3-6D), which are diagnostic of invasive colorectal adenocarcinoma.

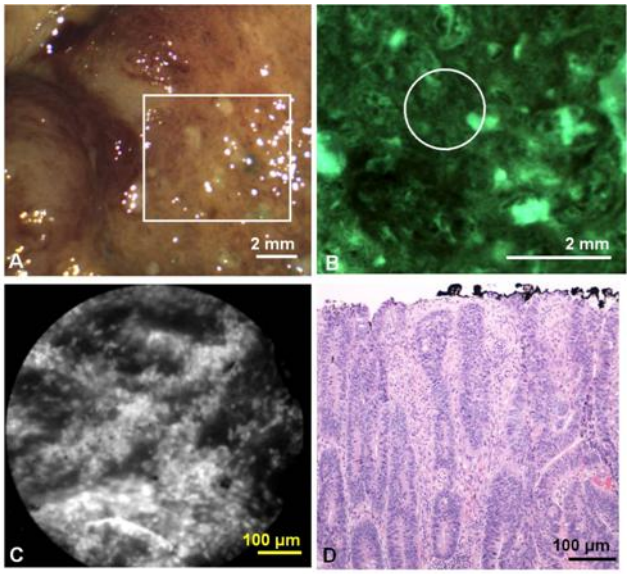

Figure 3-6. White-light image of invasive adenocarcinoma is shown (A). Widefield proflavine-fluorescence image from area indicated in (A) depicts loss of regular glandular architecture (B). High-resolution fluorescence image from area indicated in (B) shows areas of dense nuclei (C). Corresponding histopathology is shown (D).

Figure 3-7 shows images depicting mildly-active IBD. In the white-light image (Figure 3-7A) glandular detail is not easily appreciated. However, in the fluorescence images (Figure 3-7B and 3-7C), glands appear distorted and slightly more irregular in spacing than in normal colonic mucosa and in quiescent IBD (not shown). The increase in glandular distortion, cryptitis (arrow), and the expanded lamina propria seen in the high-resolution image are consistent with the abnormalities seen in the corresponding

histologic section showing active colitis (Figure 3-7D). This patient was known to have ulcerative colitis clinically.

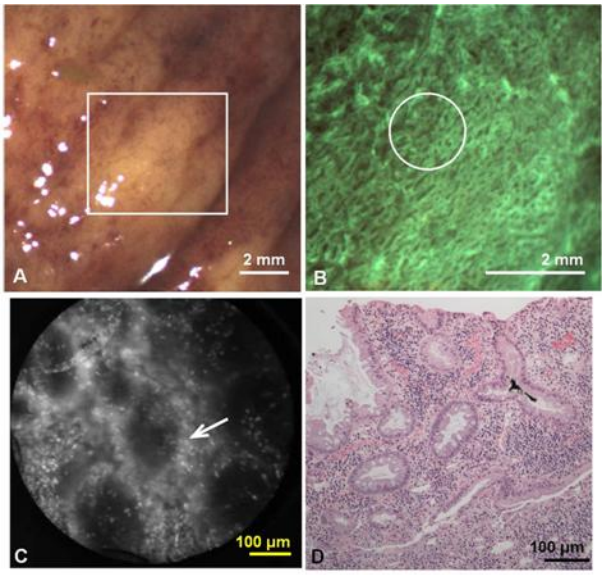

Figure 3-7. White-light image of an area of mildy active IBD is shown (A). Widefield proflavine-fluorescence image from area indicated in (A) depicts an irregular glandular pattern (B). High-resolution fluorescence image from area indicated in (B) shows an increase in distorted glands with cryptitis (arrow) and expanded lamina propria (C). Corresponding histopathology of active colitis is shown (D).

Figure 3-8 shows an example of severely-active IBD. In the white-light image (Figure 3-8A), the presence of inflammation and ulceration make glands difficult to visualize. In the widefield proflavine-fluorescence image (Figure 3-8B) the glands appear irregular and disorganized. The high-resolution image obtained from the circled region (Figure 3-8C) shows a dense population of fluorescent inflammatory cells. These features correspond to the ulcer bed seen in the corresponding histologic section showing severe colitis (Figure 3-8D), with chronic inflammatory cells in the lamina propria and

extensive gland dropout. This patient was known to have active Crohn's disease clinically.

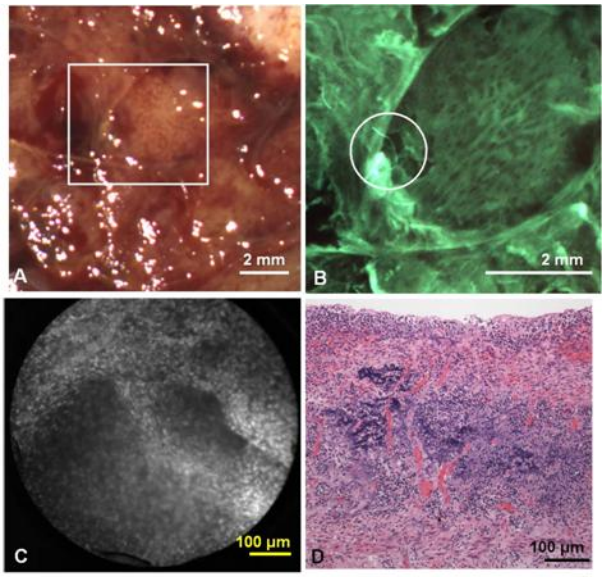

Figure 3-8. White-light image of an area of severely active IBD with ulcer is shown (A). Widefield proflavine-fluorescence image from area indicated in (A) depicts glandular irregularity (B). High-resolution fluorescence image from area indicated in (B) shows a dense nuclear presence in the lamina propria (C). Corresponding histopathology of severe colitis is shown (D).

Tables 3-1 to 3-3 summarize the morphologic features consistently observed in widefield and high-resolution imaging in Barrett's-associated neoplasia, colonic neoplasia, and IBD. Following application of proflavine, widefield fluorescence images consistently identify larger-scale architectural differences in glandular size, shape, and distribution, while high-resolution images consistently allows assessment of nuclear crowding.

Table 3-1: Image features present in proflavine-enhanced widefield and high resolution imaging of normal esophagus, Barrett's metaplasia, dysplasia, and adenocarcinoma

	Widefield Imaging Features		High Resolution Imaging Features	
Normal Esophageal Mucosa	No glands present	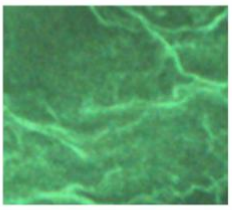	Evenly spaced, homogeneous nuclei	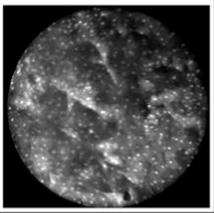
Barrett's Metaplasia	Elongated and intact glands	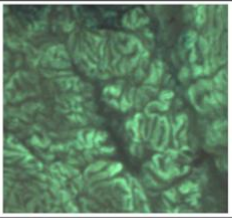	Intact glands Basal nuclei	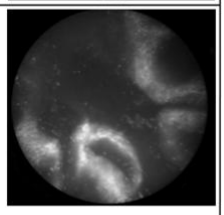
Dysplasia	Crowded and heterogeneous glands	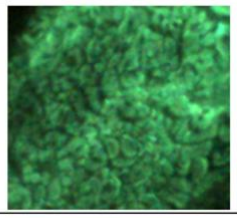	Crowded and distorted glands Nuclear crowding, enlargement and pleomorphism Loss of nuclear polarity (with high grade dysplasia)	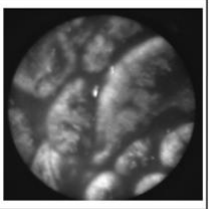
Adeno-carcinoma	Effacement of glandular architecture	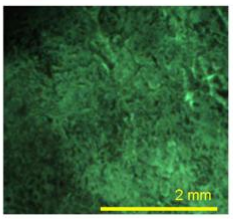	Irregular glands Invasion of lamina propria (stromal reaction)	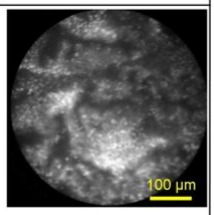

Table 3-2: Image features present in proflavine-enhanced widefield and high resolution imaging of normal colon, dysplasia, and adenocarcinoma

	Widefield Imaging Features		High Resolution Imaging Features	
Normal Colon Mucosa	Regular, intact tubular glandular pattern	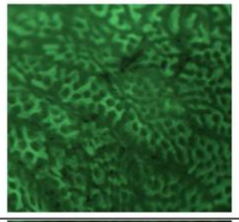	Uniform glands Regular, small, basal nuclei	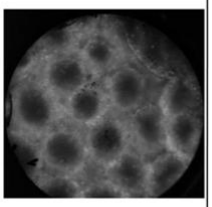
Dysplasia	Irregular, heterogeneous glands	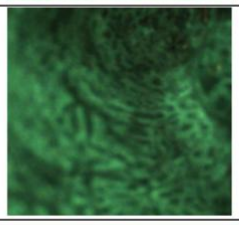	Distorted glands Nuclear crowding, enlargement and pleomorphism Loss of nuclear polarity	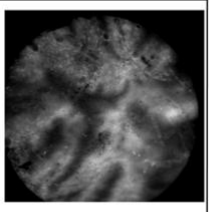
Adeno-carcinoma	Effacement of glandular architecture	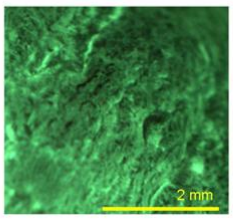	Increasingly irregular glands Invasion of lamina propria Stromal reaction	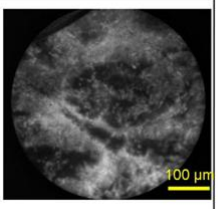

Table 3-3: Image features present in proflavine-enhanced widefield and high resolution imaging of mildly active inflammatory bowel disease (IBD) and severely active IBD.

	Widefield Imaging Features		High Resolution Imaging Features	
Mildly Active IBD	Irregular glands	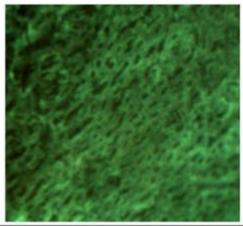	Architectural distortion and cryptitis Expanded, crowded lamina propria	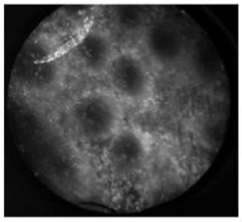
Severely Active IBD	Infrequent, heterogeneous glands	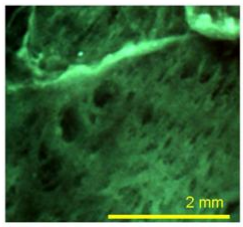	Severely atrophic glands Very expanded, crowded lamina propria	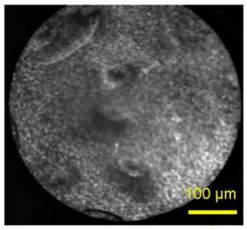

3.4 Discussion

This ex vivo pilot study demonstrates the technical feasibility of a new multi-scale imaging approach, in which sequential widefield and high-resolution fluorescence imaging is performed using a single fluorescent vital dye. Results indicate that multi-scale, proflavine-enhanced, fluorescence imaging can characterize glandular and cellular changes associated with metaplasia, neoplasia, and inflammation in gastrointestinal (GI) mucosa. Features visible with both modalities correlate well with those observed during standard histopathologic evaluation.

The results of this study provide a rationale to evaluate this multi-scale surveillance technique in vivo; further studies are necessary to determine whether similar conclusions can be drawn during endoscopic imaging of proflavine. Moreover, larger sample sizes are required to assess the sensitivity and specificity of this approach. Despite these limitations, this study suggests that multi-scale fluorescence imaging has the potential to address some of the limitations of existing widefield and high-resolution endoscopic platforms.

Existing widefield endoscopic imaging techniques are emerging as promising ways to improve early detection of precancerous lesions by scanning over a large surface area. For example, autofluorescence imaging detects changes in stromal fluorescence with high sensitivity; however, it is limited by low specificity[7, 8, 64]. Narrowband imaging detects differences in vascular density, however it only indirectly visualizes glandular architecture. In the imaging platform described here, widefield fluorescence imaging is

used to provide direct visualization of glandular morphology, providing valuable information on alterations that are visible in H&E-stained tissue sections.

The relatively poor specificity of widefield imaging motivates the need for high-resolution interrogation at the cellular level. Confocal imaging, using IV fluorescein to enhance imaging of vasculature, is the most accurate high-resolution imaging technique to date[9, 65]. Though its use in vivo is well established, cost may prevent it from being used outside tertiary care centers. Its published accuracy requires IV administration of fluorescein, further complicating the potential for widespread use. High-resolution imaging with topical proflavine can achieve sub-cellular resolution with less expensive instrumentation [54]. Topical proflavine stains nuclei, allowing direct visualization of relevant histologic features (e.g., nuclear density) associated with neoplasia. Though other promising technologies such as endocytoscopy, a probe-based technology used in conjunction with methylene blue, also allow direct visualization of histologic features [72, 73], by using the HRME with a fluorescent dye, imaging can be accomplished without having the dye interfere with standard white light imaging.

Using proflavine as a contrast agent for both widefield and high-resolution techniques provides an advantage over existing platforms which require different contrast agents for sequential imaging (e.q., methylene blue chromoendoscopy followed by confocal microendoscopy with fluorescein) [66]. Proflavine is a component of acriflavine, which has been used in vivo in GI imaging studies [59]. It is a major component of triple dye, which is widely used as an antiseptic regimen in the care of newborn umbilical cords [74]; our study concentration is ten times less than the concentration in triple dye. These

precedents, coupled with promising initial results support future in vivo use of proflavine for multi-scale imaging of GI mucosa.

Widefield fluorescence imaging of proflavine would enhance the ability of gastroenterologists to examine glandular architecture over large areas of the GI mucosa. Suspicious areas would then be interrogated further with high-resolution imaging using the same contrast agent to reveal sub-cellular changes associated with nuclear morphology. This multi-scale approach may increase sampling efficiency, enhance dysplasia detection and improve margin determination.

CHAPTER 4: MODULAR VIDEO ENDOSCOPY FOR IN VIVO DETECTION OF BARRETT'S-ASSOCIATED NEOPLASIA

4.1 Introduction

The incidence of esophageal adenocarcinoma (EAC) has dramatically increased over the last four decades; since 1975, there has been a 463% increase in men and a 335% increase in women [2]. This is of particular concern since EAC is associated with a very low five year survival rate (12%) due primarily to diagnosis at a late stage [3]. When diagnosed early, the five year survival rate of EAC is 81%, but only a small fraction of esophageal cancers are detected at this stage [12].

Patients with Barrett's esophagus (BE), a condition caused by chronic acid damage to the esophagus over time, are known to be at an increased risk of developing EAC [14, 75]. Because of the high likelihood of developing dysplasia and cancer, patients with BE are recommended to undergo regular surveillance at designated intervals [76]. During the standard surveillance procedure, white light examination is used to scan the entire Barrett's segment for visible abnormalities, such as nodules and ulcerations. Since many neoplastic lesions can appear flat and indistinguishable from non-dysplastic mucosa under white light imaging, random four quadrant biopsies are taken every 1-2 cm along the Barrett's segment [76]. Unfortunately, this method has been shown to miss as many as 57% of dysplasias and cancer [5]. Thus, there is an important need for new techniques that may improve the early diagnosis of EAC and its precursors.

In an attempt to improve image contrast and diagnostic yield, a number of widefield endoscopic imaging modalities have been developed. Autofluorescence

imaging (AFI) is sensitive to changes in stromal collagen fluorescence and increased epithelial thickness [77]; neoplasia is associated with loss of detected autofluorescence intensity. AFI has been shown to identify abnormal lesions with 91% sensitivity [7, 8]. However, inflammatory lesions can also demonstrate loss of fluorescence and the specificity of AFI can be as low as 43% [7]; other studies have also shown high rates of false positives associated with AFI [42]. Narrowband reflectance imaging uses narrow bands of blue and green illumination to enhance vascular content, indirectly enhancing the appearance of the glandular pit pattern achieving a sensitivity range of 89-100% and achieving a specificity range of 76-98% for detecting neoplasia [40, 41, 78]. Moreover, reported specificities for detecting BE are as low as 65% [79]. Though both technologies enhance mucosal changes in different ways, signal differences have been shown to aid clinical interpretation of mucosal features [8, 42], however limitations associated with false positives reinforce the need for new imaging techniques.

Recent *ex vivo* studies suggest that two emerging widefield modalities have promise to improve the early recognition of esophageal neoplasia. In the first approach, cross polarized imaging (CPI), tissue is illuminated with linearly polarized white light and light re-emitted from the tissue surface is collected via a second linear polarizer whose axis of transmission is oriented orthogonally to that of the incident light. CPI preferentially collects light scattered from sub-surface tissue structures, thereby enhancing contrast of deeper blood vessels [80]. CPI has been shown in various organ sites to improve the identification of epithelial neoplasia [71, 81], though has yet to be implemented for *in vivo* endoscopic imaging.

In the second approach, vital dye-enhanced fluorescence imaging (VFI), a fluorescent dye is used to enhance tissue fluorescence. Proflavine hemisulfate, a fluorescent contrast agent, stains cell nuclei, enabling observation of relevant changes in epithelial architecture associated with neoplastic progression. Ex vivo studies of VFI and proflavine staining in gastrointestinal tissues have shown that the agent allows the evaluation of glandular architecture during widefield imaging [82].

While the utility of CPI and VFI have been demonstrated in other organ sites or using *ex vivo* specimens, evaluating their utility for *in vivo* esophageal cancer screening requires development of an upper GI endoscope capable of acquiring images in these modalities. Here, we describe the development and initial clinical evaluation of a multimodal digital endoscope (MVE) which incorporates WLI, CPI, and VFI modalities into one endoscope. We present images acquired with the MVE from an *ex vivo* esophageal specimen with pathologically confirmed disease, as well as in vivo images acquired during endoscopic assessment of a patient with Barrett's-associated neoplasia.

4.2 Materials and Methods

4.2.1 INSTRUMENTATION

The Modular Video Endoscope (MVE) shown in Fig. 4-1, was designed to acquire images in three different modalities: conventional white light imaging (WLI); cross-polarized imaging (CPI); and vital-dye fluorescence imaging (VFI). The MVE consists of a modified high definition (1280x1024 pixels) video processor (Pentax EPK-i), a standard upper GI video endoscope (Pentax EG-29901), and stainless steel modules attached to the distal tip of the endoscope containing necessary optical filters for

implementation of CPI or VFI. Each module is coupled to the distal tip with a medium sized, commercially-available endoscope cap (Barrx Medical Inc., Sunnyvale, CA, USA) shown in the right panel of Fig. 4-1. The custom-designed filter modules maintain use of the standard features of the endoscope during CPI and VFI imaging, including the forward water jet used for irrigation and the air/water nozzle used to clear debris from the field of view (FOV) of the CCD. The dimensions are shown in Fig. 4-2. In all three imaging modalities, the system is designed to be used at the standard working distance of the endoscope, ranging from 5 - 20 mm. A digital zoom feature allows additional magnification of up to 3x. The field of view depends on both the working distance and the digital magnification; at a typical working distance of 10 mm, the FOV ranges from 15 mm to 45 mm in diameter, with a resolution of approximately 50 microns. At the minimum working distance of 5 mm, the FOV ranges from 5 mm to 15 mm in diameter, with a resolution of approximately 25 microns.

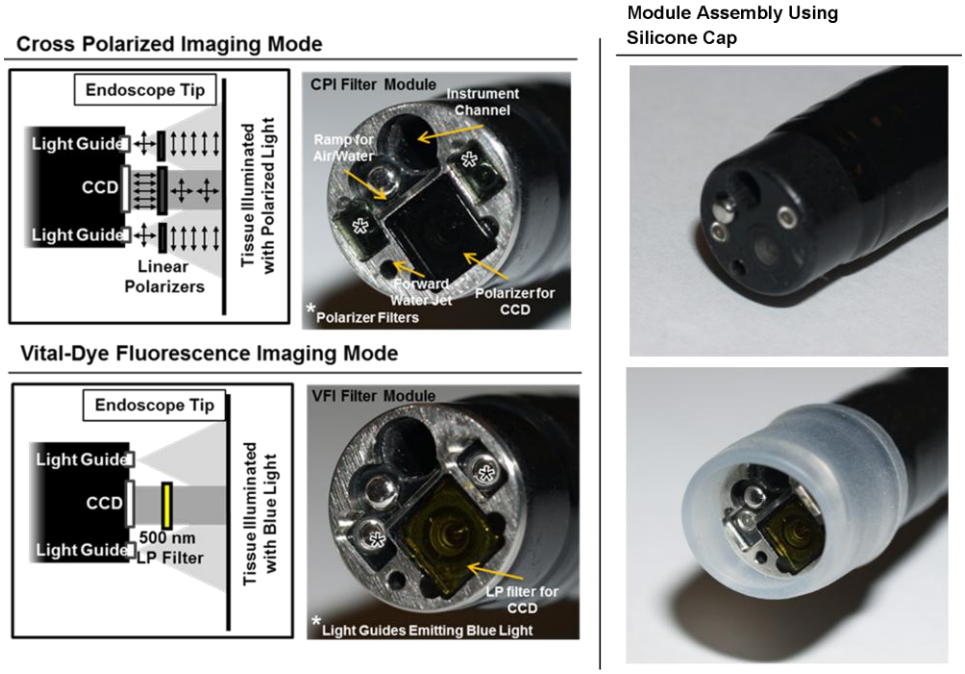

Figure 4-1. Top diagram illustrates the placement of linear polarizers in front of illumination light guides and CCD for implementation of cross polarized imaging (CPI). The image to the right of the CPI diagram shows the distal end of the endoscope tip with the CPI filter module in place. The bottom diagram illustrates the placement of the long pass filter in front of the CCD for implementation of vital-dye fluorescence imaging (VFI). The image to the right of the VFI diagram shows the distal end of the endoscope tip with the VFI filter module in place. In VFI mode, the light guides emit blue light from the laser diode. The panel on the right shows the endoscope tip (top) and module assembly (bottom) using the silicone cap.

4.2.1.1 Cross Polarized Imaging

In CPI, tissue is illuminated with linearly polarized white light, and images are acquired through a second linear polarizer oriented to transmit only reflected light with its axis of polarization oriented orthogonally to that of the illumination light. This serves both to reject specular reflection from the tissue surface, and enhance the appearance of sub-surface vasculature. The top row of Fig. 4-1 shows the module designed to adapt the standard endoscope for CPI imaging.

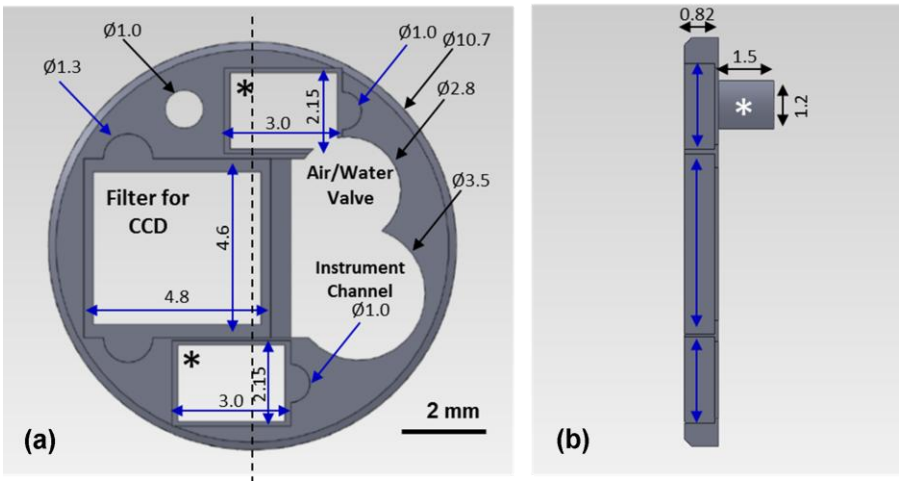

Figure 4-2. Front face of module (a) and right cross sectional profile (b) shown with dimensions (mm). Regions are labeled to indicate which

features on the endoscope tip the cuts correspond to. Black stars in (a) indicate extruded cuts created to accommodate illumination channels. Cross sectional profile (b) obtained from the dotted line in (a). Blue arrows indicate extruded cuts made for filters and epoxy. The protrusion (white star) in (b) indicates the channel for forward water jet. The protrusion was implemented to aid in alignment of the module and the endoscope tip.

To achieve CPI, white light from the endoscope light guides pass through linear polarizers (2.15 x 3.0 mm^2) contained in the cap, one in front of each end of the bifurcated light guide (indicated by the stars in the CPI filter module image of Fig. 4-1); accommodating the illumination channels that exist in the Pentax video endoscope. The module holds another linear polarizer (4.6 x 4.8 mm^2) in front of the CCD camera; the axis of this polarizer is oriented orthogonal to that of the illumination polarizers. These filters are fixed in the module using optically clear epoxy (Epo-Tek, Billerica, MA, USA). The filters are cut from HN22 polarizing sheets (Knight Optical Ltd., UK); the thickness of the film is 0.75 mm and the maximum transmission of two sheets orthogonally oriented is 0.001%. With the CPI module in place, at the center of the field of view the surface irradiance is approximately 3.6 mW/cm^2 at 5 mm and approximately 1.9 mW/cm^2 at 10 mm; both typical working distances for imaging.

4.2.1.2 Vital-Dye Fluorescence Imaging

In VFI mode, tissue is illuminated with quasi-monochromatic light designed to excite fluorescence; a long-pass filter is placed in front of the CCD camera to reject specular reflection at the excitation wavelength and allow collection of resulting fluorescence. The VFI module was designed specifically to image fluorescence

following topical application of the fluorescent antiseptic, proflavine hemisulfate which has been shown to localize in cell nuclei. The agent has an absorption maximum at 450 nm and an emission maximum at 515 nm. The bottom row of Fig. 4-1 shows the module designed to adapt the standard endoscope for VFI imaging.

To provide illumination during VFI, a 455 nm laser diode (Nichia Corporation, Tokyo, Japan) was installed in the Pentax EPK-i; light from the blue laser diode was coupled to the bifurcating light guide used during white light imaging, and a mechanical control on processor was used to switch between the two illumination modes. A driver (Wavelength Electronics, Bozeman, Montana, USA) controls the input current to the laser diode and thus allows variation of the illumination intensity. The module holds a custom-designed long pass filter (4.6 x 4.8 mm^2) passing wavelengths greater than 500 nm in front of the CCD for collection of proflavine fluorescence. The filters were cut from a custom-coated colored glass filter (Schott North America, Inc., Duryea, PA, USA); the thickness of the filter is 0.8 mm and the optical density (OD) at the illumination wavelength is 3.8. The filter was designed to have out-of-band rejection of at least OD 3 for light ranging from normal incidence to up to 70 degrees incidence, accommodating the angular FOV of the endoscope. The edges of the filter were coated black to minimize the effect of stray light on the image. The filters were installed using a medical grade, optically clear epoxy (#301-2FL, Epo-tek, Billerica, MA, USA). With the module and blue laser diode in place, at the center of the field of view the surface irradiance is approximately 14.9 mW/cm^2 at 5 mm and approximately 7.5 mW/cm^2 at 10 mm; both typical working distances for imaging.

4.2.1.3 High Resolution Microendoscopy

The MVE was designed to acquire widefield images in both CPI and VFI modes; in addition, it was designed to be compatible with a high resolution microendoscope capable of resolving subcellular detail in areas identified as suspicious during widefield imaging. The high resolution microendoscope (HRME) has been previously described [54, 68, 69] and has been used in vivo during endoscopy to visualize gastrointestinal pathology using proflavine contrast [83]. In this system, the light from a 455 nm LED is coupled to a fiber-optic bundle for tissue illumination. The fluorescence from proflavine stained tissue is collected by the bundle while in contact with the tissue and is delivered to a CCD camera through a 550 nm nm bandpass filter with a cut on wavelength of ~500 nm. The field of view of the HRME is 720 microns in diameter and the spatial resolution is 4.5 microns.

4.2.1.4 Image Capture

Image collection is achieved through a custom designed interface (Labview 2010, National Instruments, Austin, Texas, USA). The program displays the HD signal (1280x1024 pixels) via a DVI-to-USB capture card (Epiphan Systems, Ottawa, Ontario, Canada) and allows collection of both digital video and image frames. The interface also allows the user to adjust brightness and contrast where appropriate and to store information such as the date and time of procedure

4.2.1.5 Instrument Performance

The system resolution was determined by capturing an image of a U.S. Air Force resolution target (Newport Corp, Irvine, CA, USA). To assess background autofluorescence, images were acquired in VFI mode from a 2 inch diameter non-fluorescent frosted quartz disk (which approximates tissue reflectance) with settings that matched or exceeded those used for proflavine stained tissue. The measurements were used to verify the absence of excitation light leakage and assess the performance of the emission filter.

4.2.2 PILOT STUDY

The MVE was used to acquire images from clinically normal and abnormal areas of the esophagus *in vivo* during endoscopic surveillance and *ex vivo* immediately following surgical resection. Patients at Mount Sinai Medical Center were eligible to participate in the study if they met the following criteria: have or have had histologically confirmed Barrett's metaplasia, and were undergoing either routine surveillance or endoscopic treatment for Barrett's metaplasia or Barrett's-associated dysplasia. A healthcare provider described the study to eligible patients. Patients gave written informed consent prior to participation in the study. The study was reviewed and approved by the IRBs at Mount Sinai Medical Center and Rice University.

4.2.2.1 Ex Vivo Imaging Procedure

The MVE was used first to acquire images of an esophagectomy specimen. Immediately following surgical resection, the mucosal surface of the specimen was rinsed with saline and imaged with a digital single-lens reflex (SLR) camera under white light illumination. Visually abnormal and normal sites were identified by the study pathologist based on appearance; borders of these regions were marked on the white light image.

Areas identified by the pathologist as grossly normal and abnormal were imaged using all three widefield imaging modalities; images were first acquired using WLI, then CPI, and then in VFI mode. The specimen was imaged *ex vivo* at a fixed working distance of 5 mm to allow for optimal correlation between image sites and subsequent pathologic assessment. Before VFI imaging, proflavine hemisulfate (0.01% w/v) was applied to the mucosal surface of the sample using a sterile cotton tip applicator. Excess proflavine was removed with dry gauze. Finally, high resolution images were acquired using the HRME from clinically normal and abnormal areas.

In order to ensure the same FOV was imaged with each imaging modality, the distance from edge of the specimen, landmarks such as vessels, islands of squamous or columnar tissue, and the perimeter of the squamo-columnar junction were tracked as each widefield modality was used. To track high resolution imaging, widefield images were taken of the probe in contact with the mucosa, verifying that the images were obtained from the same FOV. In an effort to reduce sampling error, black or blue ink was placed at each area imaged, fixed with acetic acid, and photographed. Since the ink spread to approximately 2-4 mm in diameter, the photograph guided the approximation of image

sites on the resected specimens necessary to facilitate registration between widefield imaging, high resolution imaging, and subsequent histopathologic evaluation.

The specimen was then fixed in formalin and submitted for standard histopathologic analysis; vertical cross-sections were examined to grade and verify presence of disease. The study pathologist, blinded to the image results, assigned diagnoses to histologic sections of inked areas using standard histologic criteria.

4.2.2.2 In Vivo Imaging Procedure

The MVE was next used in vivo to acquire images during endoscopic surveillance using three high definition imaging modalities: WLI, CPI, then VFI. After endoscopic surveillance using WLI, the scope was removed and the module for CPI was placed on the distal tip and the scope was reinserted. The scope was removed again after CPI, the VFI module was installed and the scope was inserted a third time. Following the third insertion, proflavine (5-10 mL) was administered via spray catheter (Olympus America, Center Valley, Pennsylvania, USA) on the epithelial surface and VFI images were acquired. Finally, the HRME probe was introduced via the instrument channel of the endoscope by the endoscopist and placed in gentle contact with the tissue surface. HRME images were obtained from sites considered clinically abnormal using widefield imaging. Additional HRME images were obtained from sites that were considered clinically normal by widefield modalities. Widefield imaging in all three modes and high resolution imaging was performed by a single endoscopist (S.A.).

In order to ensure the images in all modalities were taken at the same site, three pieces of information were recorded during the procedure: clinical landmarks indicated

by the endoscopist (such as Barrett's borders, islands, ulceration, or bleeding), endoscope depth and quadrant, and time stamps during the procedure (upper right hand corner of every video). Post-procedure, videos were evaluated frame by frame to ensure images from the same site were extracted from each modality. All extracted image frames associated with each image site were reviewed by researchers (NT, ML, SA, RRK).

4.2.2.3 Endoscopic Image Criteria

The entire segment of Barrett's was scanned for apparent abnormalities with each image modality, using image criteria developed from previous *ex vivo* imaging studies [54, 82]. CPI images were considered suspicious if they demonstrated increased and abnormal vascularization, with crowding and branching of blood vessels, or if there were areas of glandular effacement. VFI images were considered suspicious if they demonstrated alterations in glandular architecture or glandular effacement. HRME images were considered abnormal if they exhibited enlarged, crowded, and pleomorphic nuclei. Images were also considered abnormal if they revealed overlapping glands that were heterogeneous in size and shape with irregular luminal spacing. Many abnormal areas also exhibited loss of overall glandular architecture [54, 82].

After imaging, biopsies were obtained from areas deemed suspicious in any of the imaging modes. Then, standard four quadrant biopsies were taken every 1-2 cm of the BE segment. Images acquired from suspicious sites were compared to the histologic evaluation of the biopsy from the same site. In addition, biopsies of non-neoplastic regions containing Barrett's were obtained as controls.

4.3 Results

4.3.1 INSTRUMENT PERFORMANCE

At the minimum working distance of 5 mm, the system can resolve a line spacing of at least 24.8 μm (group 4, element 3). At a typical working distance of 10 mm, the system can resolve a line spacing of at least 49.5 μm (group 3, element 3); the performance was unchanged with the incorporation of the imaging modules. The ratio of signal from proflavine-stained tissue to frosted quartz imaged using the same settings, was always greater than 10:1.

4.3.2 PILOT STUDY

4.3.2.1 **Ex Vivo: MVE Images of Esophagectomy Specimen**

The MVE was used to acquire images from 5 sites on a single esophagectomy specimen. Histopathology results were available from all 5 sites; two were diagnosed as non-neoplastic Barrett's, two were diagnosed as adenocarcinoma, and one site was diagnosed as carditis. Figures 4-3 and 4-4 show representative images of neoplastic and non-neoplastic tissue from this specimen. Figure 4-3 compares images of BE (top row) and adenocarcinoma (bottom row) in WLI and CPI modes. As expected, CPI images show reduced specular reflection (black arrows) and enhanced vascular contrast. In images of Barrett's metaplasia, vessels are better visualized in the cross polarized image

when compared to the same areas in the white light image (white boxes). In the images showing adenocarcinoma, not only are the vessels better visualized, but the increase in vasculature and vessel branching associated with neoplasia is more readily apparent (white box).

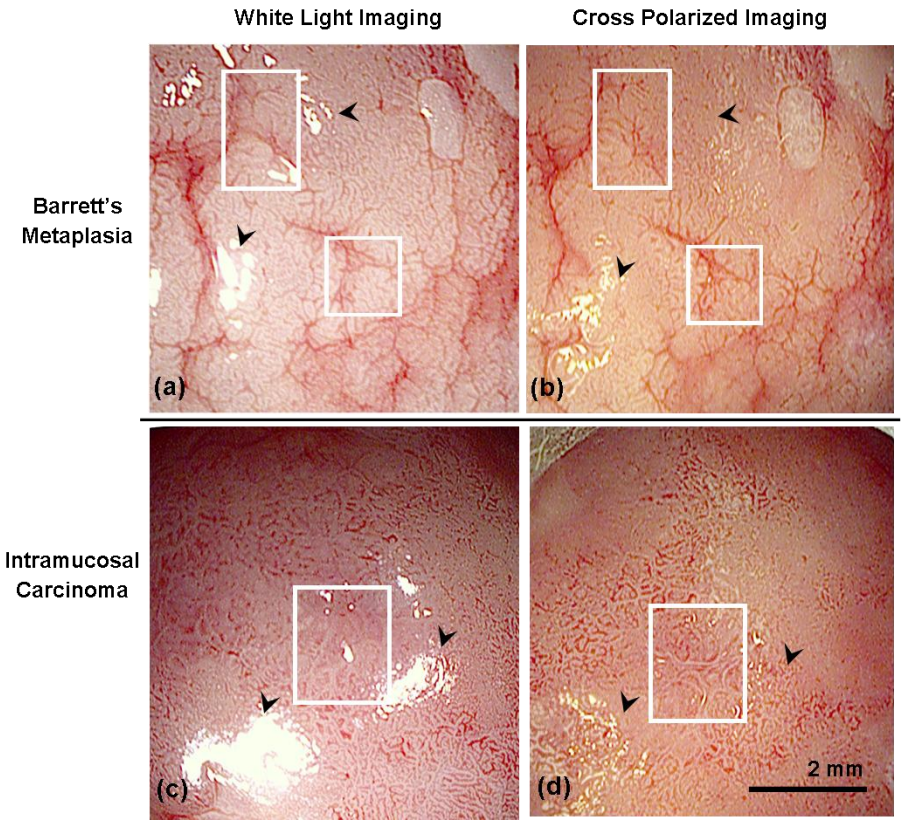

Figure 4-3. Top row shows (a) white light image and (b) cross polarized images of Barrett's metaplasia. Bottom row shows (c) white light image and (d) cross polarized image of intramucosal carcinoma. Black arrows show areas where specular reflection appears reduced in the CPI image. White boxes in the CPI image indicate areas where vessel branching is enhanced, when compared to same areas in the WLI. Images were acquired from an ex vivo esophageal specimen.

Figure 4-4 shows images acquired from BE (top row) and adenocarcinoma (bottom row) in WLI and VFI modes. The VFI image of Barrett's metaplasia allows

visualization of regular appearing glandular architecture (white box). The edges of the glands are discernible and the pattern appears consistent throughout the region. The corresponding HRME image shows nuclear staining primarily at gland edges indicating polarized nuclei, which is characteristic of non-neoplastic Barrett's metaplasia [54, 82]. This feature can also be seen in the corresponding vertical histology cross section, which shows Barrett's metaplasia.

The VFI image of adenocarcinoma allows visualization of partly effaced (yellow box) and completely effaced (white box) glandular architecture. The gland edges are no longer clearly discernible. The HRME image shows nuclear crowding, small and irregularly shaped glands (yellow arrows), loss of nuclear polarity within the glands (yellow box), and absence of glands in some areas (white box). These features are mirrored in the corresponding vertical histology cross section, which shows adenocarcinoma.

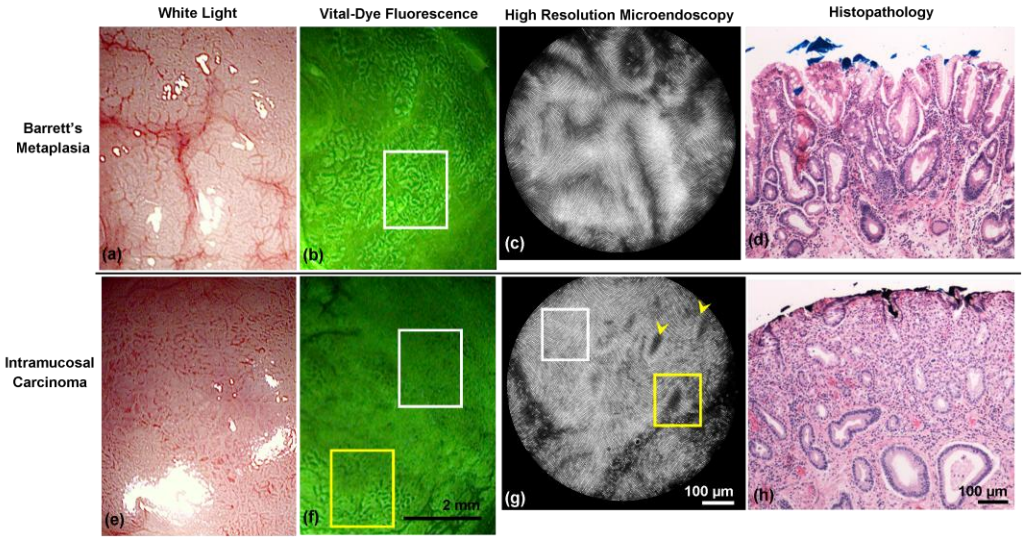

Figure 4-4. Top row shows (a) white light image, (b) vital-dye fluorescence image and (c) high resolution fluorescence image of proflavine-stained Barrett's metaplasia. The white box in the VFI image (b) indicates a region where glandular architecture is clearly visible. Bottom row shows (e) white light image, (f) vital-dye fluorescence image and (g) high resolution fluorescence image of proflavine-stained intramucosal carcinoma. In the VFI image (f), the yellow box indicates partial glandular effacement and white boxes indicate complete effacement. In the HRME image (g), yellow arrows indicate small irregularly shaped glands, and yellow box indicates a gland with disrupted edges. The white box indicates an area of nuclear crowding. Corresponding histologic cross sections are shown (d,f). Note the ink on the surface of each histologic section, verifying that the section was taken from the imaged area. Images were acquired from an ex vivo esophageal specimen.

4.3.2.2 In Vivo: MDE Images Obtained During Endoscopy

In vivo imaging was conducted on one patient. During the endoscopic procedure using the MVE, three sites were imaged using all four modalities and biopsied. Two sites were diagnosed as non-neoplastic Barrett's (BE) and one was diagnosed as adenocarcinoma.

Figure 4-5 shows representative images from a site diagnosed as BE. In Figure 4-5(A), the white light image shows glandular architecture with some vascular detail. The CPI image in Figure 4-5(B) again shows enhanced vascular contrast. Indeed, both larger vessels and smaller vessels that were not visible during WLI become clear (white box). In the VFI image shown in Figure 4-5(C), glands are present throughout the examined area. Gland borders appear wide and there is little interruption between the border edges. High resolution imaging with the HRME through the instrument channel of the endoscope in

Figure 4-5(D) allows for a magnified view of the features seen in VFI. Gland border edges appear regular (yellow boxes), and appear similar throughout the field of view. Nuclei within these regions appear polarized towards the gland edges. These features, along with intestinal-type goblet cells are apparent in the corresponding vertical histology cross section in Figure 4-5(E), showing Barrett's metaplasia which is negative for dysplasia.

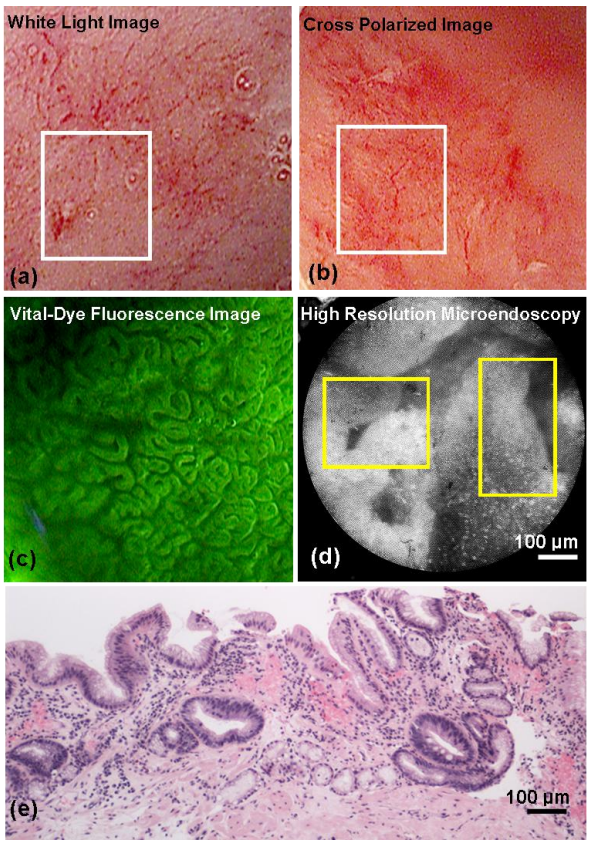

Figure 4-5. In vivo images of an area of Barrett's metaplasia in (a) white light, (b) cross-polarized, (c) vital-dye fluorescence, and (d) high resolution imaging modes. The white box in the CPI image indicate areas where appearance of vessel branching is enhanced. The yellow boxes in the HRME image (d) show regular gland edges, and indicate gland borders

where nuclei are primarily polarized towards the edge. Corresponding histopathology cross section is shown (e).

Figure 4-6 shows images from a site diagnosed as adenocarcinoma. In Figure 4-6(A), the WLI shows a flat, non-ulcerated lesion with both vascular and glandular abnormalities; in the CPI image of the same area (Figure 4-6B) the pattern of vessel branching can more easily be assessed when compared to WLI (white box). VFI of the same area (Figure 4-6C) shows glands that appear partly effaced in some regions (white boxes) and completely effaced in others (yellow boxes). Proflavine staining is heterogeneous throughout the area. The HRME image (Figure 4-6D) reveals crowded glandular structures with irregular gland borders (yellow boxes), nuclear crowding both within the glands and outside of the glands (white box). Nuclei also appear pleomorphic. The histologic section presented in Figure 4-6(E) was diagnosed as adenocarcinoma.

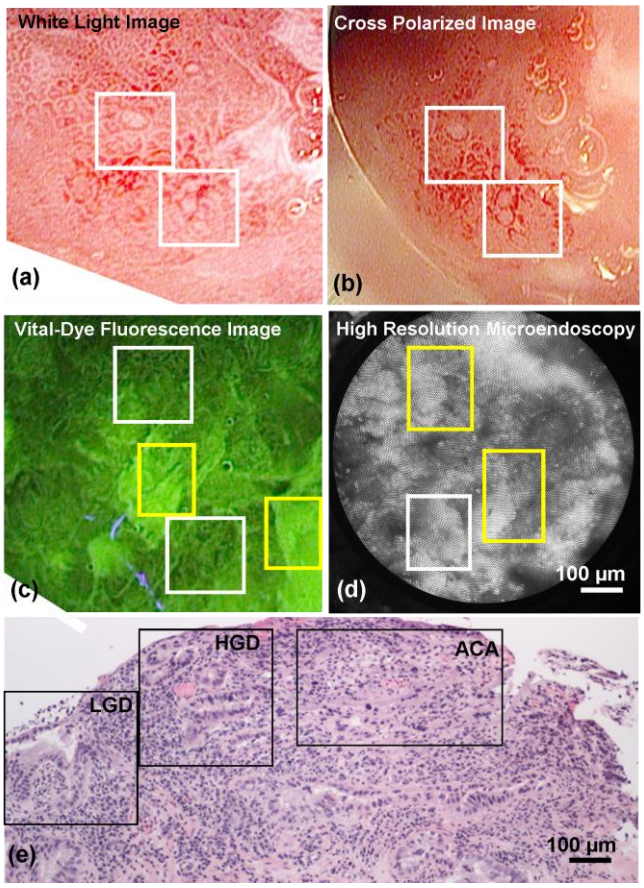

Figure 4-6. In vivo images of an area of adenocarcinoma in (a) white light, (b) cross-polarized, (c) vital-dye fluorescence, and (d) high resolution imaging modes. The white boxes in the CPI image (b) indicate areas where appearance of vessel branching is enhanced, when compared to the white light image (a). In the VFI image (c), the white boxes indicates partial glandular effacement and yellow boxes indicate complete effacement. The yellow boxes in the HRME image show irregular gland edges, and the white box indicates a border where nuclei appear crowded. Corresponding histopathology cross section is shown (e). Areas of LGD, HGD, and ACA are indicated by black boxes in (e).

4.4 Discussion

In summary, we reported the technical development and initial ex vivo and in vivo evaluation of a multimodal endoscopic imaging system which is capable of high

definition white light imaging, cross polarized reflectance imaging, vital-dye enhanced fluorescence imaging. We showed technical compatibility with a previously reported high resolution microendoscope imaging system, demonstrating the potential for the multimodal endoscope to be used in conjunction with probe-based microendoscopic technologies. CPI and VFI are novel endoscopic modalities, which probe important mucosal features; CPI enhances vasculature while VFI highlights changes in glandular architecture. Additionally, HRME imaging allows higher resolution examination of glandular morphology, including nuclear characteristics such as pleomorphism and crowding. We have demonstrated the feasibility of these modalities by imaging areas of Barrett's metaplasia and associated neoplasia on an esophagectomy specimen. We verified that the key image features of neoplastic and non-neoplastic tissue were also observed during an *in vivo* surveillance procedure. Results suggest that key pathologic features seen in CPI, VFI, and HRME imaging are not easily visible during standard endoscopic white light imaging and therefore may be useful in future *in vivo* studies for discriminating dysplasia and cancer from Barrett's metaplasia.

In this study, we find that CPI improves visualization of vasculature without significantly altering the white light appearance of the image. A number of groups have used vascular contrast enhancement to improve disease detection. Groner et al. used cross polarization to improve visualization of microcirculation [80]. Roblyer et al. used CPI to probe the diffusely reflecting light predominately coming from deep mucosal layers [71, 84]. Though vascular contrast enhancement can be valuable, an inherent trade-off of CPI is the loss of surface architecture due to the rejection of photons reflected off the tissue surface. Moreover, as the spatial resolution of white light imaging continues to improve

through the development of higher definition endoscopes, we must evaluate whether or not CPI would add a significant amount of information over those improvements. Regardless, a larger study is necessary to understand whether the trade-off which enhances the ability to visualize deeper blood vessels would improve overall accuracy.

VFI with proflavine contrast improves visualization of glandular architecture by providing contrast to epithelial cell nuclei. This is particularly important since glandular architecture changes during the progression to neoplasia [85]. Previous studies using other modalities have shown that the assessment of such features can improve Barrett's surveillance [40]. Narrowband imaging reveals some glandular features, which have been documented and have been used to identify neoplasia with high sensitivity [40, 41], but low specificity in identifying Barrett's metaplasia [79]. Since VFI uses a nuclear stain it provides a more direct assessment of glandular architecture. The added benefit of using VFI is the potential for implementing high resolution imaging at the same time, thus providing the ability to monitor nuclear changes at two different scales. For instance, the histology section presented in Fig. 4-6(E) was diagnosed as adenocarcinoma, however the histologically verified presence of both LGD and HGD within the regions indicated by black boxes in Fig. 4- 6 (E), may be contributing to the overall heterogeneity in the VFI image (Figure 4-6C). A situation like this may prompt the endoscopist to use the HRME probe on a number of sites within the area imaged by VFI to understand the differences in proflavine signal and help determine, for example, the area to biopsy.

The HRME allows more detailed interrogation of glandular architecture and allows examination of features such as nuclear size, shape, distribution, and crowding. Previous studies have shown that these features can be consistently identified in HRME

images and correlate with the appearance observed in H&E stained histologic sections [54, 68, 82]. Moreover image processing algorithms have been developed for quantitative analysis of digital HRME images; initial pilot studies show high sensitivity and specificity for identifying neoplastic lesions [56], suggesting the potential to use HRME imaging together with algorithm-assisted identification of early cancers and high grade dysplasia.

Proflavine is the principal component of acriflavine, which has been used during in vivo fluorescence imaging in Europe and Australia without any adverse effects noted [59]. Indeed, this investigational *in vivo* human study of confocal microscopy for gastrointestinal cancers, use topical acriflavine at 0.05% concentration, five times more than what is used for VFI and HRME imaging. Moreover, the agent has been clinically used as an antibacterial agent. In neonatal care, Triple dye, a combination of brilliant green, proflavine hemisulfate, and gentian violet is routinely used as a topical antibacterial agent on the umbilical stump of newborn babies [74], with a recent review of the practice categorizing toxicity as rare [86]. In this pilot study, proflavine concentration is significantly lower than that of the proflavine concentration in commercial triple dye, 0.11% (w/v) (Kerr Triple Dye, Vista Pharm, Birmingham, Alabama, USA).

Though each of the presented modalities appears to improve the visualization of relevant mucosal changes, additional studies are needed to determine the overall effectiveness in vivo of each modality. Indeed, larger in vivo studies are needed to assess 1) the sensitivity and specificity for detection of neoplasia for each modality and 2) whether or not this represents an improvement compared to white light examination and standard four quadrant biopsies. Thus the development of an instrument that can easily

implement these modalities in vivo is particularly useful. Testing each modality individually will help determine which imaging technique would be most useful to clinicians for in vivo surveillance; the result would be a potential candidate for widespread clinical testing. In the future, additional studies looking at both qualitative and quantitative image features are needed to investigate which are most relevant for endoscopic image interpretation.

The module-based imaging technique presented here allows the testing of new imaging modalities to quickly determine feasibility. This modular concept can be adapted to any video endoscope for the upper or lower gastrointestinal tract, thereby extending its utility for the detection of additional gastrointestinal abnormalities such as colon and gastric cancers. Past widefield fluorescence imaging studies using contrast agents have not fully taken advantage of recent CCD advances, potentially limiting what mucosal features can be resolved. By using a filter module to image, we can maintain the benefits of the high definition CCD (1280 by 1024 pixels) while enabling the examination of different optical markers of disease. Moreover, this dual-scale platform can be adapted to measure other molecular targets that have been used in the gastrointestinal tract with similar excitation and emission properties such as 2-NBDG [87] or other targeted fluorescence contrast agents [10, 61]. Furthermore, signal associated with these fluorescent contrast agents can be quantified and used to aid in subjective image interpretation [56, 87], thereby further increasing its potential as a surveillance tool.

CHAPTER 5: QUANTITATIVE EVALUATION OF IN VIVO VITAL-DYE FLUORESCENCE ENDOSCOPIC IMAGING FOR THE DETECTION OF BARRETT'S ASSOCIATED NEOPLASIA

5.1 Introduction

The incidence of esophageal adenocarcinoma (EAC) has increased 335% in women and 463% in men during the past 3 decades [2]. This is of particular concern because EAC is associated with a low five-year survival rate, primarily due to late stage diagnosis [3]. However, when detected before metastases occur and treated appropriately, five-year survival rates has been shown to be as high as 81% [12].

Barrett's esophagus (BE) is a condition of the esophagus caused by chronic acid reflux [14, 75]. Individuals with BE are at an increased risk for developing esophageal dysplasia and cancer; because of this increased risk, individuals with BE are recommended to undergo endoscopic surveillance at regular intervals [76]. Surveillance typically includes white light videoendoscopy, with biopsy of visually abnormal areas. Unfortunately some neoplasias are flat and often undistinguishable from BE, thus routine surveillance also includes random four quadrant biopsies every 1-2 cm of the Barrett's segment [76]. However, endoscopic surveillance protocols often fail to detect early lesions; some studies estimate that as many as 57% can be missed [5]. Thus, there is an important need to develop improved surveillance techniques that can detect early neoplastic areas with great efficiency.

A number of widefield imaging modalities have been proposed to improve the efficacy of white light videoendoscopy for detection of early neoplastic changes in the esophagus. For example, narrowband improves visualization of vascular changes

associated neoplasia [40]. Fluorescence imaging can identify areas with loss of autofluorescence, also associated with early neoplasia [77]. However, early clinical studies indicate that narrowband imaging has poor specificity for detecting BE [79], while autofluorescence imaging is associated with poor specificity for detecting neoplasia [7, 8]. The poor specificity of autofluorescence imaging is thought to be due to false positives associated with benign inflammation [42].

The use of exogenous fluorescent contrast agents that enhance the contrast between neoplastic and non-neoplastic tissue has the potential to improve efficacy of fluorescence-based endoscopic surveillance protocols. Fluorescence imaging with vital-dyes such as proflavine hemisulfate have been shown to improve visualization of mucosal architecture in the esophagus and colon [82]. Widefield imaging with proflavine contrast enhances visualization of glandular architecture in Barrett's metaplasia as well has glandular effacement which is a hallmark Barrett's-associated neoplasia.

A modular video endoscope (MVE) capable of in vivo vital-dye fluorescence imaging has recently been developed [88]. Initial in vivo images acquired with the system suggest that vital-dye fluorescence images enhance the ability to identify regions of glandular effacement [88]. Suspicious areas identified in this manner can then be interrogated with higher spatial resolution [54, 83], potentially enabling a widefield and confirmatory high resolution protocol for endoscopic surveillance. Here, we describe results from a 14 patient pilot study using the MVE. Images of 65 sites were analyzed to identify relevant quantitative image features that could be used to classify tissue as neoplastic or non-neoplastic. Results show that granulometry features, average length of gland segments, and frequency content aid in the classification of neoplasia.

5.2 Methods

5.2.1 INSTRUMENTATION

The Modular Video Endoscope (MVE) has been described in detail, previously [ref]. Briefly, it consists of a modified high definition (1280x1024 pixels) video processor (Pentax EPK-i) and a standard upper endoscope (Pentax EG-29901), modified to enable both HD white light imaging and vital-dye fluorescence imaging (VFI). For tissue illumination in VFI mode, a 455 nm laser diode (Nichia Corporation, Tokyo, Japan) was coupled to the bifurcating endoscope light guide used for white light illumination. The diode is controlled using a laser diode driver (Wavelength Electronics, Bozeman, Montana, USA), which controls the input current, thus controlling the illumination intensity. A mechanical control on the processor is used to switch between white light and laser illumination when necessary. A stainless steel filter module containing necessary optical filters for vital-dye fluorescence imaging is attached to the endoscope distal tip with a medium sized, commercially-available endoscope cap (Barrx Medical Inc., Sunnyvale, CA, USA). The filter module holds a custom-designed long pass filter in front of the endoscope CCD. The filter (4.6 x 4.8 x 0.8 mm) transmits wavelengths longer than 500 nm, enabling collection of fluorescent light. The MVE filters are designed for use with proflavine, a topically applied fluorescent dye which stains cell nuclei.

The custom-designed filter module maintains use of the forward water jet used for irrigation and the air/water nozzle used to clear debris in the field of view of the CCD. The MVE was designed for the standard working distance of the upper endoscope, ranging from 5 - 20 mm. The field of view depends on both the working distance and the

digital magnification; at a typical working distance of 10 mm, the FOV ranges from 14 mm to 45 mm in diameter, with a resolution of 50 microns.

5.2.1.2 High Resolution Microendoscope

The MVE is compatible with a high resolution microendoscope (HRME) which has been described previously [68, 69]. The HRME acquires high resolution fluorescence images with a field of view of 720 microns in diameter and a lateral spatial resolution of 4.5 microns. The HRME is also designed for use with proflavine; fluorescence is excited using a 455 nm LED and collected through 550 nm bandpass filter with a cut on wavelength of approximately 500 nm.

5.2.2 PILOT STUDY

The MVE and HRME were used to collect videos and images of clinically abnormal and normal areas of the esophagus from study participants. Patients at Mount Sinai Medical Center were eligible to participate in the study if they met the following criteria: have or have had histologically confirmed Barrett's metaplasia, and were undergoing either routine surveillance or endoscopic treatment for Barrett's metaplasia or Barrett's-associated dysplasia. A healthcare provider or a clinical research coordinator described the study to eligible patients. Patients gave written informed consent prior to participation in the study. The study was reviewed and approved by the IRBs at Mount Sinai Medical Center and Rice University.

5.2.2.1 Endoscopic Imaging Procedure

The MVE was used in vivo to evaluate Barrett's epithelium in two different imaging modes, white light imaging (WLI) and vital-dye fluorescence imaging (VFI). During white light evaluation, the endoscopist noted the location and recorded videos and images from any areas that appeared suspicious for neoplasia and at least one area that appeared non-neoplastic. After WLI, the scope was removed and the VFI filter module was attached to the distal tip for fluorescence imaging. The scope was reinserted and proflavine contrast agent (5-10 mL) was administered via spray catheter (Olympus America, Center Valley, Pennsylvania, USA) on the epithelium. Following proflavine application, the laser light was switched on for observation of proflavine fluorescence. Any areas that were imaged in WLI mode were imaged in VFI mode; the location of any additional areas that appeared abnormal in only VFI mode were documented as well and VFI video and images were acquired from these sites.

Following widefield imaging, the HRME was introduced via the instrument channel of the MVE. HRME images were obtained from the clinically abnormal and normal sites imaged and identified with WLI and VFI. At each site, the HRME probe was placed in gentle contact with the mucosal surface. Widefield imaging with the MVE, and high resolution imaging with the HRME were conducted by a single endoscopist (S.A.). Following the imaging procedure, biopsies were obtained from each of the clinically abnormal and clinically normal areas that were imaged. In addition to study biopsies, four-quadrant biopsies were obtained as standard of care. Images obtained from biopsied areas were compared to the histologic evaluation of the biopsy from the same area.

Additionally, biopsies of non-neoplastic regions of Barrett's were obtained as controls. An expert GI pathologist who was blinded to the image results read the pathology.

5.2.3 QUALITATIVE IMAGE ANALYSIS

At the time of the procedure, white light images were interpreted using standard criteria [76] and were considered abnormal if a nodule was present or if there was apparent hypervascularization [76]. Vital-dye fluorescence images were considered abnormal if there was a nodule present, if there were glandular alterations, or if there was some degree of glandular effacement [82]. HRME images were interpreted using previously developed criteria and were considered abnormal if they exhibited enlarged, crowded, and pleomorphic nuclei [54, 82]. Images were also considered abnormal if they revealed overlapping glands that were heterogeneous in size and shape with irregular luminal spacing, or if they exhibited loss of overall glandular architecture [54, 82].

5.2.4 QUANTITATIVE IMAGE ANALYSIS

Digital images and videos were reviewed for quality control. Images of Barrett's and Barrett's-associated neoplasia were included in the final evaluation only if a 250x250 pixel region of interest (ROI) within the image was clear of debris, was in focus, and did not contain movement artifact.

The diagnostic potential of various quantitative image features was explored (Table 1). For each image ROI, 49 features were computed. First order statistical features

(variance, standard deviation, etc) were computed based on individual pixel values. To explore textural image features, a grey-level co-occurrence matrix with pixel offsets (1-6) were first computed for each ROI. Then features such as correlation, contrast, energy, and homogeneity were computed from each GLCM [56, 89]. To explore spatial frequency features, a two-dimensional Fourier transform was used to calculate the power spectrum for each ROI. The resulting energy spectrum was divided up into 10 individual frequency ranges, where the contribution from each component represents the frequency content from a corresponding spatial range [90, 91]. To explore epithelial thickness, granulometry, which assesses the size distribution of elements in each ROI, was used to calculate the surface area as a function of disk size [92-94]. The plot of the surface area as a function of disk size characterizes the relative distribution of different sized disks within each ROI; statistical features (skewness, kurtosis, etc) of this distribution were computed. To explore glandular edges, two non-experts, blinded to the pathology results, segmented gland edges for each ROI in ImageJ (ImageJ 1.47D). A morphometric function in Matlab (Matlab R2011b) was used to reduce segmented edges to a single pixel perimeter. From this binary mask, the following statistical features were computed for each ROI: the number of long segments, the average length of the long segments, and the standard deviation of the length of the long segments.

A Student's t-test was used to determine whether there was a statistically significant difference ($p < 0.05$) in the mean value of each of these 49 parameters for neoplastic and non-neoplastic Barrett's. Step-wise linear discriminant analysis was used to classify images as non-neoplastic (BE/LGD) or neoplastic (HGD/EAC) using only the image features where the differences in the means were statistically significant as inputs.

The diagnostic algorithm was developed using leave-one-patient-out cross validation; for each fold, the imaged sites from all but one patient were used as a training set to develop the algorithm, this algorithm was then applied to all the image sites from the held out patient. This cycle was repeated for each individual patient. Histologic diagnosis was used as the gold standard. In each fold, a sequential forward selection algorithm was used to identify the best performing subset of up to 3 metrics to classify the image data. As the number of features increased, performance was monitored by noting whether the area under the receiver operator characteristic curve increased.

Table 5-1: Description of features calculated for each image

Metric (# of features)	Description
First order statistical values (6)	Mean, standard deviation, variance, entropy, skewness, kurtosis
GLCM*-related features (24): Correlation (6), Energy (6), Homogeneity (6), Contrast (6)	Correlation: Pixel neighborhood correlation in the GLCM (Offsets 1-6), Energy: Sum of squared elements in the GLCM (Offsets 1-6), Homogeneity: Measure of how close GLCM elements are to the GLCM diagonal (Offsets 1-6), Contrast: Intensity contrast between pixel and offset pixel over entire ROI (Offsets 1-6)
Frequency Content (10)	Fraction of power spectral density in 10 equally spaced partitions of the power spectrum
Granulometry (6)	Skewness and kurtosis of size distribution of disks in an ROI (for disks with radii of 1-100 pixels), Most prominent disk size in an ROI (for disks with radii of 1-100 pixels), Most prominent large disk size in an ROI (for disks with a radii between 50 - 100 pixels), Surface area of most prominent disk size in an ROI, Surface area of most prominent large disk size in an ROI (for disks with a radii between 50-100 pixels)
Edge-based Morphometry (3)	Sum of long segments, Average length of long segments, Standard deviation of the length of long segments

*Gray-level co-occurrence matrix

5.3 Results

A total of 20 patients were consented and underwent the study procedure. Images were obtained from 72 sites in 14 patients with biopsy confirmed Barrett's metaplasia or Barrett's- associated neoplasia. After quality control, 65 sites in 14 patients were available for analysis. Of these sites 16 sites (from 8 of the 14 patients) were diagnosed as Barrett's-associated neoplasia, and 49 (from 9 of the 14 patients) were diagnosed as Barrett's metaplasia (Table 5-2).

Table 5-2: Patient Data Summary

Category	Histopathology Dx	# Bx sites	# Bx sites	# Images
BE non-neoplasia	BE negative	13	**49 (9 pts)**	49
	BE indefinite	12		
	BE LGD	24		
BE neoplasia	BE LGD/HGD or HGD	7	**16 (8 pts)**	16
	BE HGD/ACA or ACA	9		
TOTAL			**65**	**65**

Figure 5-1 shows representative images from Barrett's metaplasia acquired during in vivo endosopic surveillance using WLI, VFI, and HRME imaging modalities. In Figure 1, WLI shows a clear distinction between squamous epithelium and Barrett's metaplasia (labeled), however glandular details are not easily discernible. In the VFI image, glandular architecture is visible. Specifically, the gland edges are distinct and the glandular pattern appears uniform throughout the indicated region (box). The corresponding HRME image shows thick glandular borders (white arrows), consistent

with the features visible in the VFI image. Additionally, the HRME image shows small, evenly-spaced nuclei (yellow arrows). These features, along with intestinal-type goblet cells are visible in the corresponding histology cross section, showing Barrett's metaplasia and low grade dysplasia.

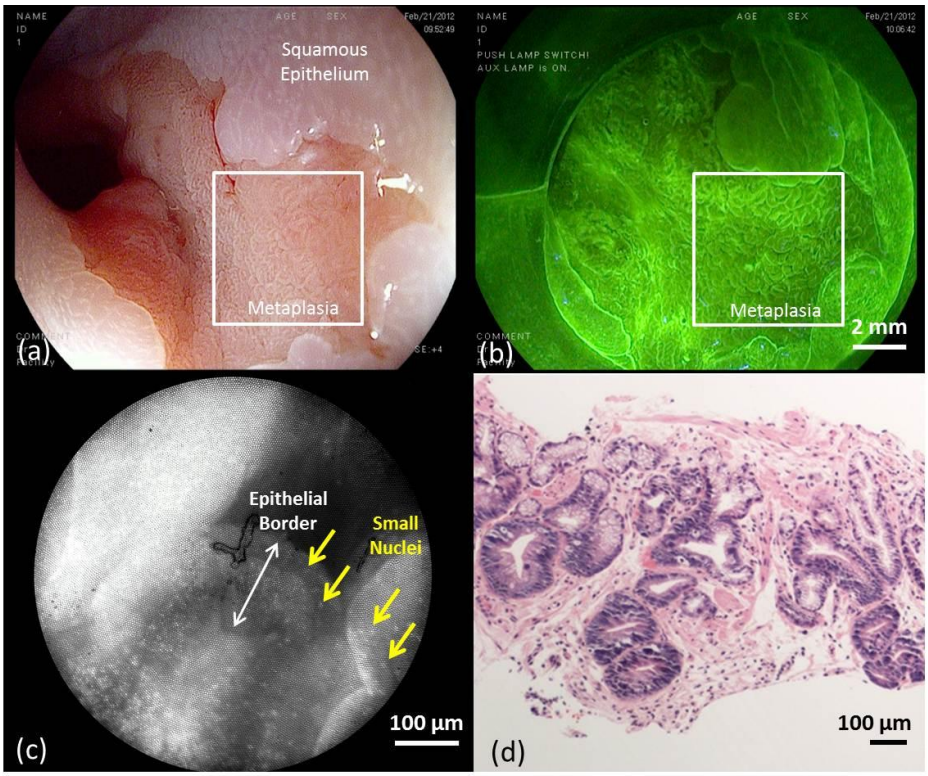

Figure 5-1. (a) White light endoscopic image, (b) vital-dye fluorescence endoscopic image, and (c) high resolution microendoscope image which were all read endoscopically as non-neoplasia. Shown in (d) is the histology section of the same site. Biopsy was diagnosed as Barrett's metaplasia with low grade dysplasia. White box in (a) and in (b) indicates area from where the biopsy was taken. White arrows in (c) indicate thick epithelial border. Yellow arrows in (c) show examples of small nuclei.

Figure 5-2 shows representative images from high grade dysplasia acquired during in vivo endoscopic surveillance using WLI, VFI, and HRME imaging modalities.

In the white light image, glandular architecture appears uniform throughout the image and there is no apparent indication of increased vasculazation. There is an area (box) that appears slightly raised. In the VFI image of the same area (box), some distorted glandular architecture is apparent. Glands appear thin and irregular (left arrow); glandular effacement is also present (right arrow). The corresponding HRME image shows irregularly sized glands (white arrow) as well as nuclear crowing (yellow circle) throughout the image. These features are also visible in the corresponding histologic cross-section taken from that image site; the H&E image was read as high grade dysplasia.

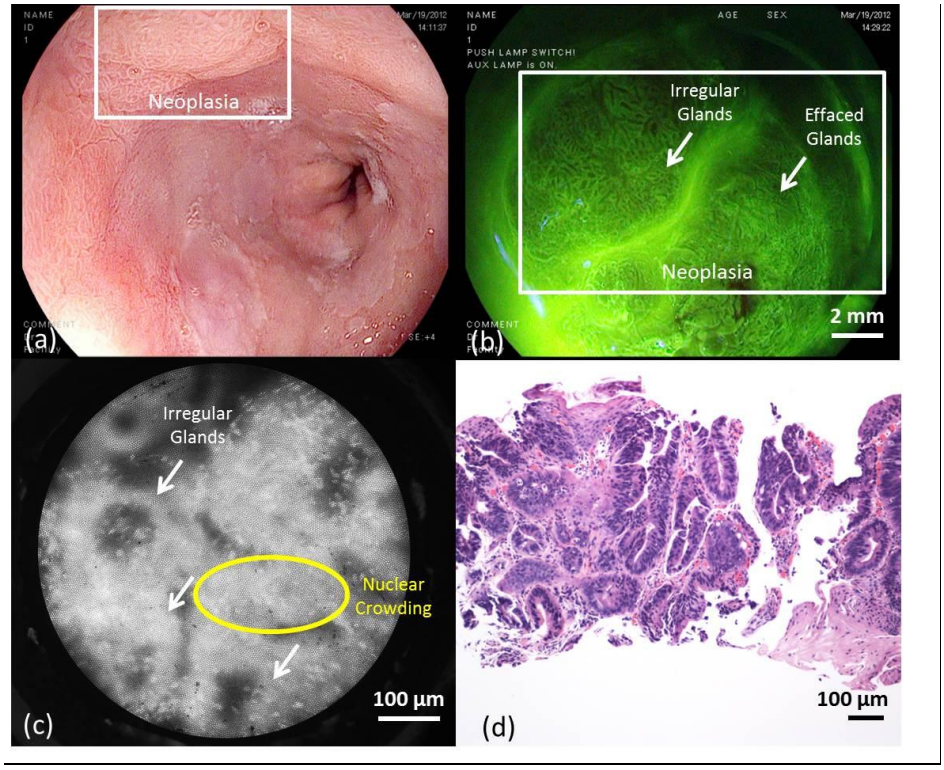

Figure 5-2. (a) White light endoscopic image, (b) vital-dye fluorescence endoscopic image, and (c) high resolution microendoscope image which were all considered endoscopically suspicious for neoplasia. Shown in (d) is a histology section of the same site. Biopsy was diagnosed as Barrett's-associated high grade dysplasia. White box in (a) and (b) indicates area

from where the biopsy was taken. White arrows in (b) indicate irregular and effaced glands. White arrows in (c) indicate examples of glands with irregular borders. Yellow circle in (c) indicates an example of area with nuclear crowding.

Figure 5-3 shows representative images from adenocarcinoma acquired during in vivo endosopic surveillance using WLI, VFI, and HRME imaging modalities. In the white light image, a nodule is visible (box); areas of hyper-vascularization are also apparent (star). In the corresponding VFI image, glandular effacement is observed throughout the same neoplastic region (box). In the HRME image obtained from the nodule, thick brush borders associated with metaplasia are not present and crowded pleomorphic nuclei are prominent (circle). These features are visible in the corresponding histology cross section from that image site showing Barrett's-associated high grade dysplasia and adenocarcinoma.

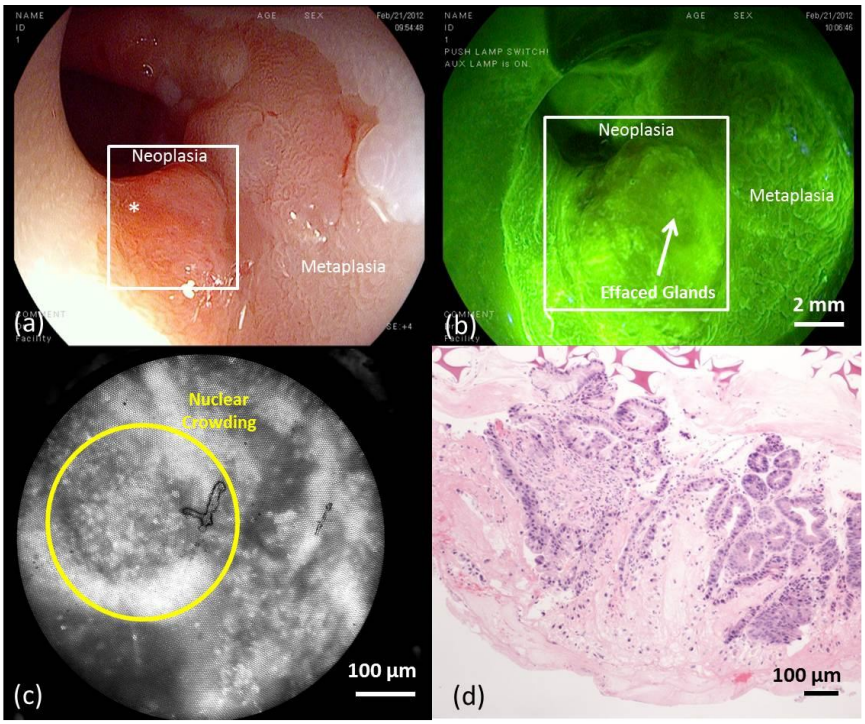

Figure 5-3. (a) White light endoscopic image, (b) vital-dye fluorescence endoscopic image, and (c) high resolution microendoscope image were all endoscopically suspicious for neoplasia. Shown in (c) is the histology section of the same site. Biopsy was diagnosed as Barrett's-associated adenocarcinoma. White box in (a) and (b) indicates the nodule from which the biopsy was taken. Star in (a) indicates hyper-vascularization. White arrow in (b) indicates glandular effacement. Yellow circle in (c) indicates nuclear crowding.

Figure 5-4 demonstrates an instance where the WLI image shows areas of hypervascularization (arrows), prompting a false positive read. The VFI image from the same area shows characteristic metaplastic patterns where gland edges are easily discernible. The corresponding HRME image verifies this observation. The histology cross section from this image site was read as Barrett's metaplasia.

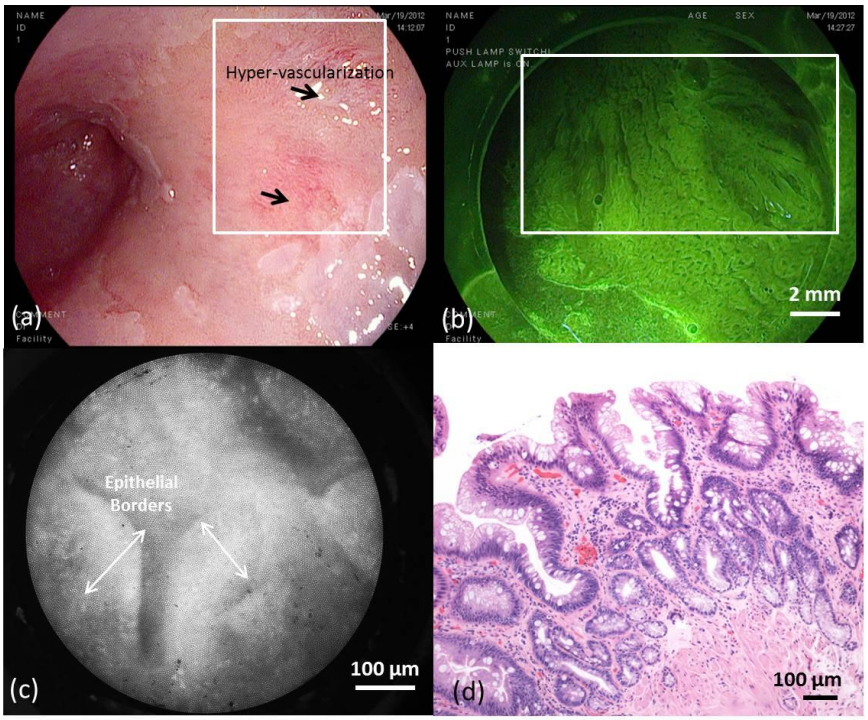

Figure 5-4. (a) White light endoscopic image of an area endoscopically suspicious for neoplasia. (b) Vital-dye fluorescence endoscopic image of the same area and (c) corresponding high resolution microendoscope image were both read endoscopically as non-neoplasia. Shown in (c) is

histology section of the same site. Biopsy was diagnosed as Barrett's metaplasia. White box in (a) and (b) indicates the area from which the biopsy was taken. Black arrows in (a) indicates areas of apparent hyper-vascularization. White arrows in (c) indicate examples of thick epithelial borders, which are characteristic of HRME metaplasia images.

Figure 5-5(a) shows a scatter plot of the posterior probability values for each site based on a two class linear classifier developed using leave-one-out cross validation. The sites are organized by diagnosis. Figure 5-5(b) shows the resulting receiver operator characteristic (ROC) curve; at the Q-point, the sensitivity is 88% and the specificity is 86% with an area under the ROC curve of 0.86. Table 5-4 shows the percentage of data points in each diagnostic category that were categorized correctly.

Table 5-3. Image analysis features with statistically significant differences in mean values for non-neoplastic and neoplastic tissue sites (p-value < 0.05)

Metric	**p-value**
Frequency content in first partition of the power spectrum	0.016
Skewness of size distribution of disks in an ROI (for disks with radii of 1-100 pixels)	0.023
Frequency content in the seventh partition of the power spectrum	0.025
Kurtosis of size distribution of disks in an ROI (for disks with radii of 1-100 pixels)	0.034
Surface area of most prominent disk size in an ROI	0.034
Average length of long segments	0.036

Differences in the mean values of six of the 49 image features for neoplastic and non-neoplastic tissue were found to be statistically significant ($p<0.05$). Table 3 lists these features ranked by p-value. Step-wise linear discriminant analysis was performed using these features as inputs. Leave-one-patient-out cross validation was used; the features selected in each cross-valdiation fold were tracked to those selected most frequently. Most frequently selected features include: average length of gland segments in an ROI (100%), skewness of size distribution of disks in an ROI (57%), and frequency content in the first partition of the power spectrum (79%).

Figure 5-5(a) shows a scatter plot of the posterior probability values for each site based on a two class linear classifier developed. Figure 5-5(b) shows the resulting receiver operator characteristic (ROC) curve; at the Q-point, the sensitivity is 88% and the specificity is 86% with an area under the ROC curve of 0.86. Table 5-4 shows the percentage of data points in each diagnostic category that were categorized correctly.

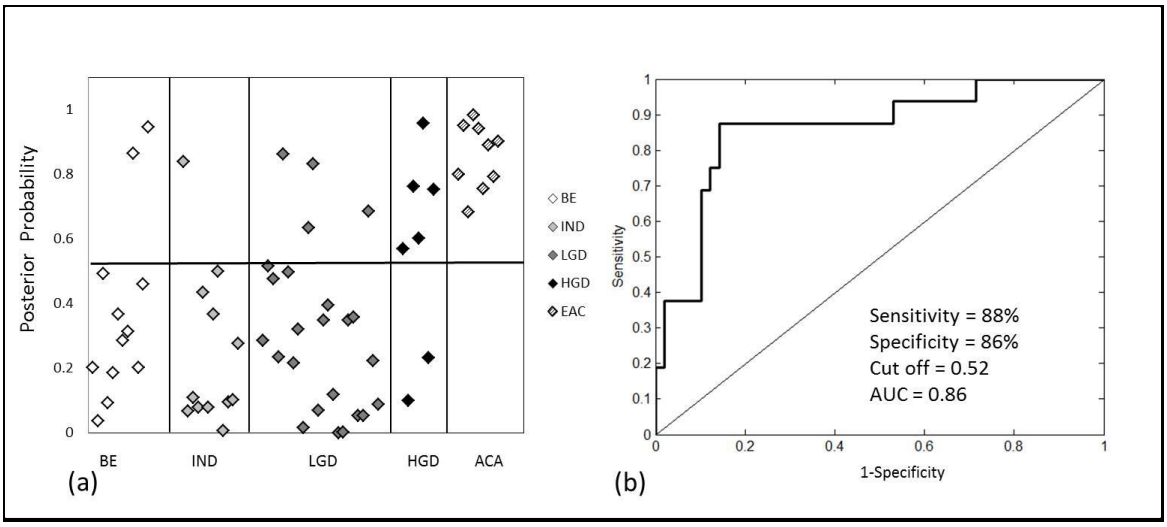

Figure 5-5. Scatter plot (a) shows posterior probability of neoplasia organized by diagnostic category. Corresponding receiver operator characteristic curve is shown (b). At the Q-point, the sensitivity and specificity are 88% and 86%, respectively; the area under the curve is 0.86.

Table 5-4. Percentage of sites in each diagnostic category which are classified correctly

Category	Histopathology Dx	# Bx sites	Correctly Categorized	Correctly Categorized
BE non-neoplasia	BE negative	13	85%	86%
	BE indefinite	12	92%	
	BE LGD	24	88%	
BE neoplasia	BE HGD	7	71%	88%
	BE ACA	9	100%	

5.4 Discussion

In summary, we report results from an *in vivo* study of VFI; images from 65 sites in 14 patients were collected and analyzed to assess the classification potential of VFI using quantitative image features. Three quantitative image features were found to

consistently aid in the identification of neoplasia. The first feature is the skewness of the distribution of disk sizes, which we hypothesize characterizes the presence of glandular structure within each ROI. Results indicate that, as glandular structure is lost, the skewness of this distribution decreases. The second feature is the average perimeter of glands; gland perimeters were typically longer in metaplastic lesions than in neoplastic lesions. The third feature is the frequency content in the first partition of the power spectrum; the low frequency content is higher in neoplastic images, again likely corresponding to loss of glandular structure. Linear discriminant analysis using a combination of these three features resulted in sensitivity and specificity of 88% and 86% respectively, with an AUC of 0.86.

We examined possible factors that resulted in images being incorrectly classified. Of the 49 images classified as neoplastic, 12 were falsely positive when histology was considered the gold standard. Images of these 12 sites showed many of the same image characteristics as truly neoplastic lesions, primarily loss of clearly discernible glands. There are number of factors that may have contributed to this. Many of the study participants had recently undergone an endoscopic procedure including biopsy and had come to Mt. Sinai for further assessment and treatment. Recent biopsy and resulting re-epithelialization may also be associated with lack of glandular structure. Regenerative mucosa was shown to substantially contribute to false positives in a study evaluating fluorescence induced by a different contrast agent [95]. In the future it will be important to characterize the differences associated recently biopsied sites in order to improve specificity.

Two of the 16 sites with a histologic diagnosis of neoplasia were falsely negative by VFI. These sites were both histologically diagnosed as high grade dysplasia, without adenocarcinoma; one corresponded to a focal dysplasia. While the VFI image of both of these sites shows some glandular structure, the glands appear more fragmented when compared to metaplasia. Larger studies are needed to determine whether image characteristics seen in these false negatives are consistent in a significant number of HGDs.

This *in vivo* pilot study marks an important step in clinical translation of vital-dye fluorescence endoscopy. There are many advantages to VFI; video endoscopes can be easily modified to achieve VFI, contrast is provided by a topically applied dye and VFI image results can be quantified. However, our study has a number of limitations that need to be addressed. This study was conducted retrospectively in a small population with a high prevalence of disease; larger studies are needed to assess overall accuracy and determine whether VFI improves the detection rate for neoplasia when compared to white light endoscopic surveillance and standard four-quadrant biopsies in both high and low prevalence populations. At the same time, the role of high resolution imaging in improving overall diagnostic accuracy should be further investigated; VFI should be tested in conjunction with high resolution imaging modalities such as confocal microendscopy and high resolution microendscopy to determine how the addition of higher resolution imaging might improve overall detection of neoplastic lesions.

Finally, this study demonstrates the potential for quantitative features to aid in interpretation of widefield images. Subjective interpretation of endoscopic imaging is variable and highly dependent on clinician experience [96]. Quantifying image features

provides a means for objective interpretation, and may also be helpful in guiding the endoscopist's index of suspicion regarding the presence or absence of neoplasia within a lesion. In order to optimize potential benefit of this technique, quantitative results must be automated and presented in real-time during endoscopy, allowing endoscopists to use quantitative features to make informed, real-time decisions regarding patient care.

CHAPTER 6: PRE-CLINICAL EVALUATION OF FLUORESCENT DEOXYGLUCOSE AS A TOPICAL CONTRAST AGENT FOR THE DETECTION OF BARRETT'S-ASSOCIATED NEOPLASIA DURING CONFOCAL IMAGING

6.1 Introduction

The incidence of esophageal adenocarcinoma (EAC) is rapidly rising in the United States, with an estimated 300-400% increase over the past 3 decades [97, 98]. This increased incidence is particularly worrisome, given that the overall five-year-survival rate for patients diagnosed with EAC is a dismal 12% [3], an outcome resulting from detection of late-stage disease. Indeed, more than 60% of patients with EAC are diagnosed with local, regional, and distant metastases [13]. Detecting and treating esophageal neoplasia at an early stage has been reported to increase five-year survival to rates as high as 81% [12]; however, current surveillance methods have considerable limitations.

EAC arises primarily in patients with Barrett's esophagus (BE) [14, 15], a highly prevalent condition caused by chronic esophageal reflux[99]. In patients with BE, the squamous epithelium of the esophagus near the gastroesophageal junction is replaced by specialized columnar epithelium [16-18] known as intestinal metaplasia (IM). BE/IM is of clinical importance because it is a risk factor for EAC. Because of this increased risk, patients with BE undergo regular surveillance at designated intervals according to level of dysplasia in an attempt to identify neoplastic lesions at an early, treatable stage [4, 19]. The current standard of endoscopic surveillance involves random four-quadrant biopsies taken every 1-2 cm along the BE segment [4]. However, dysplasia within BE is often

unidentifiable under standard white light endoscopy and as many as 43-57% of early cancers can go undetected by this method [5]. Thus, there is a pressing need to improve the clinician's ability to visualize neoplastic lesions during endoscopy. Improving the ability to discriminate high grade dysplasia (HGD) and early EAC from IM and low grade dysplasia (LGD) could significantly impact clinical decision-making. The diagnosis of either HGD or EAC prompts endoscopic based therapy or surgical resection [100-102], while diagnosis of either IM or LGD warrants continued surveillance [4].

Various optical imaging techniques are being explored to improve current surveillance strategies [9, 20, 42]. Widefield endoscopic optical imaging techniques, such as autofluorescence [7] and narrowband imaging [41], have shown high sensitivity but suboptimal specificity, largely due to the confounding effect of inflammation. Moreover, the lack of spatial resolution prevents cellular-level interrogation of suspicious areas, motivating the need for high resolution imaging technologies, which may aid in reducing false positives.

Confocal endomicroscopy is thought to achieve the highest sensitivity and specificity of any high-resolution modality to date [9, 46]. This technology is most commonly coupled with intravenously administered fluorescein. Unfortunately, fluorescein is a non-specific contrast agent with diffuse uptake in both normal as well as neoplastic mucosa. While it permits the visualization of subcellular epithelial changes and the subepithelial vasculature, it does not specifically target neoplastic epithelium. Moreover, the number of cases needed to train endoscopists to interpret these images and characterize the morphologic features of neoplasia interpretation is high [103]. The increased availability and utilization of confocal endoscopy necessitates the need for

novel, safe, easily-applied contrast agents that can be used to increase the diagnostic accuracy of endoscopic surveillance.

Several molecular-specific, optically active contrast agents have been developed to enhance the optical detection of neoplasia in a variety of organ sites using confocal microendoscopy [60, 104]. Topical application of a fluorescently labeled deoxyglucose, 2-NBDG (2-[N-(7-nitrobenz-2-oxa-1,3-diazol-4-yl)amino]-2-deoxy-D-glucose), was recently shown to improve visualization of early oral neoplasia. The application of 2-NBDG was shown to increase fluorescence contrast in specimens with neoplasia, relative to that available with autofluorescence [105]. The staining method was based on experiments by O'Neil and colleagues in cancer cell lines [106]. The increase in 2-NBDG uptake is associated with increased rates of glucose metabolism in cancer cells relative to normal cells [106], thought to be due to over-expression of glucose transporters (GLUTs) and increased activity of hexokinase enzymes [107]. The deoxyglucose is actively transported into the cell by the GLUTs and is phosphorylated by the hexokinase enzyme [108]. The phosphorylated deoxyglucose molecule is then selectively entrapped within the cell cytoplasm, resulting in increased contrast during fluorescence imaging [109, 110], with peak excitation at 475 nm and peak emission at 550 nm. When coupled with the appropriate imaging technology, 2-NBDG can be a useful marker for detecting areas with increased levels of cellular metabolism associated with the over-expression of GLUTs.

An increase in expression of GLUTs has been reported in many epithelial cancers, including EAC [111, 112]. GLUTs are currently targeted in cancer imaging using a radioactively-labeled glucose analog (^{18}FDG) during positron emission tomography (PET) [113]. PET is routinely used to stage potentially operable patients with EAC [114].

However, there are obstacles to using PET for routine surveillance, including a high number of false positives associated with inflammation [115-117], patient exposure to radiation, and a relatively poor spatial resolution. Indeed, PET is used to evaluate increased uptake over a large field of view and cannot delineate neoplasia occurring at microscopic level. Optical molecular imaging using a fluorescently labeled deoxyglucose, a contrast agent with similar mechanism of uptake as ^{18}FDG [118], has the potential to address these limitations when used as an adjunct to endoscopic surveillance with confocal endomicroscopy. When coupled with confocal imaging, 2-NBDG could potentially permit the simultaneous characterization of the morphologic and metabolic features of neoplasia.

The goal of this study was to carry out a pre-clinical pilot study to evaluate the feasibility of topical 2-NBDG as a contrast agent for the evaluation of Barrett's-associated neoplasia. Fluorescently labeled deoxyglucose (2-NBDG) was topically applied ex vivo to fresh esophageal biopsy specimens. Samples were imaged using confocal fluorescence microscopy, and resulting fluorescence images were evaluated to assess the contrast between metaplastic (IM/LGD) and neoplastic (HGD/EAC) mucosa. Results of this pre-clinical study provide preliminary data to guide future translation to *in vivo* confocal endoscopic imaging in patients with BE.

6.2 Materials and Methods

6.2.1 Patient Enrollment and Data Collection

Patients who participated in this study had been previously diagnosed with BE, BE with dysplasia, or BE with EAC and were scheduled for endoscopic examination.

This study was reviewed and approved by the Institutional Review Boards at Rice University, the University of Texas M.D. Anderson Cancer Center, and the Mount Sinai Medical Center. All patients gave written informed consent to participate in the study.

For each patient, up to 4 research biopsies were obtained from the gastroesophageal junction, 1 biopsy for every 1-2 cm of BE segment. The endoscopist noted whether the esophageal mucosa was intact or ulcerated at the site of each biopsy. Biopsies were excluded if they were too small to process for imaging, were too small for histologic processing, or if the epithelial layer was not present for assessment after histologic staining.

Immediately following forceps removal, biopsies were incubated in 100 μL of a 210 μM solution of 2-NBDG (Invitrogen, Carlsbad, CA, USA) in isotonic PBS for 40 minutes at 37° C. Following incubation, specimens were washed in isotonic PBS on a shaker three times at 4°C for 10 minutes each to remove any excess 2-NBDG. PBS was replaced after each washing step. The tissue was then placed between two cover slips and imaged *en face* on a confocal microscope (LSM Meta 510, Zeiss, Inc., Germany). Fluorescence images were obtained at 488 nm laser excitation, with a 488 nm dichroic and a bandpass emission filter (520-580 nm) with a 20X objective. Images were acquired at different sites across the entire epithelial surface of each biopsy, resulting in 2-10 images acquired from different sites within each biopsy. At each site, the focal plane was located between 16 and 23 microns below the surface of the biopsy specimen. Differential interference contrast (DIC) images were obtained from the same 500x500 μm field of view as the confocal fluorescence images to provide a guide to tissue morphology. All the fluorescence images used for analysis were taken at the same laser

power and gain settings. The use of a benchtop confocal system allows the ability to control these settings, necessary during this initial pre-clinical evaluation of 2-NBDG in BE.

Following confocal imaging, biopsy specimens were fixed in formalin and submitted for standard histologic evaluation; the diagnosis of the research biopsy was considered the gold standard in this study. Pathology slides were reviewed by a single GI pathologist with expertise in BE and EAC. The pathologist who reviewed the biopsy was blinded from the interpretation of confocal images. Pathologic diagnosis of IM, LGD, HGD and/or EAC was determined using previously defined standard criteria [4], which included loss of goblet cells, increased cellular atypia and glandular irregularity during neoplastic progression, among others. The presence of chronic and/or acute inflammation was based on the presence of lymphocytes/plasma cells in the lamina propria or neutrophils within the glandular epithelium, respectively [119]. When present, the degree of chronic inflammation was graded (mild, moderate, marked).

6.2.2 Qualitative Image Evaluation

All confocal fluorescence images were analyzed visually by two investigators (N.T. and D.M.) to identify key morphologic and architectural features visualized by fluorescence contrast associated with 2-NBDG uptake, which correspond to features present in H&E-stained histology. These include architectural features such as complexity of glandular architecture, glandular density, and glandular arrangement, as well as cytologic features such as the presence/absence of goblet cells, nuclear crowding, and nuclear enlargement.

Initial review of images indicated distinct 2-NBDG staining patterns for EAC samples depending on whether or not the tumor appeared ulcerated at the time of endoscopy. Therefore, images from samples diagnosed as HGD/EAC were divided into two sub-groups based on endoscopic tumor appearance (intact mucosa, ulcerated surface). Images categorized as ulcerated EAC were excluded from further quantitative analysis, due to the clinicians' ability to easily visualize these lesions during endoscopy.

6.2.3 Quantitative Image Evaluation

Due to the low-risk of progression associated with LGD, and the known high inter-observer variability in histologic diagnosis of LGD [4], for quantitative evaluation both IM and LGD were grouped as metaplasia, and both HGD and EAC were grouped as neoplasia. This classification is consistent with the current confocal endoscopic grading system and is the most relevant to clinical utility for disease management [9].

GLUT over-expression and activity are known to be significantly elevated in HGD/EAC [111], therefore specimens diagnosed as such may exhibit increased uptake of 2-NBDG relative to IM/LGD. To determine whether the intensity of 2-NBDG fluorescence correlated with histopathologic diagnosis, two quantitative image features were calculated. First, the mean glandular intensity (MGI), which included fluorescence only from glands, was calculated for each site imaged. Glands were segmented by a single observer, blinded to histopathologic diagnosis. Second, the mean fluorescence intensity (MFI) of the entire field of view, including fluorescence from both glands and the lamina propria, was calculated for each site imaged. The average MGI and MFI were calculated for all sites with the same histopathologic diagnosis and compared. One-way unbalanced

ANOVA was performed to determine whether differences in the mean value of calculated features between each pathologic category were significant.

6.2.4 Diagnostic Algorithm

Linear discriminant analysis was used to develop an algorithm to classify samples as neoplastic (HGD/EAC) or non-neoplastic (IM/LGD) based on each of the two quantitative image features using histologic diagnosis as the gold standard. Due to the exploratory nature of this study, the same data set was used to train the algorithm and test its performance. For each input feature, a receiver operator characteristic (ROC) curve was constructed and the associated area under the curve (AUC) was calculated. Performance of the algorithm was assessed on a per-site basis; in addition, quantitative features from each site within a biopsy were averaged together in order to assess algorithm performance on a per biopsy basis.

6.3 Results

A total of 206 sites were imaged from 44 biopsies, as described in Table 6-1; 34 biopsies were obtained from UT MD Anderson Cancer Center and 10 biopsies were obtained from Mount Sinai Medical Center.

Table 6-I: Patient Data Summary

Pathologic Diagnosis	Individual Biopsies	Sites Imaged
IM/LGD	28 (in 14 patients)	113
HGD/EAC with no ulceration	10 (in 7 patients)	55
EAC with ulceration	6 (in 5 patients)	38

6.3.1 Qualitative Image Evaluation

Figures 6-1 to 6-3 show representative endoscopic images, 2-NBDG stained confocal fluorescence images, and corresponding H&E histology from specimens with intact and ulcerated surfaces. Figure 6-1A shows a representative endoscopic image of BE with intact mucosa (non-ulcerated). Figure 6-1B shows a representative confocal fluorescence image of a biopsy from that area incubated with 2-NBDG. While uptake of the contrast agent is minimal, glands are still visible due to uptake of the contrast agent in epithelial cell cytoplasm. Goblet cells and nuclei appear to take up less 2-NBDG in comparison, making them appear dark. These features are indicated in the magnified confocal image (Figure 6-1D). The diagnosis of IM was verified by histopathology from the same biopsy (Figure 6-1C).

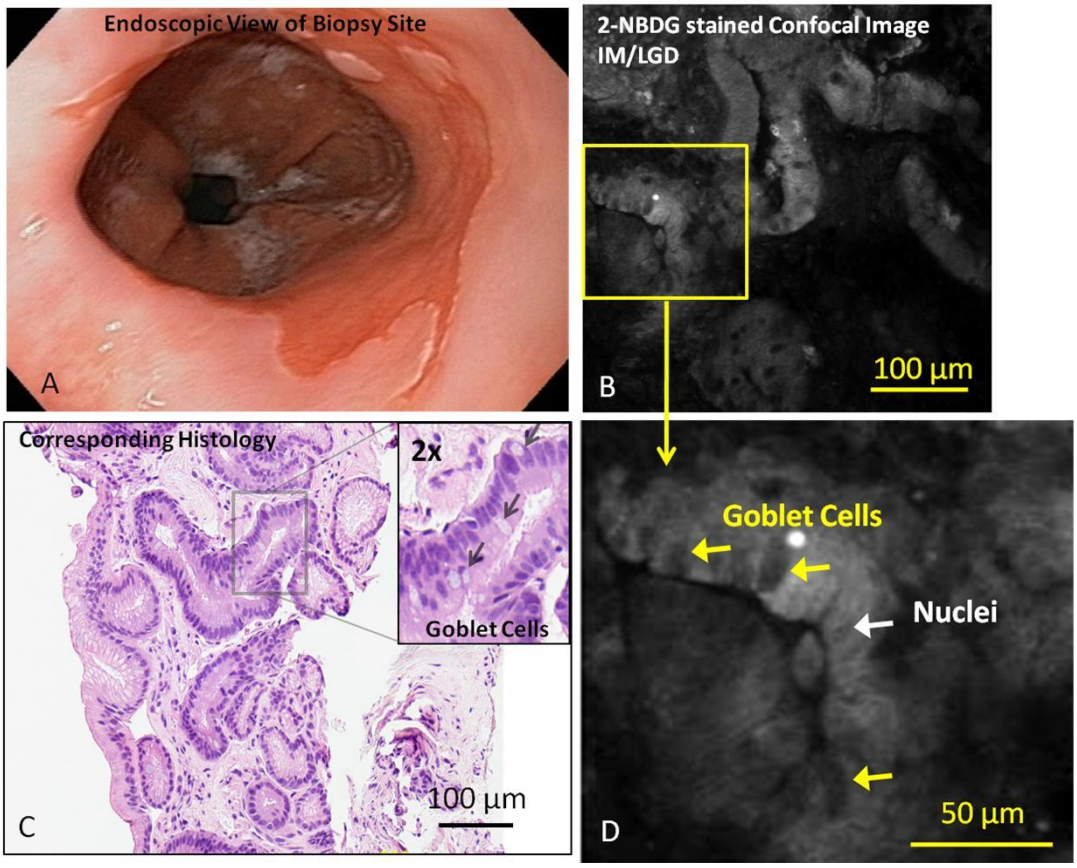

Fig. 6-1. Representative endoscopic image (A), confocal fluorescence images (B, D) and histologic images (C) of samples diagnosed as IM/LGD are shown. Relevant features such as goblet cells and nuclei are indicated.

Figure 6-2A shows an endoscopic image of mucosa diagnosed as HGD with intact mucosa (non-ulcerated). Figure 6-2B shows a confocal fluorescence image of a biopsy from that area incubated with 2-NBDG; uptake of the contrast agent is higher than in the specimen diagnosed as IM (shown in previous Figure 6-1B), resulting in increased glandular fluorescence intensity. Irregularly shaped glands and an increased density of glands are visible in the confocal fluorescence image, with strong uptake of 2-NBDG making the glandular patterns clear. Incomplete glands and nuclei are indicated in the magnified confocal image (Figure 6-2D). Visible cytologic changes include a decrease in

goblet cell density and enlargement of nuclei. The diagnosis of HGD was verified by histology (Figure 6-2C).

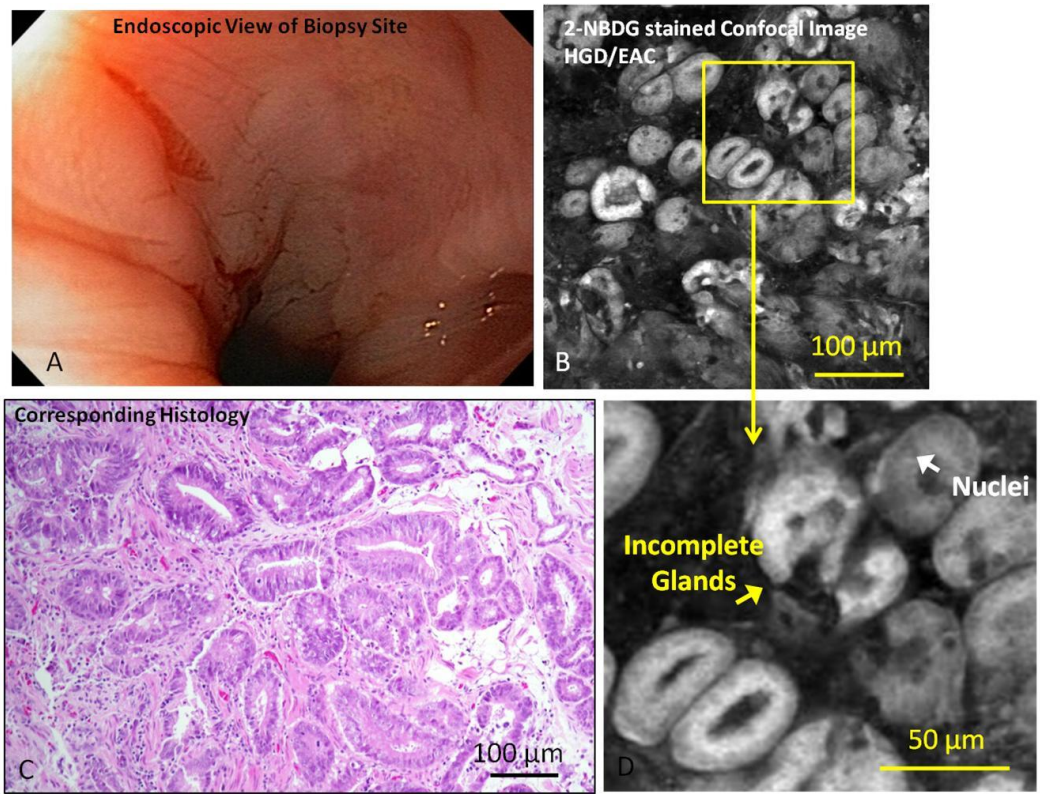

Fig. 6-2. Representative endoscopic image (A), confocal fluorescence images (B, D) and histologic images (C) of samples diagnosed as HGD with intact mucosal surface are shown. Relevant features such nuclei and incomplete glands are indicated. There is no apparent lesion or ulceration indicating neoplasia in endoscopy image; however, biopsy-confirmed neoplasia is present and neoplastic features are visible in the confocal image.

Figure 6-3A shows an endoscopic image of ulcerated mucosa diagnosed as carcinoma. Figure 6-3B shows a confocal fluorescence image of a biopsy from that area incubated with 2-NBDG. Cells appear to take up the contrast agent, resulting in high fluorescence intensity; however, due to the lack of recognizable glandular structure, it is difficult to

differentiate tumor cells from stromal invasion. The lack of glandular structure and the diagnosis of ulcerated EAC were verified on the corresponding histology section (Figure 6-3C).

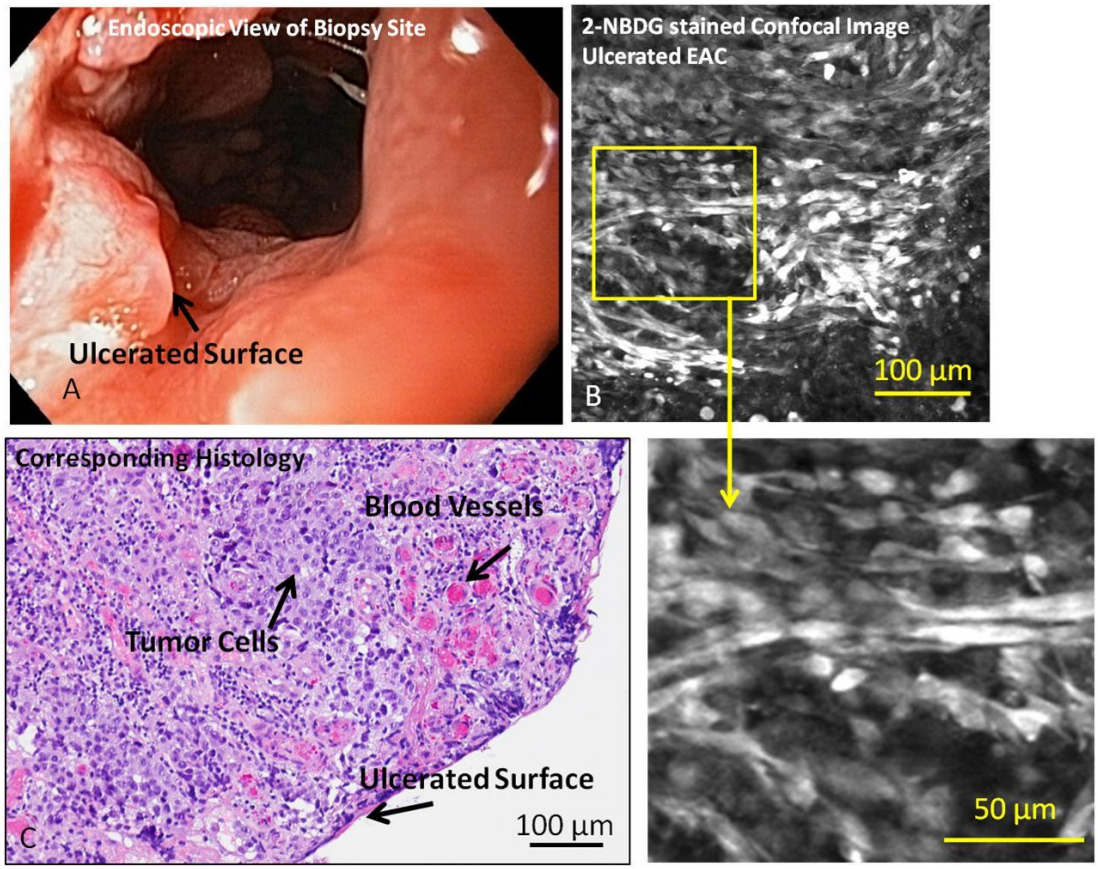

Fig. 6-3. Representative endoscopic image (A), confocal fluorescence images (B, D) and histologic images (C) of samples diagnosed as EAC with ulcerated mucosal surface are shown. Relevant features such as tumor cells, blood vessels, and the ulcerated surface are indicated. Apparent tumor and ulcerated surface visible during surveillance endoscopy is verified with biopsy-confirmed invasive cancer with surface ulceration.

Figures 6-4A, C, and E, show representative images of 2-NBDG stained tissue from IM/LGD with zero to mild levels of inflammation, IM/LGD with moderate to marked inflammation, and HGD/EAC with moderate to marked inflammation. All specimens were obtained from areas with endoscopically-intact mucosal surfaces. Corresponding histology is also shown (Figure 6-4B, D, and F). While fluorescence intensity associated with 2-NBDG uptake is minimal in the sample diagnosed with IM/LGD with zero to mild levels inflammation (Figure 6-4A), the 2-NBDG uptake within the gland enhances the visibility of mucin within goblet cells, making them appear dark in contrast. A representative goblet cell is indicated by the white arrow. Dark nuclei are made apparent by the uptake of the agent in the surrounding cytoplasm and are identified by their smaller size and position within the gland; they are not as dark as goblet cells.

Figure 6-4C shows a representative confocal image of IM/LGD with moderate to marked inflammation. The pattern of glandular uptake is similar to that of IM/LGD with mild inflammation; the image shows characteristic crypts with dark goblet cells associated with IM/LGD. However, the presence of inflammatory cells in the lamina propria is associated with increased 2-NBDG and increased fluorescence intensity, characterized by the bright areas between the glands.

Figure 6-4E shows a representative confocal fluorescence image of HGD/EAC with moderate to marked inflammation. Glandular uptake of 2-NBDG is significantly higher than is found with IM/LGD, resulting in increasingly bright glands. The particularly high intensity associated with these glands allows visualization of glandular irregularity and disruption –hallmarks of HGD and early EAC. Glands are crowded,

irregular, and fragmented and goblet cells are not visible. Uptake of 2-NBDG is visible in areas of lamina propria, making visible a few scattered fibers, most likely representing disrupted muscularis mucosa. Among the patients diagnosed as HGD/EAC with intact mucosa, the majority were graded as having moderate to marked levels of chronic inflammation (53/55); thus, the impact of lower levels of inflammation on 2-NBDG uptake could not be evaluated.

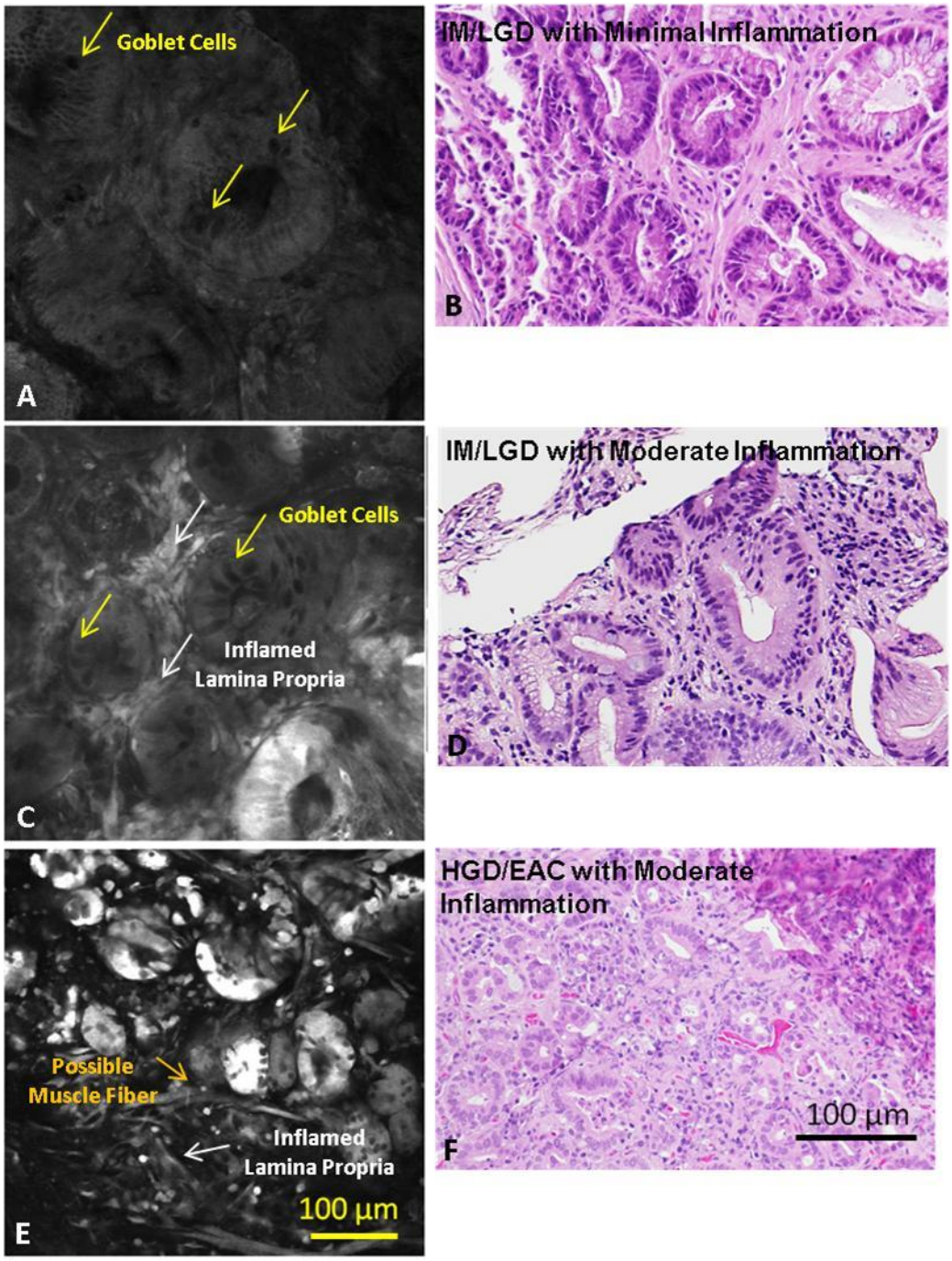

Fig. 6-4. Representative confocal fluorescence images of samples diagnosed as (A) IM/LGD with zero to mild levels of chronic inflammation, (B) IM/LGD with moderate to marked levels of chronic inflammation, (C) HGD/EAC with moderate to marked levels of chronic inflammation, and corresponding histopathology (D-F). The presence of moderate-marked inflammation is associated with increased fluorescence

in the lamina propria, while the presence of neoplasia is associated with increased glandular fluorescence.

6.3.2 Quantitative Image Evaluation

Figure 6-5 demonstrates gland selection for MGI calculation. Figure 6-6A shows the mean and standard deviation of the MGI of each site as a function of histologic diagnosis and grade of inflammation. On average, the MGI is lowest for sites with IM/LGD with zero to mild levels of inflammation (42.3 ± 17.0), and is highest for sites with HGD/EAC (84.0 ± 10.2). Figure 6-6B shows a corresponding scatter-plot of the MGI for each site; the MGI of the majority of the sites diagnosed as HGD/EAC are greater than for a majority of the sites diagnosed as IM/LGD, irrespective of the presence or degree of inflammation. Differences in the overall MGI of biopsies histologically categorized as IM/LGD and HGD/EAC were found to be significantly different ($p<0.001$). The ability of high resolution imaging to separate glandular changes from changes in the lamina propria is particularly useful.

The mean and standard deviation of the MFI feature, which includes both glands and lamina propria, was 29.3±9.3 for IM/LGD with zero to mild levels of inflammation, 67.0 ± 35.7 for IM/LGD with moderate to marked levels of inflammation, and 53.0 ± 13.9 for HGD/EAC with mild to marked levels of inflammation. Due to the inflamed lamina propria, there is considerable overlap in the distribution of the MFI for sites diagnoses as IM/LGD with moderate to marked inflammation and sites diagnosed as HGD/EAC. Differences in the overall MFI of biopsies histologically categorized as IM/LGD and HGD/EAC were not found to be significantly different.

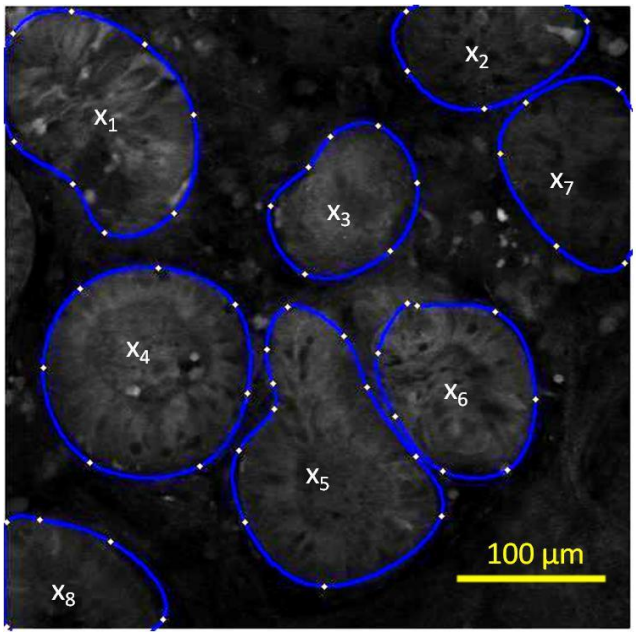

Fig. 6-5. Demonstration of gland selection for mean glandular intensity (MGI) calculation on a confocal image of Barrett's metaplasia stained with 2-NBDG. MGI is the average of x, where x is the average intensity of each gland.

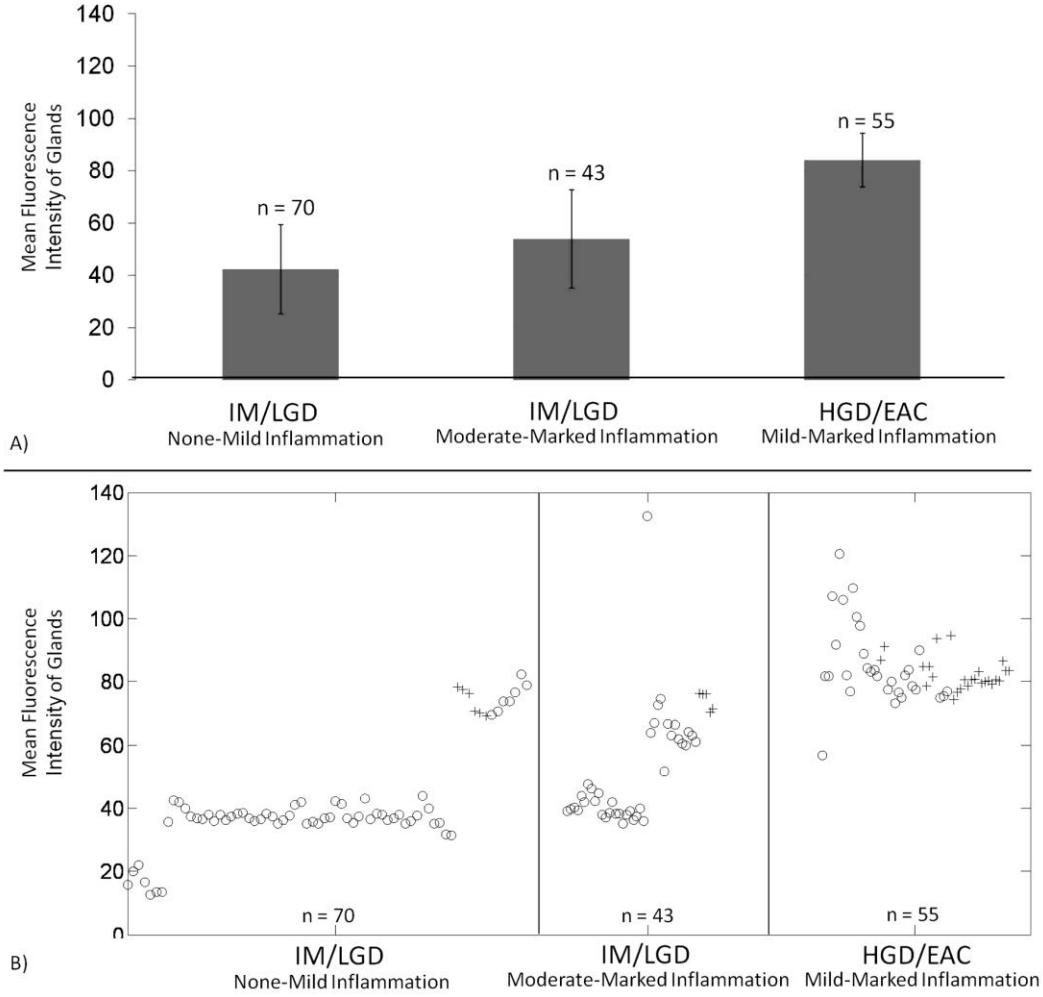

Fig. 6-6. (A) Plot showing mean glandular fluorescence intensity ± one standard deviation, separated according to histologic diagnosis and presence/grade of inflammation: IM/LGD with zero-mild chronic inflammation; IM/LGD with moderated-marked chronic inflammation; and HGD/EAC with zero-marked chronic inflammation. (B) Scatter-plot showing mean glandular fluorescence intensity for each site according to histologic diagnosis and presence/grade of inflammation. Samples with acute inflammation present are indicated by "+" symbols; samples with no acute inflammation present are indicated by "o" symbols. n = the number of images evaluated per category.

Diagnostic algorithms were developed to classify samples as neoplastic or metaplastic based on each of these two quantitative features; algorithms based on the

MGI gave best performance relative to the gold standard of histopathology. Figure 6-7 shows the resulting ROC curves for this feature, with accuracy calculated on a per-site or per-biopsy basis. At the Q-point, the algorithm based on MGI has a sensitivity of 96% and a specificity of 90% calculated per site (AUC = 0.97), and a sensitivity of 100% and a specificity of 93% calculated per biopsy (AUC = 0.96).

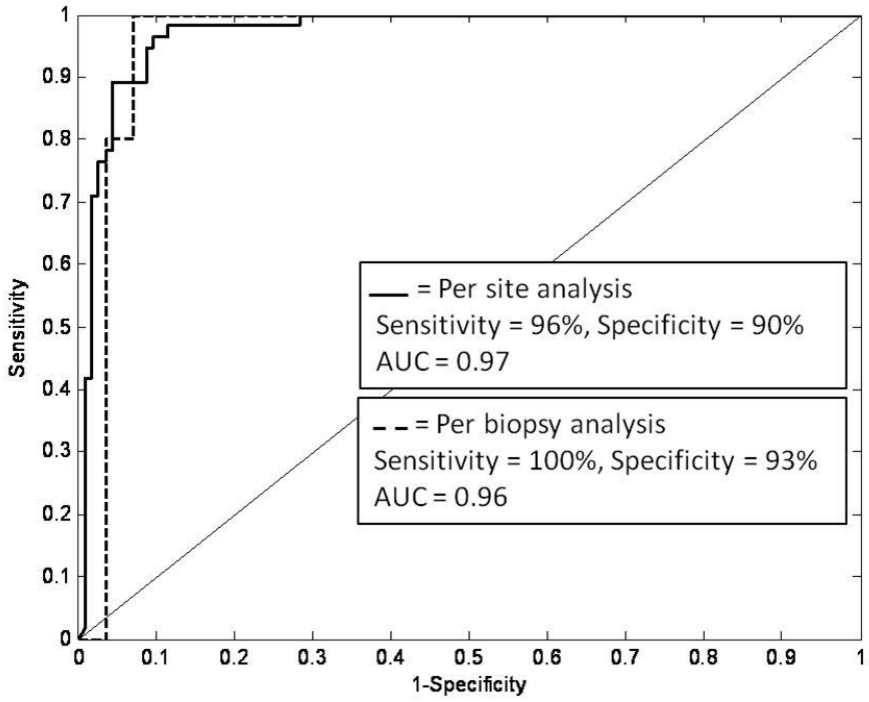

Fig. 6-7. ROC curve for algorithm discriminating samples with HGD/EAC from samples with IM/LGD based on mean glandular fluorescence intensity. Results are shown for a per-site and a per-biopsy analysis using histology as the gold standard.

6.4 Discussion

This prospective, pre-clinical study evaluates the potential of fluorescent deoxyglucose as a topical contrast agent for adjuvant confocal microscopic examination of Barrett's esophagus. Our results suggest that topical 2-NBDG provides quantifiable

image features that can be used to discriminate neoplastic sites from metaplastic sites with high sensitivity and specificity. By combining high-resolution morphologic information provided by confocal microscopy with the metabolic information provided by 2-NBDG, this imaging method offers the ability to visualize and quantify key pathologic features to differentiate neoplasia. While glandular staining can be heterogeneous, likely due to pathologic heterogeneity known to be present in individual biopsy fragments [120], the effect appears to mitigated when the mean glandular intensity is used as a classifying feature. Indeed, the ability to delineate glandular uptake of 2-NBDG from the surrounding lamina propria provides the critical advantage of differentiating neoplasia from inflammation, a significant confounder with other imaging technologies.

Emerging targeted, optically labeled contrast agents such as antibodies, peptides, or aptamers can be advantageous over commonly used non-targeted agents, such as fluorescein, due to the specificity towards known markers of neoplasia. However, due to the size of the targeted agents (kDa range), it may be difficult to achieve relevant penetration depth using topical delivery. An advantage of 2-NBDG is its low molecular weight (330 Da); thus it may have the potential to penetrate deeper through tissue [57]. This is especially useful since confocal imaging has the ability to image sub-surface cell layers. Moreover, due to its small size, 2-NBDG has the potential to overcome difficulties associated with tissue clearance; agent not taken up by the cells can be removed through simple washing steps.

Like ^{18}FDG PET, 2-NBDG imaging provides a tool to assess tissue metabolic activity [118]. Despite its benefits, ^{18}FDG PET is typically only used for disease staging and monitoring [121]. Moreover, false positives associated with inflammation are common

[115]. While duplicating many of the benefits of ^{18}FDG PET, the use of 2-NBDG during optical imaging offers additional advantages. The spatial resolution of optical imaging is limited by diffraction and can thus be used to visualize the location of 2-NBDG uptake. This can aid in determining whether the signal comes from inflammatory cells in the lamina propria or neoplastic cells of the glands. These advantages support the broader use of metabolic monitoring during endoscopic surveillance. Finally, due to the long history of safe use of intravenous ^{18}FDG [122, 123] and the limited amounts (3-5 ml) of 2-NBDG required for topical application in the esophagus, the use of this contrast agent should be readily translatable to clinical application.

This ex vivo study highlights the potential benefits of using 2-NBDG to image and quantify signal contrast associated with neoplasia and serves as an important step towards eventual clinical translation. However, further clinical studies are necessary to determine whether similar conclusions can be drawn during in vivo imaging. In this study, tissue samples were incubated with 2-NBDG post excision to allow the uptake of the agent. An in vivo study will be necessary to determine whether topical application will require an incubation time similar to that used in the ex vivo study. If so, an optimal medium for application, such as a paste or a gel, will need to be explored. Furthermore, larger sample sizes are necessary to assess clinical utility. In such a study, the effects of acute inflammation on the glandular mean intensity could be further evaluated and the differences between low grade and high grade dysplasia could be explored in more detail. Despite these limitations, this study demonstrates the potential benefits of optically monitoring metabolic activity to identify neoplasia.

Results of this *ex vivo* pre-clinical study provide preliminary data to guide future translation to *in vivo* confocal endoscopic surveillance in patients with BE. Advances in widefield imaging have given endoscopists the ability to detect areas suspicious of neoplasia with high sensitivity but limited specificity. Topically applied 2-NBDG coupled with appropriate high resolution imaging techniques could be used to further optically sample those areas and rule out false positives based on relevant cellular and biochemical changes associated with neoplastic progression. Objective visualization of relevant biochemical changes provides clinicians with an added dimension of information, thus appropriate decisions regarding diagnosis and treatment can be made. Since these features are quantifiable, there exists the potential to develop computer-aided analysis software for real-time endoscopic interpretation. This information may increase sampling efficiency, enhance the detection of neoplasia and improve margin determination during surveillance.

CHAPTER 7: CONCLUSION

7.1 Summary and Research Contributions

Widefield optical imaging allows scanning of large epithelial surface areas for lesions suspicious of neoplasia. The technology can be used in conjunction with existing, highly specific, high resolution technologies [9, 54, 59] in order to eventually implement a two-step detection process, widefield identification of suspicious areas and high resolution verification of disease [124, 125]. While both widefield and high resolution optical imaging platforms have been used to probe various endogenous tissue features associated with disease progression [7, 24], both have more recently been used to probe exogenous contrast agent dyes in order to increase the visibility of important disease biomarkers [82, 126].

The pathologic disease progression from Barrett's metaplasia to associated adenocarcinoma is well-documented making it an ideal candidate for testing new imaging techniques. To date, various widefield imaging techniques have been tested for in vivo Barrett's surveillance [7, 40, 77, 79], however, these individual techniques have yet to achieve the accuracy needed to be incorporated into standard of care [127]. While these endoscopic technologies have significantly advanced optical imaging in vivo, there remains a need for an imaging platform which utilizes both widefield and high resolution imaging for Barrett's surveillance. This dissertation describes the development and testing of new widefield and high resolution imaging techniques for the optical detection of Barrett's associated neoplasia.

Chapter 3 describes the first research contribution of this dissertation, the development of vital-dye fluorescence imaging (VFI) with proflavine hemisulfate

contrast, a fluorescent dye which binds to DNA. Our goal in this *ex vivo* 15-patient pilot study was to evaluate the feasibility of a single topical contrast agent using a benchtop fluorescence-based platform for both widefield and high resolution imaging of the gastrointestinal tract. This approach elucidated the clinically relevant features that can be visualized using two different imaging scales, highlighting the benefit of first examining glandular architecture and then probing nuclear morphology. Results from this study demonstrated the diagnostically relevant image features found in VFI. Widefield fluorescence imaging was used to resolve features on the order of 50-100 microns with a field of view of approximately 2 cm in diameter. This mode of imaging coupled with proflavine contrast enhanced visualization of glandular architecture when compared to white light imaging. In metaplasia, glandular edges were enhanced, and a distinct glandular pattern appeared throughout a given region of interest. The spatial distribution of glands appeared regular and there was little distortion or crowding of the pattern. In high grade dysplasia, partial effacement of the glands was visible and heterogeneous staining was present. In adenocarcinoma, glandular architecture often became completely effaced with little to no visible gland edges.

High resolution imaging was used to resolve features on the order of 4-5 microns with a field of view of approximately 750 microns in diameter. HRME imaging has previously been shown to improve visualization of both glandular and nuclear morphology. Indeed, in this *ex vivo* study, HRME of metaplastic epithelium showed evenly distributed glands, clear epithelial borders, where the nuclei were polarized towards the outer edges. In neoplasia, glands appear heteregenous and unevenly distributed with various levels of glandular dropout associated with the increased

progression to neoplasia. In HRME images, nuclear crowing is also an important visible indicator of neoplasia.

These results led to the second research contribution of this dissertation; the design, construction, and implementation of the module-based video endoscope (MVE), an endoscope which can image in three widefield imaging modes and that can accommodate the existing HRME imaging probe via endoscope instrument channel for high resolution imaging. The MVE can collect white light, cross-polarized reflectance, and vital-dye fluorescence *in vivo*. At a typical working distance of 10 mm, the field of view is adjustable due to a digital zoom function and can vary between 14 mm and 45 mm in diameter. At this working distance the system can easily resolve blood vessels and glandular architecture (50 microns).

To implement cross-polarized imaging (CPI), a stainless steel filter module designed to work with the Pentax high definition upper endoscope was used to hold necessary optical filters. White light from the existing xenon arc lamp passes through linear polarizers contained in the module, one in front of each end of the bifurcated light guide. This module holds another orthogonally oriented linear polarizer in front the CCD to achieve CPI. Though cross polarized imaging has been demonstrated in other organ sites [80, 84], this is the first in vivo implementation of cross-polarized imaging through an endoscope.

To implement vital-dye fluorescence imaging (VFI), a custom 455 nm laser illumination system was implemented to achieve sufficient excitation to image proflavine fluorescence. The quasi-monochromatic illumination light excites proflavine contrast, and emitted fluorescence is collected through a custom-designed long pass filter held by a

second stainless steel filter module. This filter was designed to accommodate the angular FOV of the endoscope (up to 70 degrees). Fluorescence imaging has been demonstrated to probe endogenous contrast [7, 8] and exogenous contrast [82] in Barrett's, but this is a unique instance where widefield endoscopic fluorescence imaging has been achieved through a replaceable filter module and the first instance where widefield proflavine fluorescence was measured *in vivo* in the gastrointestinal tract.

Results show that CPI enhances vessel architecture while VFI enhances glandular architecture when compared to white light imaging; this was demonstrated during in vivo endoscopic imaging. In neoplasia, CPI images show an increase in vessel density and VFI images show an increase in glandular effacement when compared to non-neoplastic images. Moreover, the changes in glandular architecture seen in widefield VFI images were further visualized during high resolution imaging of the same agent. For in vivo HRME images, both glandular and nuclear morphology can be assessed.

The third contribution of this dissertation was the development of a classification algorithm for the identification of neoplasia in MVE images obtained endoscopically. In a 14 patient pilot study, 65 pathologically correlated images of metaplasia and neoplasia were obtained. Step-wise linear discriminant analysis was used to classify images as metaplasia (BE/LGD) or neoplasia (HGD/EAC) using quantitative image features. The diagnostic algorithm, developed using leave-one-out cross validation, classified neoplasia with a sensitivity and specificity of 88% and 86% respectively, with an area under the receiver operator characteristic curve of 0.86. This contribution is unique due to its focus on quantitatively evaluating widefield images of esophageal mucosa stained with proflavine.

The final contribution of this dissertation is the evaluation of an additional contrast agent for the identification of neoplasia in Barrett's. Chapter 6 examines 2-NBDG, a fluorescent deoxyglucose, a well-documented optical indicator of cellular metabolism that has been shown to aid in identifying neoplasia in the oral cavity [105]. The excitation and emission wavelengths of 2-NBDG closely correspond to those of proflavine, making it a candidate for future in vivo surveillance using the MVE and the HRME. The study presented here focuses on high resolution evaluation of the agent, a necessary step towards eventual widefield examination. A total of 206 sites were images from 44 biopsies. Each biopsy was incubated with 2-NBDG for 30 minutes at 37ºC and imaged using benchtop confocal microscope. Qualitatively, confocal images of 2-NBDG stained biopsies highlights the glandular pattern. Nuclei and characteristic goblet cells appear dark, whereas cell cytoplasm appears bright due to accumulation of 2-NBDG. Diagnostic algorithms were used to classify image sites as neoplasia. By using the mean glandular intensity of each image, the algorithm could classify neoplasia with a sensitivity of 96% and specificity of 90% with an area under the receiver operator characteristic curve of 0.97. This is the first pre-clinical evaluation of 2-NBDG as a topical contrast agent for the detection of Barrett's-associated neoplasia using confocal imaging.

7.2 Future Research Directions

Various steps are needed to translate the technology developed in this dissertation from research-based pilot studies to clinical care. Based on the research presented here, there are important instrumentation modifications, clinical studies, and laboratory experiments that are needed to determine whether or not these research contributions can

influence the current clinical paradigm for cancer detection. By executing these steps, there exists the potential to further develop a multimodal/dual-scale imaging platform that can probe various exogenous contrast agents.

Firstly, while the instrumentation designed and constructed here was an important first-step towards in vivo endoscopic fluorescence imaging, the limitations associated with the number of scope insertions (two to achieve white light imaging and VFI) were not anticipated. In order to promote widescale use of the MVE, the endoscope must achieve the same imaging results using one scope insertion. Moreover, the endoscopist should be able to switch easily between white light and VFI imaging modalities. Without this improvement, adoption of this technique in community surveillance centers may not be easily achievable. By exciting proflavine with a shorter wavelength (~405 nm) we can take advantage of long pass filter with a shorter cut-on (~435 nm) wavelength; the benefit of this long pass filter is that it can be used to image in white light mode as well, reducing the number of insertions for widefield examination. However, appropriately designed experiments are needed to determine whether sufficient proflavine excitation can be achieved at this wavelength and if the use of a long pass filter during white light imaging affects the interpretation of mucosal features.

Secondly, large-scale statistically significant clinical studies are needed to understand the benefits of VFI. Moreover, understanding the effectiveness of the widefield/high-resolution detection scheme is an important step to understanding how essential the role of each play in surveillance. For this to happen, two different studies need to be conducted. Since confocal imaging has emerged as a high performing high resolution imaging technology [9], and the HRME has emerged as a potential cost-effective

alternative [54, 56], the first is a statistically significant study comparing the sensitivity and specificity of the WLI/VFI/confocal detection scheme to the WLI/VFI/HRME detection scheme. Once the optimal high resolution technology is determined, the second study needed is a randomized clinical trial to compare that platform to the current standard of care.

In addition to what WLI/VFI/HRME can do to improve the detection of new neoplastic lesions, there is also the potential for the technology to aid in endoscopic margin determination. The advent of a variety of new imaging techniques and surveillance programs has the potential to improve the detection of adenocarcinoma at early stages. As technology improves early detection of neoplastic lesions, endoscopic treatments are becoming available. By introducing VFI technology that elucidates changes in glandular architecture, the technology could be used for margin determination, though additional in vivo studies are needed to assess the potential in this area.

VFI imaging was designed to not only image proflavine contrast but also to image additional contrast agents that may aid in identifying neoplasia such as 2-NBDG. We tested 2-NBDG as an alternative contrast agent, however there are more steps needed for clinical translation of the agent. In order eventually conduct widefield and high resolution fluorescence imaging of 2-NBDG in vivo, short term animal toxicity studies are needed to obtain an FDA exemption to use 2-NBDG for IRB approved in vivo research protocols. Additionally, medium of delivery must be explored due to the necessary incubation step.

In addition to 2-NBDG, due to the development of the MVE the opportunity exists to test additional highly specific contrast agents developed for the esophagus such as a recently described, fluorescently-labeled, high affinity peptide [10, 128]. The development of this system also motivates the development of new contrast agents. Biomarkers such as EGFR have been shown to increase in certain subsets of patients with Barrett's [129]. By identifying these patients early using optical contrast agents targeting these biomarkers, we can potentially personalize their care at the point of surveillance.

The future of endoscopic surveillance will be multifaceted and a potential solution will require not only larger scale clinical studies but cost analysis to understand the overall effectiveness compared to existing practice. This dissertation emphasizes the importance of a solution involving a two-step detection process using both widefield and high resolution imaging and the importance of developing topical contrast agents that will work with the proposed platform. The steps laid out in this chapter are necessary to move the platform from research into clinical practice. Once these steps are taken, we can evaluate how to transition this technology beyond the high-risk Barrett's patient population and into screening and evaluating other endoscopically accessible cancers.

REFERENCES

1. Petersen, P.E. Oral cancer prevention and control--the approach of the World Health Organization. *Oral Oncol* **45**, 454-60 (2009).
2. Brown, L.M., Devesa, S.S. & Chow, W.H. Incidence of adenocarcinoma of the esophagus among white Americans by sex, stage, and age. *J Natl Cancer Inst* **100**, 1184-7 (2008).
3. Sihvo, E.I., Luostarinen, M.E. & Salo, J.A. Fate of patients with adenocarcinoma of the esophagus and the esophagogastric junction: a population-based analysis. *Am J Gastroenterol* **99**, 419-24 (2004).
4. Sampliner, R.E. Updated guidelines for the diagnosis, surveillance, and therapy of Barrett's esophagus. *Am J Gastroenterol* **97**, 1888-95 (2002).
5. Vieth, M., Ell, C., Gossner, L., May, A. & Stolte, M. Histological analysis of endoscopic resection specimens from 326 patients with Barrett's esophagus and early neoplasia. *Endoscopy* **36**, 776-81 (2004).
6. Thekkek, N., Anandasabapathy, S. & Richards-Kortum, R. Optical molecular imaging for detection of Barrett's-associated neoplasia. *World J Gastroenterol* **17**, 53-62 (2011).
7. Kara, M.A. et al. Endoscopic video autofluorescence imaging may improve the detection of early neoplasia in patients with Barrett's esophagus. *Gastrointest Endosc* **61**, 679-85 (2005).
8. Kara, M.A. et al. A randomized crossover study comparing light-induced fluorescence endoscopy with standard videoendoscopy for the detection of early neoplasia in Barrett's esophagus. *Gastrointest Endosc* **61**, 671-8 (2005).
9. Kiesslich, R. et al. In vivo histology of Barrett's esophagus and associated neoplasia by confocal laser endomicroscopy. *Clin Gastroenterol Hepatol* **4**, 979-87 (2006).
10. Lu, S. & Wang, T.D. In vivo cancer biomarkers of esophageal neoplasia. *Cancer Biomark* **4**, 341-50 (2008).
11. Devesa, S.S., Blot, W.J. & Fraumeni, J.F., Jr. Changing patterns in the incidence of esophageal and gastric carcinoma in the United States. *Cancer* **83**, 2049-53 (1998).
12. Portale, G. et al. Modern 5-year survival of resectable esophageal adenocarcinoma: single institution experience with 263 patients. *J Am Coll Surg* **202**, 588-96; discussion 596-8 (2006).
13. Farrow, D.C. & Vaughan, T.L. Determinants of survival following the diagnosis of esophageal adenocarcinoma (United States). *Cancer Causes Control* **7**, 322-7 (1996).
14. Blot, W.J., Devesa, S.S., Kneller, R.W. & Fraumeni, J.F., Jr. Rising incidence of adenocarcinoma of the esophagus and gastric cardia. *JAMA* **265**, 1287-9 (1991).
15. Cameron, A.J. EPIDEMIOLOGY OF COLUMNAR-LINED ESOPHAGUS AND ADENOCARCINOMA. *Gastroenterol Clin North Am* **26**, 487-494 (1997).
16. Morales, T.G., Sampliner, R.E. & Bhattacharyya, A. Intestinal metaplasia of the gastric cardia. *American Journal of Gastroenterology* **92**, 414-418 (1997).

17. Mueller, J., Werner, M. & Stolte, M. Barrett's esophagus: histopathologic definitions and diagnostic criteria. *World J Surg* **28**, 148-54 (2004).
18. Spechler, S.J. Columnar-lined esophagus: Definitions. *Chest Surgery Clinics of North America* **12**, 1-13 (2002).
19. Katz, D. et al. The development of dysplasia and adenocarcinoma during endoscopic surveillance of Barrett's esophagus. *American Journal of Gastroenterology* **93**, 536-541 (1998).
20. Georgakoudi, I. et al. Fluorescence, reflectance, and light-scattering spectroscopy for evaluating dysplasia in patients with Barrett's esophagus. *Gastroenterology* **120**, 1620-9 (2001).
21. Wallace, M.B. et al. Endoscopic detection of dysplasia in patients with Barrett's esophagus using light-scattering spectroscopy. *Gastroenterology* **119**, 677-82 (2000).
22. DaCosta, R.S., Wilson, B.C. & Marcon, N.E. Photodiagnostic techniques for the endoscopic detection of premalignant gastrointestinal lesions. *Digestive Endoscopy* **15**, 153-173 (2003).
23. Georgakoudi, I. et al. NAD(P)H and collagen as in vivo quantitative fluorescent biomarkers of epithelial precancerous changes. *Cancer Res* **62**, 682-7 (2002).
24. Kara, M.A. et al. Characterization of tissue autofluorescence in Barrett's esophagus by confocal fluorescence microscopy. *Dis Esophagus* **20**, 141-50 (2007).
25. Auvinen, M.I. et al. Incipient angiogenesis in Barrett's epithelium and lymphangiogenesis in Barrett's adenocarcinoma. *Journal of Clinical Oncology* **20**, 2971-2979 (2002).
26. Couvelard, A. et al. Angiogenesis in the neoplastic sequence of Barrett's oesophagus. Correlation with VEGF expression. *J Pathol* **192**, 14-8 (2000).
27. Mobius, C. et al. The 'angiogenic switch' in the progression from Barrett's metaplasia to esophageal adenocarcinoma. *Eur J Surg Oncol* **29**, 890-4 (2003).
28. Gono, K. et al. Appearance of enhanced tissue features in narrow-band endoscopic imaging. *J Biomed Opt* **9**, 568-77 (2004).
29. Herszenyi, L. et al. Alteration of glutathione S-transferase and matrix metalloproteinase-9 expressions are early events in esophageal carcinogenesis. *World Journal of Gastroenterology* **13**, 676-682 (2007).
30. Salmela, M.T., Karjalainen-Lindsberg, M.L., Puolakkainen, P. & Saarialho-Kere, U. Upregulation and differential expression of matrilysin (MMP-7) and metalloelastase (MMP-12) and their inhibitors TIMP-1 and TIMP-3 in Barrett's oesophageal adenocarcinoma. *British Journal of Cancer* **85**, 383-392 (2001).
31. DaCosta, R.S., Wilson, B.C. & Marcon, N.E. Spectroscopy and fluorescence in esophageal diseases. *Best Pract Res Clin Gastroenterol* **20**, 41-57 (2006).
32. Georgakoudi, I. & Van Dam, J. Characterization of dysplastic tissue morphology and biochemistry in Barrett's esophagus using diffuse reflectance and light scattering spectroscopy. *Gastrointest Endosc Clin N Am* **13**, 297-308 (2003).
33. DaCosta, R.S., Andersson, H. & Wilson, B.C. Molecular fluorescence excitation-emission matrices relevant to tissue spectroscopy. *Photochem Photobiol* **78**, 384-92 (2003).

34. Drezek, R. et al. Autofluorescence microscopy of fresh cervical-tissue sections reveals alterations in tissue biochemistry with dysplasia. *Photochem Photobiol* **73**, 636-41 (2001).
35. Pavlova, I. et al. Microanatomical and biochemical origins of normal and precancerous cervical autofluorescence using laser-scanning fluorescence confocal microscopy. *Photochem Photobiol* **77**, 550-5 (2003).
36. Gulledge, C.J. & Dewhirst, M.W. Tumor oxygenation: a matter of supply and demand. *Anticancer Res* **16**, 741-9 (1996).
37. Mayevsky, A. & Chance, B. Intracellular oxidation-reduction state measured in situ by a multichannel fiber-optic surface fluorometer. *Science* **217**, 537-40 (1982).
38. Harris, D.M. & Werkhaven, J. Endogenous porphyrin fluorescence in tumors. *Lasers Surg Med* **7**, 467-72 (1987).
39. Panjehpour, M. et al. Endoscopic fluorescence detection of high-grade dysplasia in Barrett's esophagus. *Gastroenterology* **111**, 93-101 (1996).
40. Kara, M.A., Ennahachi, M., Fockens, P., ten Kate, F.J. & Bergman, J.J. Detection and classification of the mucosal and vascular patterns (mucosal morphology) in Barrett's esophagus by using narrow band imaging. *Gastrointest Endosc* **64**, 155-66 (2006).
41. Sharma, P. et al. The utility of a novel narrow band imaging endoscopy system in patients with Barrett's esophagus. *Gastrointest Endosc* **64**, 167-75 (2006).
42. Curvers, W.L. et al. Endoscopic tri-modal imaging for detection of early neoplasia in Barrett's oesophagus: a multi-centre feasibility study using high-resolution endoscopy, autofluorescence imaging and narrow band imaging incorporated in one endoscopy system. *Gut* **57**, 167-72 (2008).
43. Evans, J.A. et al. Optical coherence tomography to identify intramucosal carcinoma and high-grade dysplasia in Barrett's esophagus. *Clin Gastroenterol Hepatol* **4**, 38-43 (2006).
44. Qi, X., Sivak, M.V., Isenberg, G., Willis, J.E. & Rollins, A.M. Computer-aided diagnosis of dysplasia in Barrett's esophagus using endoscopic optical coherence tomography. *J Biomed Opt* **11**, 044010 (2006).
45. Pohl, H. et al. Evaluation of endocytoscopy in the surveillance of patients with Barrett's esophagus. *Endoscopy* **39**, 492-6 (2007).
46. Pohl, H. et al. Miniprobe confocal laser microscopy for the detection of invisible neoplasia in patients with Barrett's oesophagus. *Gut* **57**, 1648-53 (2008).
47. Endo, T. et al. Classification of Barrett's epithelium by magnifying endoscopy. *Gastrointestinal Endoscopy* **55**, 641-647 (2002).
48. Curvers, W. et al. Chromoendoscopy and narrow-band imaging compared with high-resolution magnification endoscopy in Barrett's esophagus. *Gastroenterology* **134**, 670-9 (2008).
49. Curvers, W.L. et al. Mucosal morphology in Barrett's esophagus: interobserver agreement and role of narrow band imaging. *Endoscopy* **40**, 799-805 (2008).
50. Kara, M.A., Peters, F.P., Fockens, P., ten Kate, F.J. & Bergman, J.J. Endoscopic video-autofluorescence imaging followed by narrow band imaging for detecting early neoplasia in Barrett's esophagus. *Gastrointest Endosc* **64**, 176-85 (2006).

51. Cobb, M.J. et al. Imaging of subsquamous Barrett's epithelium with ultrahigh-resolution optical coherence tomography: a histologic correlation study. *Gastrointest Endosc* **71**, 223-230.
52. Suter, M.J. et al. Comprehensive microscopy of the esophagus in human patients with optical frequency domain imaging. *Gastrointest Endosc* **68**, 745-53 (2008).
53. Tomizawa, Y. et al. Endocytoscopy in esophageal cancer. *Gastrointest Endosc Clin N Am* **19**, 273-81 (2009).
54. Muldoon, T.J., Anandasabapathy, S., Maru, D. & Richards-Kortum, R. High-resolution imaging in Barrett's esophagus: a novel, low-cost endoscopic microscope. *Gastrointest Endosc* **68**, 737-44 (2008).
55. Dunbar, K.B., Okolo, P., 3rd, Montgomery, E. & Canto, M.I. Confocal laser endomicroscopy in Barrett's esophagus and endoscopically inapparent Barrett's neoplasia: a prospective, randomized, double-blind, controlled, crossover trial. *Gastrointest Endosc* **70**, 645-54 (2009).
56. Muldoon, T.J. et al. Evaluation of quantitative image analysis criteria for the high-resolution microendoscopic detection of neoplasia in Barrett's esophagus. *J Biomed Opt* **15**, 026027.
57. Pierce, M.C., Javier, D.J. & Richards-Kortum, R. Optical contrast agents and imaging systems for detection and diagnosis of cancer. *Int J Cancer* **123**, 1979-90 (2008).
58. Olliver, J.R., Wild, C.P., Sahay, P., Dexter, S. & Hardie, L.J. Chromoendoscopy with methylene blue and associated DNA damage in Barrett's oesophagus. *Lancet* **362**, 373-4 (2003).
59. Polglase, A.L. et al. A fluorescence confocal endomicroscope for in vivo microscopy of the upper- and the lower-GI tract. *Gastrointest Endosc* **62**, 686-95 (2005).
60. Hsiung, P.L. et al. Detection of colonic dysplasia in vivo using a targeted heptapeptide and confocal microendoscopy. *Nat Med* **14**, 454-8 (2008).
61. Goetz, M. & Wang, T.D. Molecular imaging in gastrointestinal endoscopy. *Gastroenterology* **138**, 828-33 e1.
62. Rubin, D.T., Rothe, J.A., Hetzel, J.T., Cohen, R.D. & Hanauer, S.B. Are dysplasia and colorectal cancer endoscopically visible in patients with ulcerative colitis? *Gastrointestinal Endoscopy* **65**, 998-1004 (2007).
63. Dekker, E. et al. Narrow-band imaging compared with conventional colonoscopy for the detection of dysplasia in patients with longstanding ulcerative colitis. *Endoscopy* **39**, 216-21 (2007).
64. van den Broek, F.J. et al. Endoscopic tri-modal imaging for surveillance in ulcerative colitis: randomised comparison of high-resolution endoscopy and autofluorescence imaging for neoplasia detection; and evaluation of narrow-band imaging for classification of lesions. *Gut* **57**, 1083-9 (2008).
65. Kiesslich, R. et al. Confocal laser endoscopy for diagnosing intraepithelial neoplasias and colorectal cancer in vivo. *Gastroenterology* **127**, 706-13 (2004).
66. Kiesslich, R. et al. Chromoscopy-Guided Endomicroscopy Increases the Diagnostic Yield of Intraepithelial Neoplasia in Ulcerative Colitis. *Gastroenterology* **132**, 874-882 (2007).

67. Pohl, H. et al. Accuracy of Miniprobe Confocal Laser Microscopy for the Detection of Barrett Neoplasia. *Gastrointestinal Endoscopy* **67**, AB125-AB125 (2008).
68. Muldoon, T.J. et al. Subcellular-resolution molecular imaging within living tissue by fiber microendoscopy. *Opt Express* **15**, 16413-23 (2007).
69. Pierce, M., Yu, D. & Richards-Kortum, R. High-resolution fiber-optic microendoscopy for in situ cellular imaging. *J Vis Exp*.
70. Kiesslich, R. & Neurath, M.F. Endoscopic detection of early lower gastrointestinal cancer. *Best Pract Res Clin Gastroenterol* **19**, 941-61 (2005).
71. Roblyer, D. et al. Multispectral optical imaging device for in vivo detection of oral neoplasia. *J Biomed Opt* **13**, 024019 (2008).
72. Inoue, H. et al. In vivo observation of living cancer cells in the esophagus, stomach, and colon using catheter-type contact endoscope, "Endo-Cytoscopy system". *Gastrointest Endosc Clin N Am* **14**, 589-94, x-xi (2004).
73. Inoue, H. et al. Endoscopic in vivo evaluation of tissue atypia in the esophagus using a newly designed integrated endocytoscope: a pilot trial. *Endoscopy* **38**, 891-5 (2006).
74. Janssen, P.A., Selwood, B.L., Dobson, S.R., Peacock, D. & Thiessen, P.N. To dye or not to dye: a randomized, clinical trial of a triple dye/alcohol regime versus dry cord care. *Pediatrics* **111**, 15-20 (2003).
75. Cameron, A.J. Epidemiology of columnar-lined esophagus and adenocarcinoma. *Gastroenterol Clin North Am* **26**, 487-94 (1997).
76. Wang, K.K. & Sampliner, R.E. Updated guidelines 2008 for the diagnosis, surveillance and therapy of Barrett's esophagus. *Am J Gastroenterol* **103**, 788-97 (2008).
77. Kara, M., DaCosta, R.S., Wilson, B.C., Marcon, N.E. & Bergman, J. Autofluorescence-based detection of early neoplasia in patients with Barrett's esophagus. *Dig Dis* **22**, 134-41 (2004).
78. Wolfsen, H.C. et al. Prospective, controlled tandem endoscopy study of narrow band imaging for dysplasia detection in Barrett's Esophagus. *Gastroenterology* **135**, 24-31 (2008).
79. Mannath, J., Subramanian, V., Hawkey, C.J. & Ragunath, K. Narrow band imaging for characterization of high grade dysplasia and specialized intestinal metaplasia in Barrett's esophagus: a meta-analysis. *Endoscopy* **42**, 351-9.
80. Groner, W. et al. Orthogonal polarization spectral imaging: a new method for study of the microcirculation. *Nat Med* **5**, 1209-12 (1999).
81. Balas, C. A novel optical imaging method for the early detection, quantitative grading, and mapping of cancerous and precancerous lesions of cervix. *IEEE Trans Biomed Eng* **48**, 96-104 (2001).
82. Thekkek, N. et al. Vital-dye enhanced fluorescence imaging of GI mucosa: metaplasia, neoplasia, inflammation. *Gastrointest Endosc* **75**, 877-87.
83. Pierce, M.C., Vila, P.M., Polydorides, A.D., Richards-Kortum, R. & Anandasabapathy, S. Low-cost endomicroscopy in the esophagus and colon. *Am J Gastroenterol* **106**, 1722-4.

84. Roblyer, D. et al. Comparison of multispectral wide-field optical imaging modalities to maximize image contrast for objective discrimination of oral neoplasia. *J Biomed Opt* **15**, 066017.
85. Haggitt, R.C. Barrett's esophagus, dysplasia, and adenocarcinoma. *Hum Pathol* **25**, 982-93 (1994).
86. McConnell, T.P., Lee, C.W., Couillard, M. & Sherrill, W.W. Trends in umbilical cord care: Scientific evidence for practice. *Newborn and Infant Nursing Reviews* **4**, 211-222 (2004).
87. Thekkek, N. et al. Pre-clinical evaluation of fluorescent deoxyglucose as a topical contrast agent for the detection of Barrett's-associated neoplasia during confocal imaging. *Technol Cancer Res Treat* **10**, 431-41.
88. Thekkek, N. et al. Modular Video Endoscopy for In Vivo Cross Polarized and Vital-Dye Fluorescence Imaging of Barrett's Neoplasia. *J Biomed Opt* **18** (2013).
89. Argenti, F., Alparone, L. & Benelli, G. Fast algorithms for texture analysis using co-occurrence matrices. *Radar and Signal Processing, IEE Proceedings F* **137**, 443-448 (1990).
90. Gossage, K.W., Tkaczyk, T.S., Rodriguez, J.J. & Barton, J.K. Texture analysis of optical coherence tomography images: feasibility for tissue classification. *J Biomed Opt* **8**, 570-5 (2003).
91. Srivastava, S., Rodriguez, J.J., Rouse, A.R., Brewer, M.A. & Gmitro, A.F. Computer-aided identification of ovarian cancer in confocal microendoscope images. *J Biomed Opt* **13**, 024021 (2008).
92. Di Ruberto, C., Dempster, A., Khan, S. & Jarra, B. Analysis of infected blood cell images using morphological operators. *Image and Vision Computing* **20**, 133-146 (2002).
93. -Costa, L. & Ayala, G. Classifying human endothelial cells based on individual granulometric size distributions. *Image and Vision Computing* **20**, 783-791 (2002).
94. Gonzalez, R.C. Digital Image Processing Using Matlab (Prentice-Hall Europe).
95. Mayinger, B., Neidhardt, S., Reh, H., Martus, P. & Hahn, E.G. Fluorescence induced with 5-aminolevulinic acid for the endoscopic detection and follow-up of esophageal lesions. *Gastrointestinal endoscopy* **54**, 572-578 (2001).
96. Meining, A. et al. Inter- and intra-observer variability of magnification chromoendoscopy for detecting specialized intestinal metaplasia at the gastroesophageal junction. *Endoscopy* **36**, 160-4 (2004).
97. Cameron, A.J. Epidemiology of Barrett's esophagus and adenocarcinoma. *Dis Esophagus* **15**, 106-8 (2002).
98. DeVault, K.R. Epidemiology and significance of Barrett's esophagus. *Dig Dis* **18**, 195-202 (2000).
99. Winters Jr, C., Spurling, T.J. & Chobanian, S.J. Barrett's esophagus. A prevalent, occult complication of gastroesophageal reflux disease. *Gastroenterology* **92**, 118-124 (1987).
100. Muller, J.M., Erasmi, H., Stelzner, M., Zieren, U. & Pichlmaier, H. Surgical therapy of oesophageal carcinoma. *Br J Surg* **77**, 845-57 (1990).
101. Rice, T.W., Falk, G.W., Achkar, E. & Petras, R.E. Surgical management of high-grade dysplasia in Barrett's esophagus. *Am J Gastroenterol* **88**, 1832-6 (1993).

102. Ell, C. et al. Endoscopic mucosal resection of early cancer and high-grade dysplasia in Barrett's esophagus. *Gastroenterology* **118**, 670-677 (2000).
103. Kiesslich, R., Goetz, M., Vieth, M., Galle, P.R. & Neurath, M.F. Confocal laser endomicroscopy. *Gastrointest Endosc Clin N Am* **15**, 715-731 (2005).
104. Goetz, M. et al. In vivo molecular imaging of colorectal cancer with confocal endomicroscopy by targeting epidermal growth factor receptor. *Gastroenterology* **138**, 435-46 (2009).
105. Nitin, N. et al. Molecular imaging of glucose uptake in oral neoplasia following topical application of fluorescently labeled deoxy-glucose. *Int J Cancer* **124**, 2634-42 (2009).
106. O'Neil, R.G., Wu, L. & Mullani, N. Uptake of a fluorescent deoxyglucose analog (2-NBDG) in tumor cells. *Mol Imaging Biol* **7**, 388-92 (2005).
107. Medina, R.A. & Owen, G.I. Glucose transporters: expression, regulation and cancer. *Biol Res* **35**, 9-26 (2002).
108. Yoshioka, K. et al. Intracellular fate of 2-NBDG, a fluorescent probe for glucose uptake activity, in Escherichia coli cells. *Biosci Biotechnol Biochem* **60**, 1899-901 (1996).
109. Lloyd, P.G., Hardin, C.D. & Sturek, M. Examining glucose transport in single vascular smooth muscle cells with a fluorescent glucose analog. *Physiol Res* **48**, 401-10 (1999).
110. Yamada, K. et al. Measurement of glucose uptake and intracellular calcium concentration in single, living pancreatic beta-cells. *J Biol Chem* **275**, 22278-83 (2000).
111. Younes, M., Ertan, A., Lechago, L.V., Somoano, J. & Lechago, J. Human erythrocyte glucose transporter (Glut1) is immunohistochemically detected as a late event during malignant progression in Barrett's metaplasia. *Cancer Epidemiol Biomarkers Prev* **6**, 303-5 (1997).
112. Younes, M., Lechago, L.V., Somoano, J.R., Mosharaf, M. & Lechago, J. Wide expression of the human erythrocyte glucose transporter Glut1 in human cancers. *Cancer Res* **56**, 1164-7 (1996).
113. Nabi, H.A. & Zubeldia, J.M. Clinical applications of (18)F-FDG in oncology. *J Nucl Med Technol* **30**, 3-9; quiz 10-1 (2002).
114. Flamen, P. et al. Utility of positron emission tomography for the staging of patients with potentially operable esophageal carcinoma. *J Clin Oncol* **18**, 3202-10 (2000).
115. Strauss, L.G. Fluorine-18 deoxyglucose and false-positive results: a major problem in the diagnostics of oncological patients. *Eur J Nucl Med* **23**, 1409-15 (1996).
116. Cook, G.J., Wegner, E.A. & Fogelman, I. Pitfalls and artifacts in 18FDG PET and PET/CT oncologic imaging. *Semin Nucl Med* **34**, 122-33 (2004).
117. Rosenbaum, S.J., Lind, T., Antoch, G. & Bockisch, A. False-positive FDG PET uptake--the role of PET/CT. *Eur Radiol* **16**, 1054-65 (2006).
118. Sheth, R.A., Josephson, L. & Mahmood, U. Evaluation and clinically relevant applications of a fluorescent imaging analog to fluorodeoxyglucose positron emission tomography. *J Biomed Opt* **14**, 064014 (2009).

119. Cestari, R. et al. The pathology of gastric cardia: a prospective, endoscopic, and morphologic study. *Am J Surg Pathol* **31**, 706-10 (2007).
120. Reid, B.J. et al. Observer variation in the diagnosis of dysplasia in Barrett's esophagus. *Hum Pathol* **19**, 166-78 (1988).
121. Yasuda, S. et al. Application of positron emission tomography imaging to cancer screening. *Br J Cancer* **83**, 1607-11 (2000).
122. Som, P. et al. A fluorinated glucose analog, 2-fluoro-2-deoxy-D-glucose (F-18): nontoxic tracer for rapid tumor detection. *J Nucl Med* **21**, 670-5 (1980).
123. Gallagher, B.M. et al. Metabolic trapping as a principle of oradiopharmaceutical design: some factors resposible for the biodistribution of [18F] 2-deoxy-2-fluoro-D-glucose. *J Nucl Med* **19**, 1154-61 (1978).
124. Bedard, N. et al. Emerging roles for multimodal optical imaging in early cancer detection: a global challenge. *Technol Cancer Res Treat* **9**, 211-7 (2010).
125. Pierce, M.C. et al. Accuracy of in vivo multimodal optical imaging for detection of oral neoplasia. *Cancer Prev Res (Phila)* **5**, 801-9 (2012).
126. Nitin, N. et al. Optical molecular imaging of epidermal growth factor receptor expression to improve detection of oral neoplasia. *Neoplasia* **11**, 542-51 (2009).
127. Sharma, P. et al. The American Society for Gastrointestinal Endoscopy PIVI (Preservation and Incorporation of Valuable Endoscopic Innovations) on imaging in Barrett's Esophagus. *Gastrointest Endosc* **76**, 252-4 (2012).
128. Li, M. et al. Affinity peptide for targeted detection of dysplasia in Barrett's esophagus. *Gastroenterology* **139**, 1472-80 (2010).
129. Cronin, J. et al. Epidermal growth factor receptor (EGFR) is overexpressed in high-grade dysplasia and adenocarcinoma of the esophagus and may represent a biomarker of histological progression in Barrett's esophagus (BE). *Am J Gastroenterol* **106**, 46-56 (2011).